SDL/89-083

CONCEPTUAL DESIGN STUDY FOR INFRARED LIMB EXPERIMENT (IRLE)

FINAL REPORT

Doran J. Baker
Jim Ulwick
Roy Esplin
J. C. Batty
Gene Ware
Craig Tew

September 1989

Submitted to:

National Aeronautics and Space Administration
Langley Research Center
Hampton, Virginia 23665-5225

NASA Research Grant NAG-1-899

SPACE DYNAMICS LABORATORY
UTAH STATE UNIVERSITY LOGAN, UTAH 84322-4140

FOREWORD

This final report documents the phase A engineering design study for the Infrared Limb Experiment (IRLE) instrument, the infrared portion of the Mesosphere-Lower Thermosphere Explorer (MELTER) satellite payload. The Space Dynamics Laboratory at Utah State University (SDL/USU) conducted this engineering design study under NASA research grant NAG-1-899.

TABLE OF CONTENTS

TABLE OF CONTENTS (CONT)

TABLE OF CONTENTS (CONT)

LIST OF FIGURES

LIST OF FIGURES (CONT)

LIST OF TABLES

1. INTRODUCTION

The Infrared Limb Experiment (IRLE) instrument is a satellite instrument, based on the heritage of the Limb Infrared Monitor of the Stratosphere (LIMS) program, that will make global measurements of O_3, CO_2, NO, NO_2, H_2O, and OH from earth limb emissions. These measurements will be used to provide improved understanding of the photochemistry, radiation, dynamics, energetics, and transport phenomena in the lower thermosphere, mesosphere, and stratosphere. The IRLE instrument is the infrared portion of the Mesosphere-Lower Thermosphere Explorer (MELTER) satellite payload. A NASA Langley artist's concept of the MELTER satellite is shown in Figure 1-1. MELTER is being proposed to NASA Goddard by a consortium consisting of the University of Michigan, University of Colorado, and NASA Langley. It is proposed that the Space Dynamics Laboratory at Utah State University (SDL/USU) build the IRLE instrument for NASA Langley. MELTER is scheduled for launch in November 1994 into a sun-synchronous, 650-km circular orbit with an inclination angle of 97.8 deg and an ascending node at 3:00 p.m. local time.

This publication is the final report for the phase A engineering design study conducted by SDL/USU under NASA research grant NAG-1-899. Doran J. Baker and Jim Ulwick were Co-Principal Investigators for this study. System Engineering was performed by Roy Esplin, Thermal Engineering by Clair Batty, Structural Engineering by Craig Tew, Mechanical Designing by Donn Goode, and Electronic Engineering by Gene Ware. NASA technical direction was provided by James Russell III and Jack Dodgen, NASA Langley Research Center.

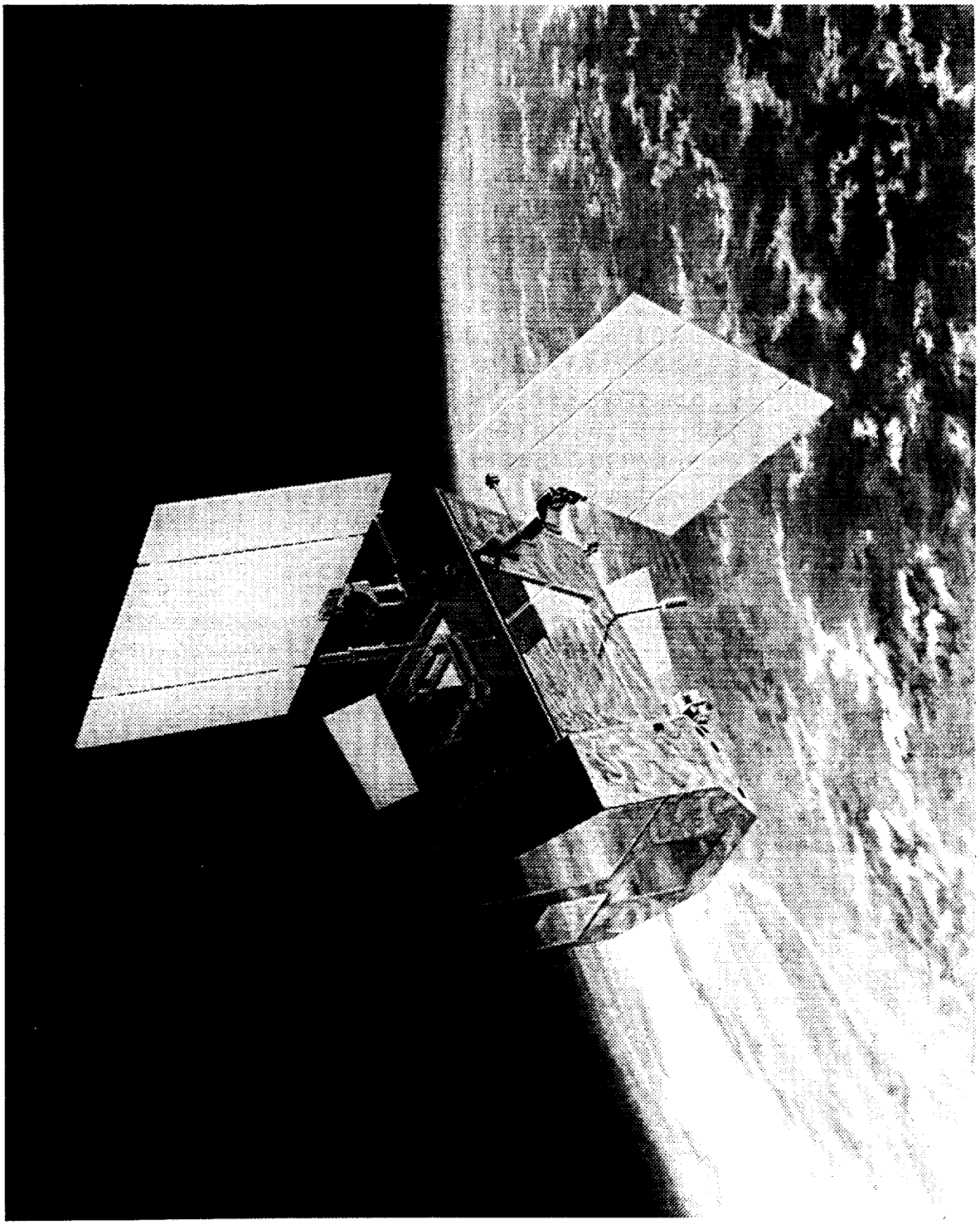

Figure 1-1. MELTER Satellite - NASA Langley Artist's Conception

2. IRLE SYSTEM DESCRIPTION

2.1 FUNCTIONAL DESCRIPTION

2.1.1 System Block Diagram

The IRLE instrument is a 9-channel radiometer whose line of sight (LOS) is scanned vertically through the earth limb by means of a one-dimensional scanning mirror. A functional system block diagram of the IRLE instrument is shown in Figure 2.1-1. The instrument collects radiance from the earth limb in nine spectral channels, digitizes it, synchronously demodulates and filters it, and finally formats the data and transmits it to the spacecraft in a serial data stream. A cryogenic mechanical refrigerator cools a detector array consisting of seven HgCdTe and two InSb detectors that sample the spectral wavelength region from 1 to 17 μm. The telescope cavity emission is subtracted from each measurement, allowing use of an ambient temperature telescope even though the IRLE instrument operates in the thermal IR. The magnitude of this emission is ascertained by measuring the signal when the instrument is looking at deep space.

2.1.2 Limb Scan Sequence

The limb scan sequence is illustrated in Figure 2.1-2 which plots the depression angle versus time. The depression angle is defined as the angle of the LOS below the spacecraft's local horizon. The local horizon is perpendicular to the nadir direction with zero spacecraft tilt. The limb scan sequence consists of two scan patterns, an acquisition scan pattern and an adaptive scan pattern. In addition to these scan patterns, the scan mirror is moved once per orbit so that the IRLE instrument looks at a full-aperture blackbody for calibration purposes. When IRLE is commanded to take data, the first four scans use the acquisition pattern to ascertain the reference tangent height and then IRLE switches over to the adaptive pattern. The scan rate for both patterns is 0.25 deg/sec. The data rate is the same for both scan patterns.

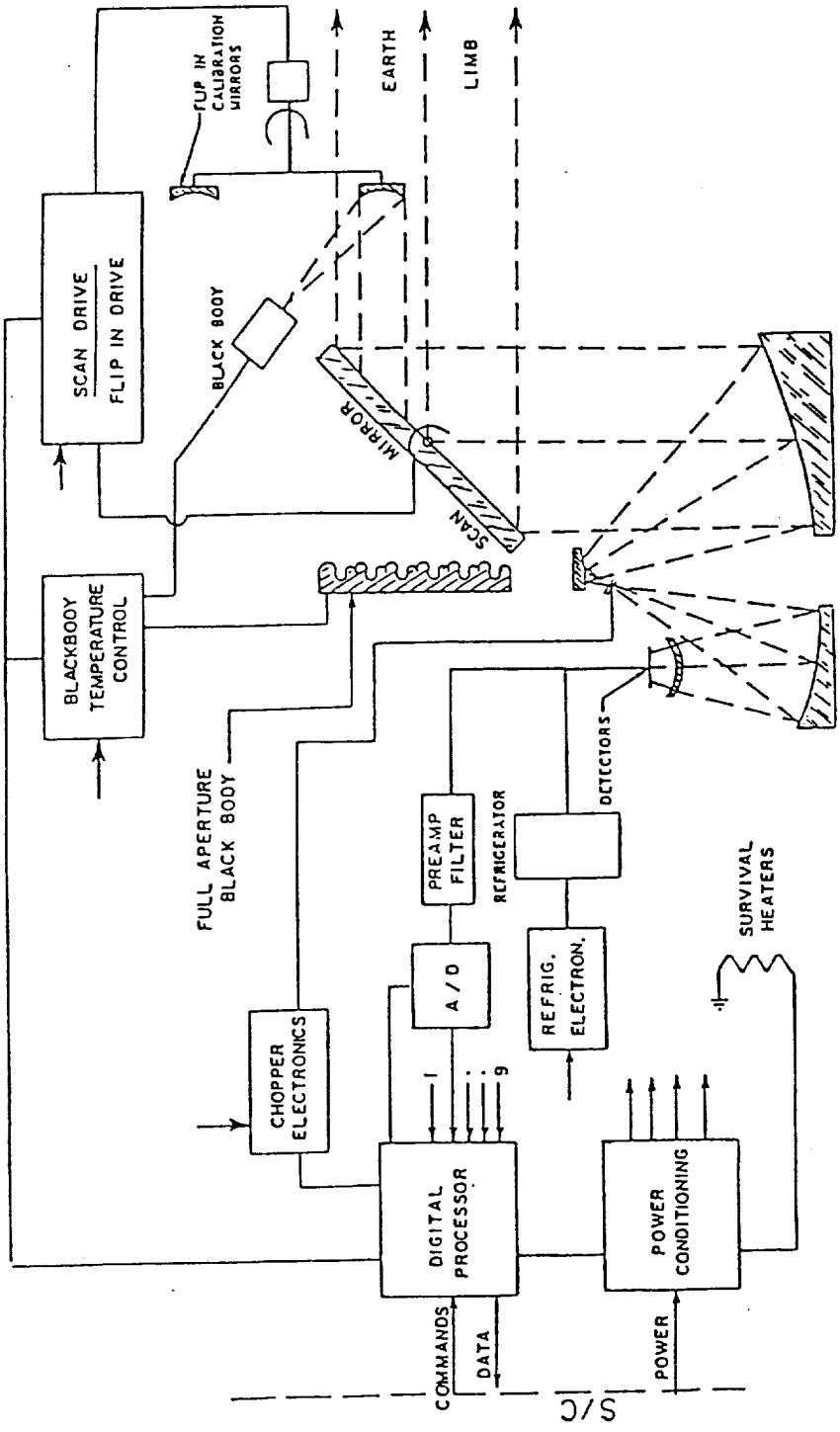

Figure 2.1-1. IRLE Instrument Functional Block Diagram

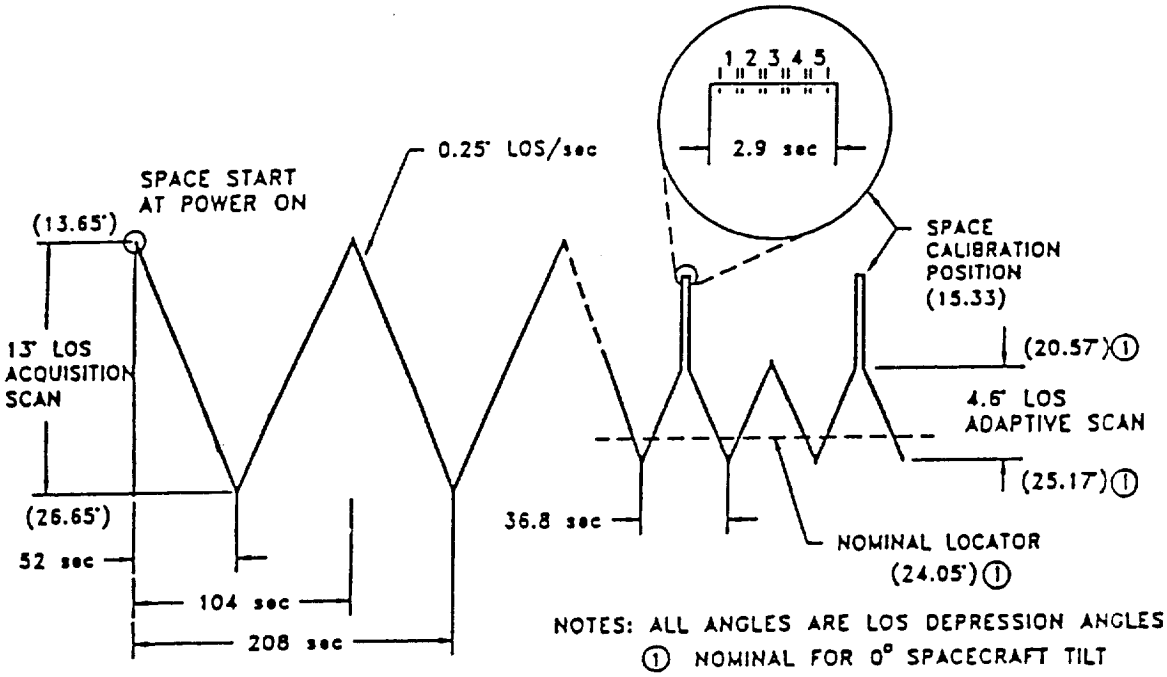

Figure 2.1-2. Limb Scan Sequence

2.1.2.1 Acquisition Scan Pattern. The acquisition scan pattern is used to ascertain the reference tangent height. IRLE uses this pattern for the first four scans after being commanded to take data. The acquisition scan pattern allows the IRLE to scan the LOS linearly over a range of 13 deg between depression angles of 13.65 and 26.65 deg. Given the 650-km orbit height, these angles correspond, respectively, to tangent heights of 452 and -95 km. Negative tangent heights are below the tangent point with the earth, indicating that the sensor is looking at the earth. Each of the four acquisition scans takes 52 seconds.

The reference tangent height is ascertained by processing the radiance versus tangent height profiles of channels 1, 2, and 3, the CO_2 wide channels and the CO_2 narrow channel. The nominal value for this horizon locator height is 40 km, which corresponds to a depression angle of 24.05 deg.

2.1.2.2 Adaptive Scan Pattern. After the reference tangent height has been determined from the acquisition scan data, IRLE switches to the adaptive scan pattern and continues in this pattern until commanded to do otherwise. The adaptive scan mode allows the IRLE to scan the LOS linearly over a 4.6-deg range that is registered to the reference tangent height. For the nominal reference angle of 24.05 deg, the adaptive scan angular limits are 20.57 and 25.17 deg. These angular limits correspond, respectively, to tangent heights of 200 and -20 km. During the adaptive scan the reference angle is continually undated to compensate for spacecraft altitude changes. After every two adaptive scan cycles, the scan mirror is moved to a calibration position for 2.9 seconds. The in-flight calibration procedure is described in the next paragraph.

2.1.3 In-Flight Calibration

To maintain the 1-percent radiometric accuracy, calibration of the IRLE instrument is updated after every two adaptive scan cycles. This is accomplished by moving the LOS to a tangent height of 400 km for a deep space look and then flipping three different mirrors in front of the telescope. Two of the flip-in mirrors introduce radiance from a controlled blackbody source for calibrating channels 1 through 8. These two mirrors are of different sizes to cover 25 and 2.5 percent of the IRLE aperture, providing calibration signals that differ by a factor of 10 in amplitude so that

channels 1 through 8 can be calibrated at two points in their dynamic range. The third flip-in mirror introduces radiance from a calibrated tungsten lamp for calibrating channel 9, the OH channel. Measurements taken without the flip-in mirrors provide the zero reference signal level, which make it possible to subtract the chopped signal from the warm telescope cavity.

Once per orbit the scan mirror is rotated so that IRLE looks at a full-aperture blackbody. This full-aperture blackbody is used to monitor contamination on all optical surfaces. This source is also a redundant calibration source for channels 1, 6, 7, and 8. It cannot be used for the other channels because it saturates channels 2 through 5 and it does not provide enough radiant energy to calibrate channel 9.

2.2 HARDWARE DESCRIPTION

2.2.1 System Overview

A perspective view of the IRLE instrument is shown in Figure 2.2-1. During launch the rocket velocity vector is in the Y direction. During orbital operation, the Z and X axes are in the orbit plane; the Z axis points in the nadir direction while the X axis defines the local horizon. Side and front views of IRLE are shown in Figures 2.2-2 and 2.2-3, respectively. The PDE box identified in these figures represents the power distribution electronics, and the PCE box represents the processor/control electronics. When the scan mirror is in its central position, the sensor's field of view is mid-way between the acquisition scan limits; that is, the local depression angle equals (26.65 + 13.65)/2 = 20.15 deg. Orthogonal projection views of IRLE are shown in Figure 2.2-4.

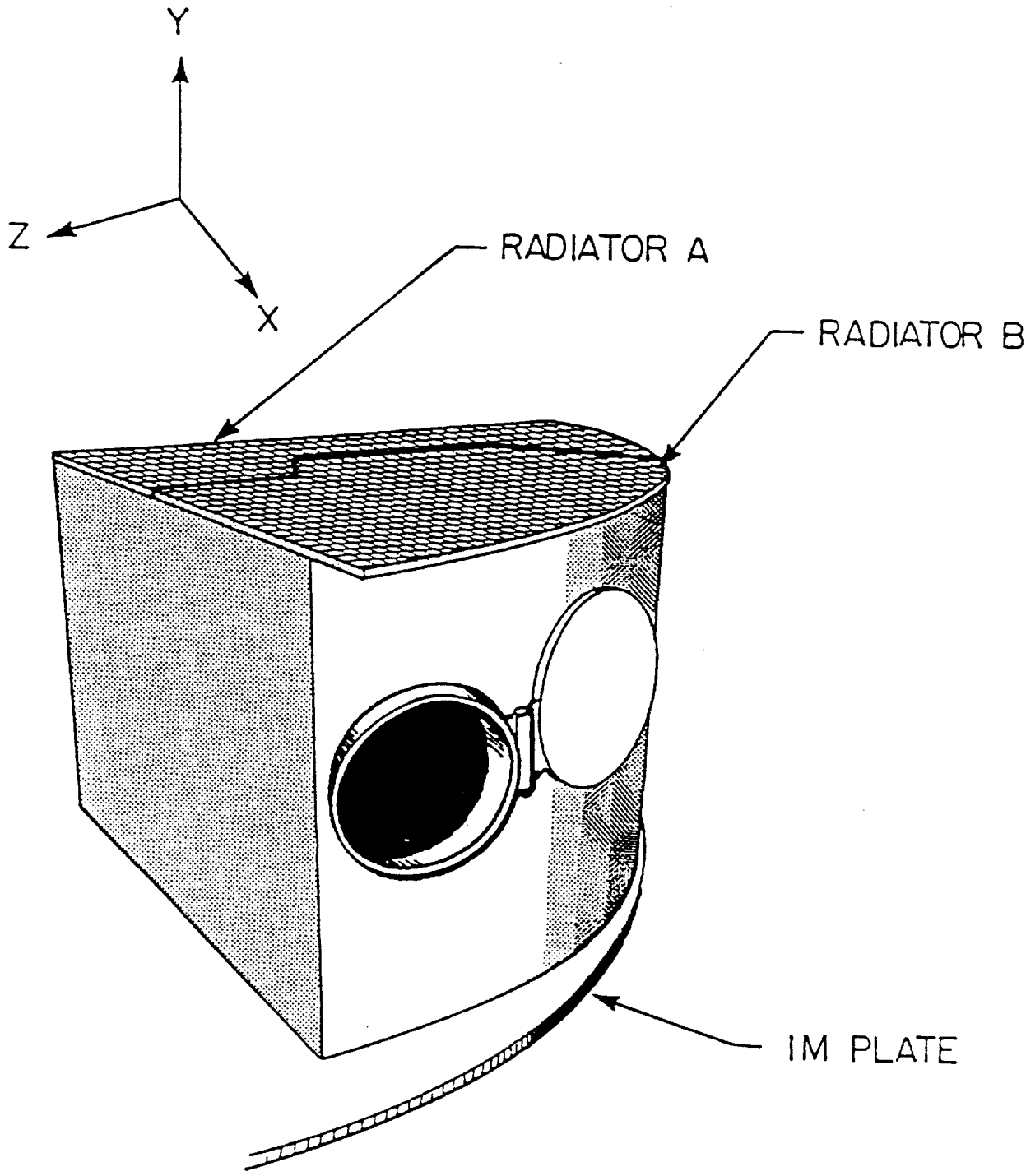

Figure 2.2-1. IRLE Instrument Perspective View

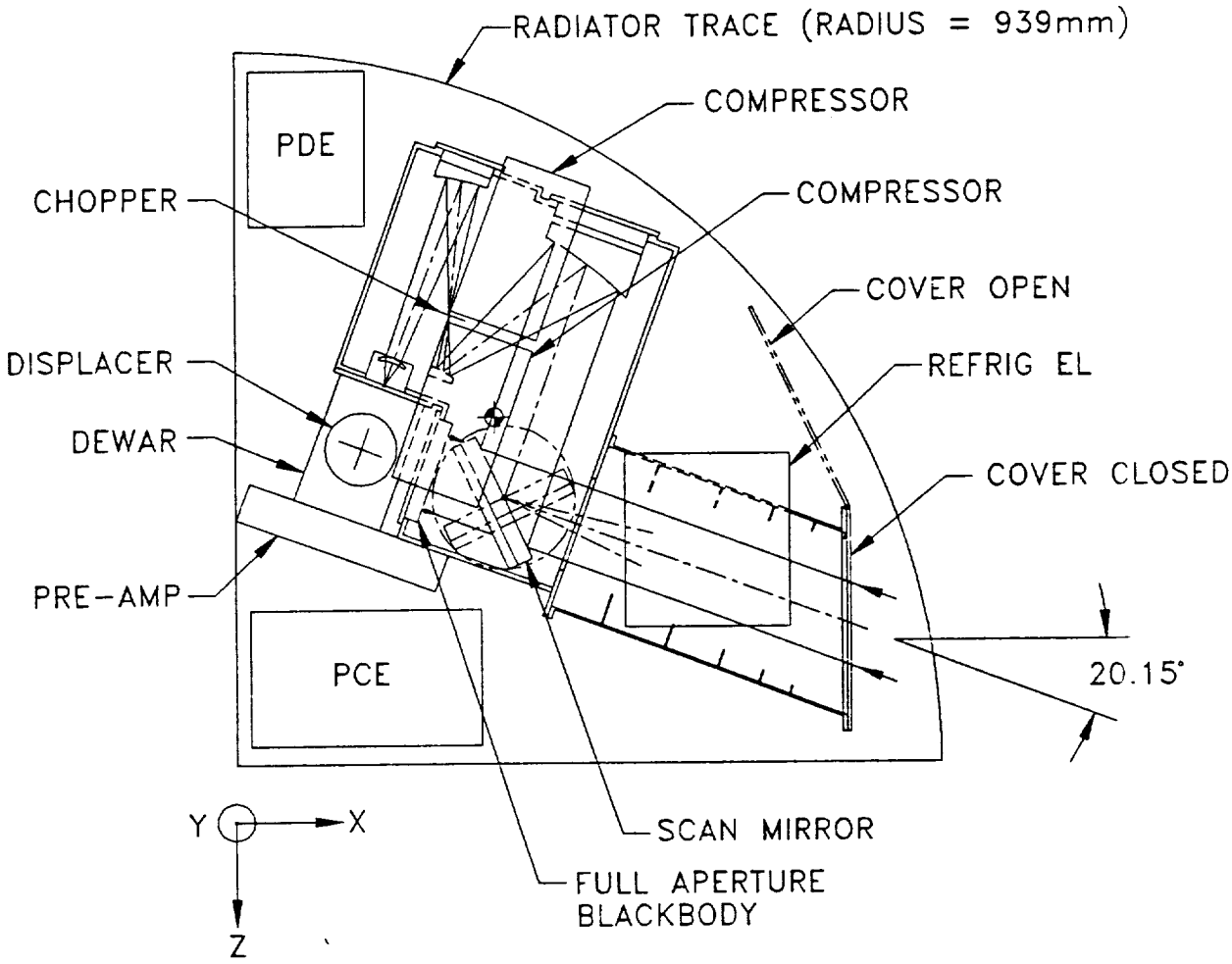

Figure 2.2-2. IRLE Instrument Side View

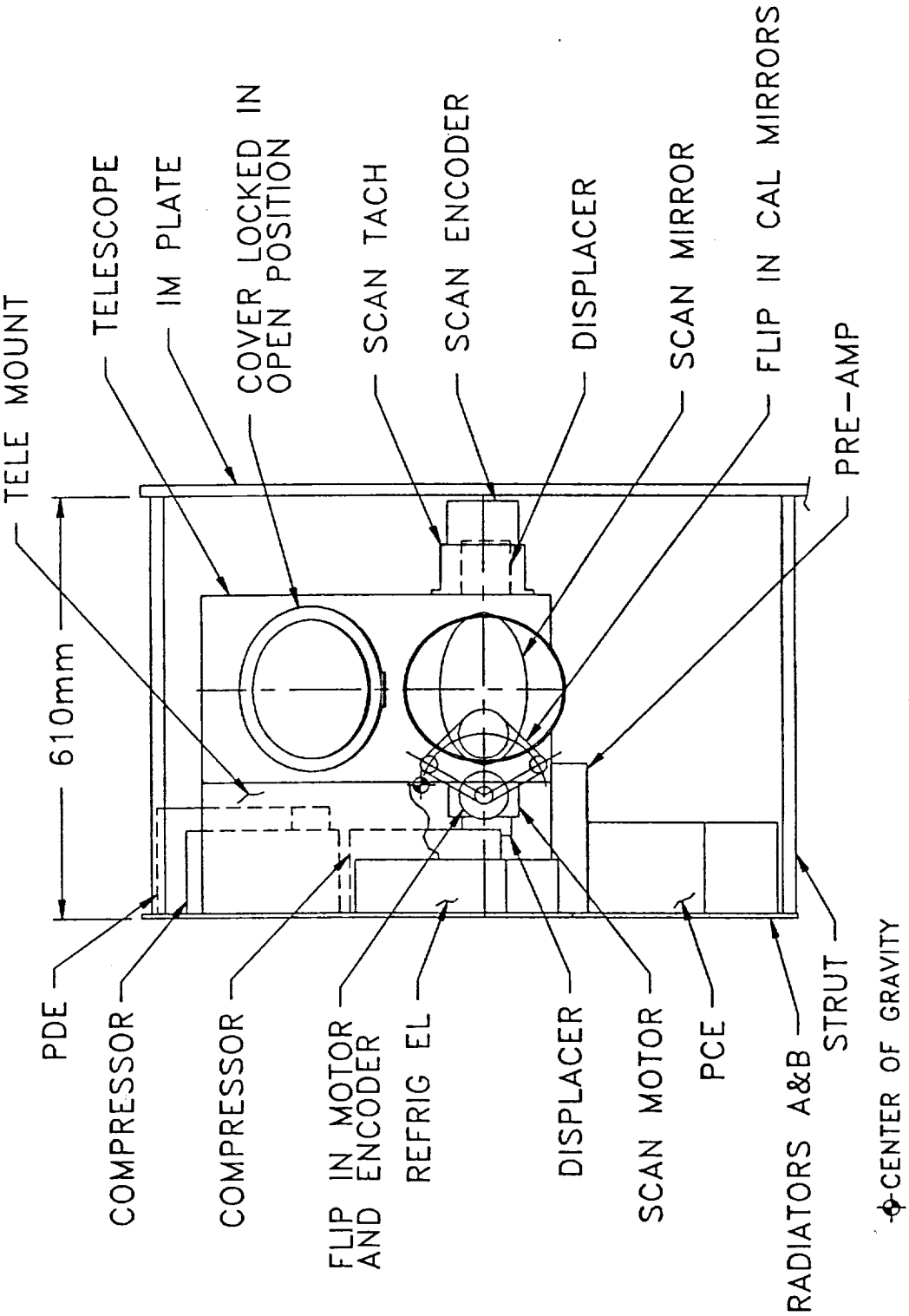

Figure 2.2-3. IRLE Instrument Front View

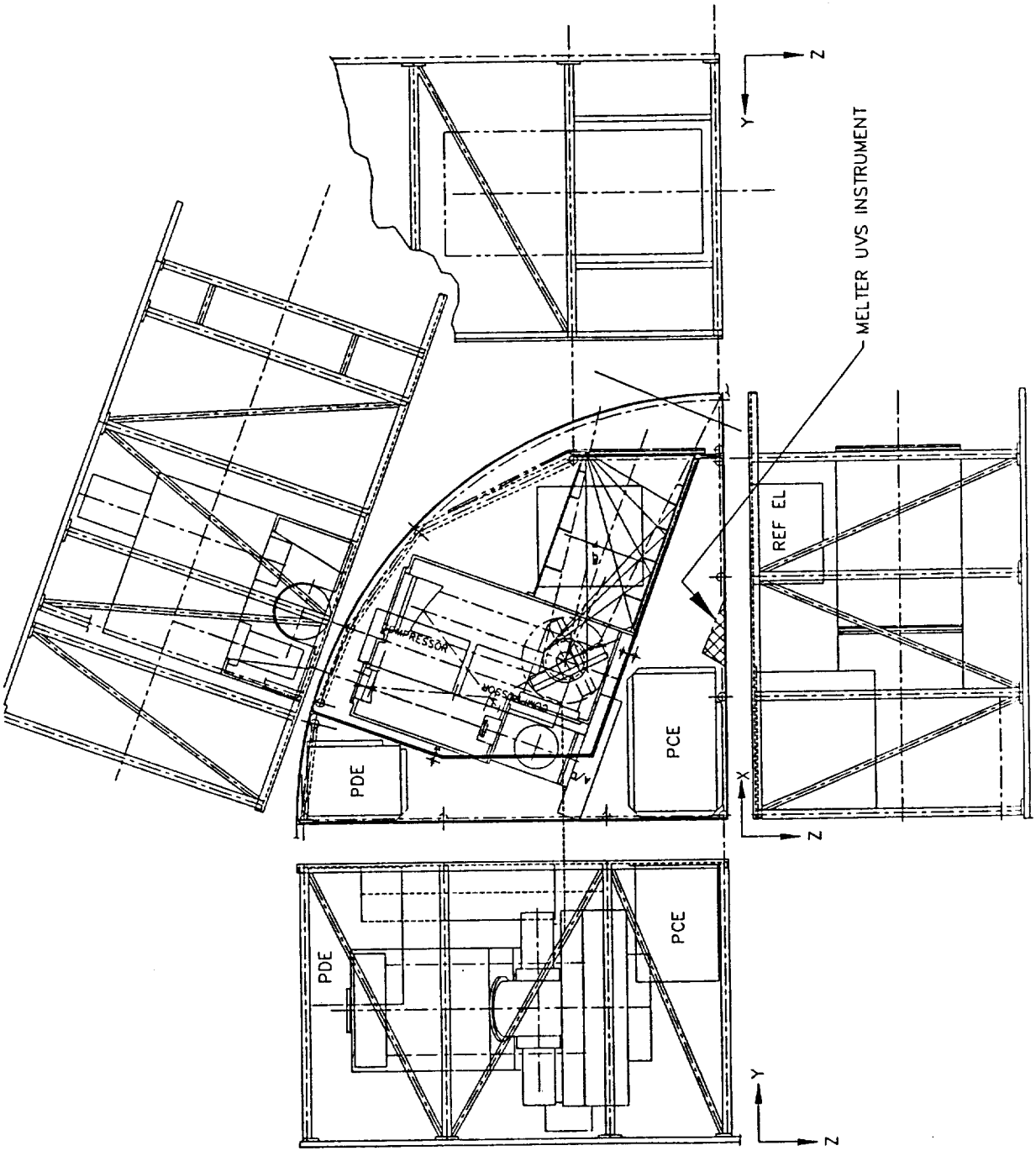

Figure 2.2-4. IRLE Instrument Orthogonal Projection Views

2.2.2 Subsystem Summaries

The IRLE instrument consists of the following subsystems: detectors, cryocooler, dewar, radiators, optics, chopper, electronics, scan mechanisms, in-flight calibration, and structure. Summary descriptions of the subsystems follow.

2.2.2.1 Detectors. The IRLE instrument has nine discrete detectors, seven HgCdTe and two InSb. The 75-Kelvin detector operating temperature is determined by the long wavelength CO_2 channels. Detectors are long lead items due to the special material that must be fabricated for long wavelength CO_2 detectors.

2.2.2.2 Cyrocooler. Two Stirling-cycle mechanical coolers, operating in opposition for momentum compensation, are used to cool the detector array. An in-progress life test of this type of mechanical cooler, which is built by British Aerospace, has now passed the 3-year mark with no degradation in cooling capacity. The compressor and the displacer of each cooler are split apart and connected with a flexible tube. The displacers are mounted directly to the detector dewar and connected to the compressors with a flexible tube. This approach minimizes the effects of compressor vibration. The heat sink thermal path for each displacer is symmetrical to ensure that both displacers operate at the same temperature, thus optimizing momentum compensation. The total thermal load on the cooler is 660 mW, and the two coolers together require a total of 44 W of input power to maintain the detector array at 75 Kelvin.

2.2.2.3 Detector Dewar. The detector dewar uses concentric fiberglass G-10 isolators to support the focal plane within an aluminum vacuum shell. The dewar window is a CdTe lens which is also part of the telescope. The dewar contains a detector cold shield that is also the aperture stop of the system. The cooler displacers are mounted directly to the dewar, and their cold stings are attached to the focal plane by thermal switches and a flexible strap. These switches make it possible to remove the thermal load of a malfunctioning cooler. One cooler has sufficient capacity to maintain the detectors at 77 Kelvin. The detector dewar's total heat load is 660 mW while the IRLE instrument is in operation.

2.2.2.4 Radiators. Two radiators are mounted in an antisolar position so that they are completely shaded from the sun by the spacecraft. One radiator, which dumps the 78 W from the coolers and telescope, has an area of 0.49 m_2 and operates near 264 Kelvin. The second radiator, which dumps the 45 W from the electronics, has an area of 0.20 m^2 and operates near 283 Kelvin.

2.2.2.5 Optics. The telescope is an off-axis, three mirror, one lens design. The lens also serves as the dewar window. The off-axis design maximizes the rejection of stray light so that IRLE can make accurate measurements at low tangent heights. This design minimizes background photon noise because the close proximity of the telescope aperture to the focal plane allows it to be placed inside the detector dewar.

2.2.2.6 Chopper. The chopper, a tuning-fork design built by Philamon, Inc., is the same type used on the Solar Mesospheric Explorer (SME). Multi-aperture shutters (or "picket-fence" shutters) will be used to maintain the amplitude of the chopper motion well under the long-life amplitude limit. The 700-Hz chopping frequency is determined by the 1/f noise of the HgCdTe detectors.

2.2.2.7 Electronics. Microprocessors are used extensively for both signal processing and control. Most of the microprocessors are the extremely low-power NSC 800, which with 2K of memory and a NSC 810 RAM-I/O-Timer, requires only 110 mW. This NSC combination is used in three areas: system control and data formatting, scan and flip-in mirror control, and signal processing. Digital filtering uses a high-speed, two-port RAM and the Texas Instruments TMS 320/20 microprocessor. These devices are higher power devices; the two-port RAM requires 1.6 W and the TMS 320/20 requires 1.3 W. A separate low-power, 16-bit, A/D (Crystal CZ5116) is used for each channel to maximize reliability. Each A/D requires only 250 mW. NASA's Synchronous Intelligent Report Terminal (SIRT) units will be used to put data on and get data off the spacecraft 1553 bus.

2.2.2.8 Scan Mechanism. The scan mechanism consists of a 17.6 cm by 22.0 cm flat beryllium mirror, a dc torque motor (Aeroflex model TQ34W-1), a tachometer (Aeroflex model TG34W-12), a shaft angle encoder (Itek RI 36K/40), and two greaseless BarTemp bearings. The scan mirror is made from beryllium to minimize the angular impulse when the mirror is moved rapidly.

2.2.2.9 In-Flight Calibration (IFC) System. The flip-in mirrors are off-axis parabolic mirrors. They are used with bending flats so that the small area blackbody source and the tungsten lamp will not obscure the optics. The flip-in mirrors are inserted by means of a mechanism that uses a MPC type 9-2D stepping motor and gear head, an Itek RI 1.0K/20 angular encoder, and a greaseless bearing. The full-aperture blackbody is 13 mm thick aluminum with hundreds of holes drilled on the emitting side. An array of platinum resistance thermometers (PRTs) will monitor temperature.

2.2.2.10 Structure. A carbon/graphite composite material will be used to produce an extremely lightweight structure while providing the required strength and thermal isolation. The structure is designed for a Delta II launch vehicle. The entire structure has a mass of 5.76 kg.

2.3 INSTRUMENT PARAMETERS

2.3.1 Science Measurement Parameters

The spectral passbands, emitting gas species, and sensitivity in terms of noise equivalent radiance (NEN) are tabulated in Table 2.3-1.

Table 2.3-1. Spectral Passbands, Gas Species, and NEN for Nine IRLE Channels

Channel	Gas Species	$\Delta\lambda$ 10^{-9} (μm)	NEN ($Wcm^{-2}sr^{-1}$)
1	CO_2 (N)	14.99-15.58	7.7
2	CO_2 (W)	13.70-16.53	12
3	CO_2 (W)	13.70-16.53	12
4	O_3	9.05-10.46	10
5	H_2O	6.52-7.15	7
6	NO_2	6.14-6.35	7
7	NO	5.12-5.60	7
8	CO_2 (4.3)	4.19-4.36	0.7
9	OH	1.5-1.8	0.3

Channels 2 and 3 have identical passbands, but they measure CO_2 at two different tangent heights. This information is used during data reduction to refine the estimate of the location in the earth limb that is actually being measured.

The instantaneous field of view (IFOV) of each detector is 2 km vertical by 28 km horizontal at the earth limb. Two measurements are taken per IFOV. The integration time per measurement is 0.083 seconds.

The modulation transfer function (MTF) of the IRLE instrument is given by

$$MTF_{Total} = MTF_{IFOV} \times MTF_{Telescope} \times MTF_{Int.\ Time}.$$

The instantaneous field-of-view modulation transfer function, which is determined by the detector size and the focal length, is given by

$$MTF_{IFOV} = Sinc(2.1435\ S_o),$$

where

S_o is the object spatial frequency in cy/km.

The integration time modulation transfer function, which describes the image smearing caused by a finite integration time and a finite scan rate, is given by

$$MTF_{Int.\ Time} = Sinc(1.072\ S_o),$$

where

S_o is again the spatial frequency of the object in cy/km.

These two functions and their products are plotted in Figure 2.3-1. The IRLE instrument is specified to collect data for spatial periods equal to or greater than 4 km. This point corresponds to a spatial frequency of 0.25 cy/km. The MTF is different for each channel due to geometrical aberrations in the telescope. For a spatial period of 4 km, it ranges form 0.82 to 0.97. Thus, the IRLE instrument MTF is dominated by the instantaneous field-of-view modulation transfer function, MTF_{IFOV}.

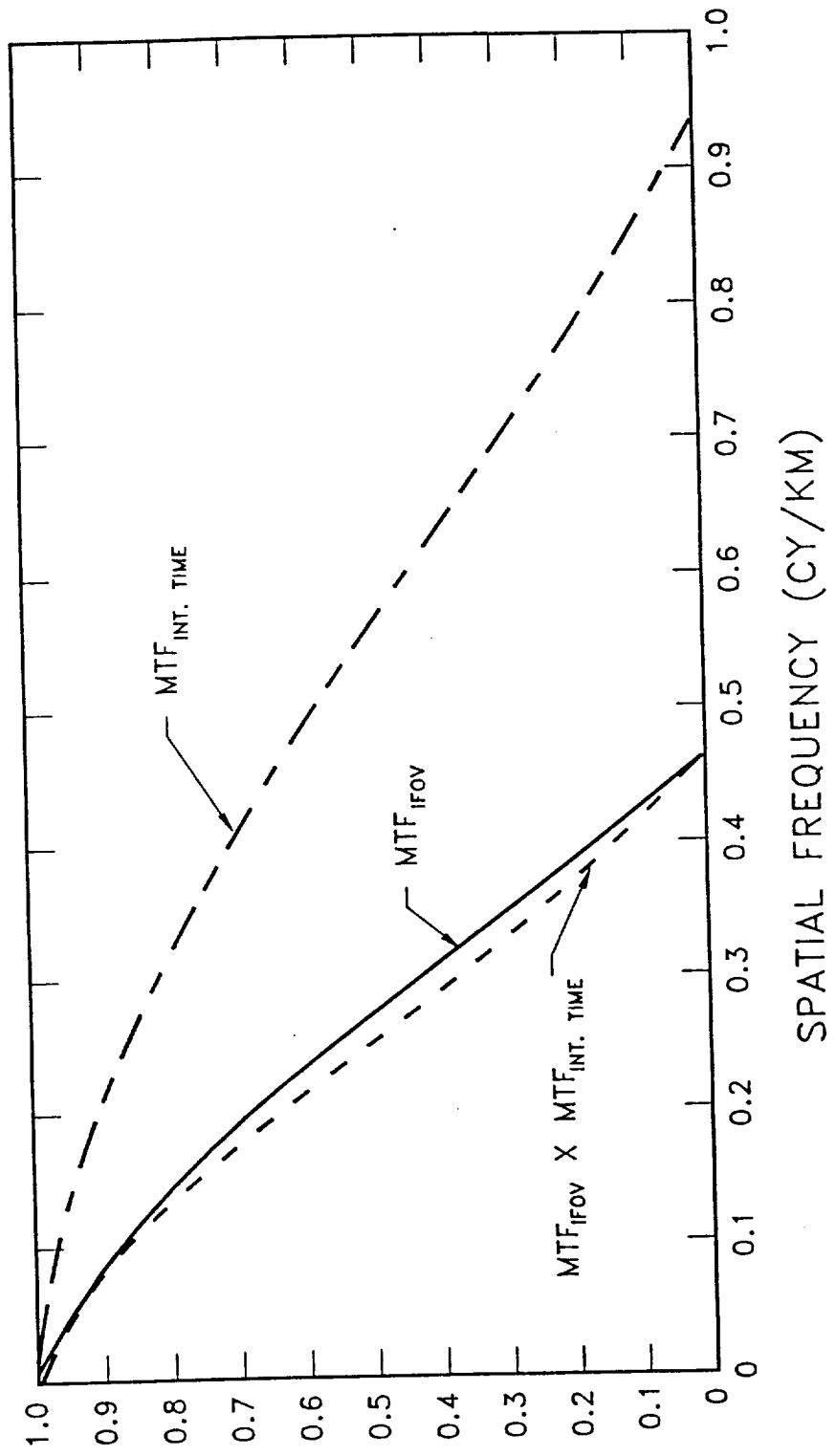

Figure 2.3-1. Instantaneous Field of View MTF and Integration Time MTF Plots

2.3.2 Instrument Package Dimensions

As shown in Figure 2.2-3, the IRLE package extends 610 mm above the instrument mounting (IM) plate. The IRLE package occupies one quadrant of the 0.939-m radius MELTER instrument plate, except for the small cross-hatched area shown in Figure 2.2-4. This area is reserved for penetration by the Ultraviolet Spectrometer (UVS), a University of Colorado instrument. The dimensions of this area are given in Figure 2.3-2.

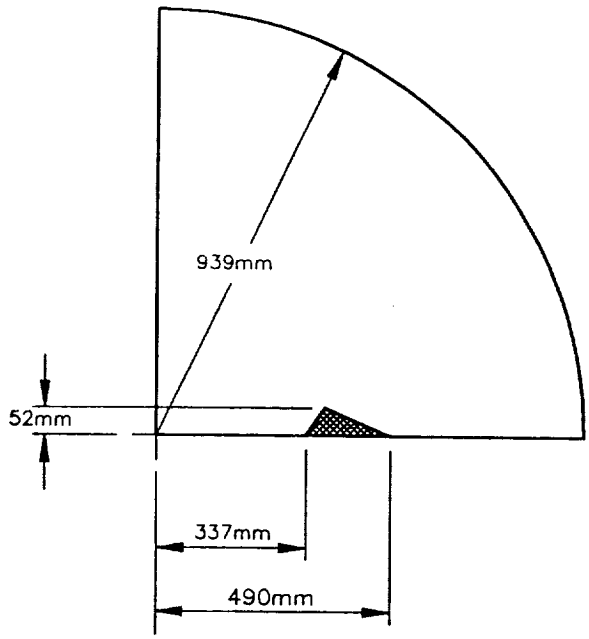

Figure 2.3-2. Projection of UVS Instrument Penetration into IRLE Quadrant

2.3.3 Mass

The total mass of the IRLE instrument is 71.6 kg. The center of mass location is identified in Figures 2.2-2 and 2.2-3. The mass of each major component and subassembly is tabulated in Table 2.3-2. The structure mass includes 4.5 kg for a telescope mount, 2.5 kg for the displacer mounts, and 3.0 kg for the compressor mounts. These mounts also function as thermal links.

Table 2.3-2. Mass of Major Components and Subassemblies

Item	Component (kg)	Assembly (kg)
Optics		17.5
Telescope	9.1	
Scan Mirror System	3.0	
IFC	3.2	
Chopper	0.2	
Baffle	2.0	
Contamination Cover	1.1	1.1
Cryogenics		11.0
Dewar	3.2	
Compressors (2)	6.0	
Displacers (2)	1.8	
Thermal Control		12.9
Radiators	12.2	
Thermal Links	0.7	
Electronics		15.5
PCE	4.25	
Preamplifiers	1.75	
PDE	5.0	
Cryocooler Electronics	4.5	
Structure	13.6	13.6
TOTAL	71.6	71.6

2.3.4 Power Requirements

The IRLE instrument power requirements for a detector temperature of 75 Kelvin are tabulated in Table 2.3-3. Decreasing the detector temperature to 70 Kelvin would require an additional 4 W of power for the compressors.

Table 2.3-3. IRLE Power Requirements

Major Element	Power (W) Average	Peak
Electronics, Motors, Tach, and Encoders:		
Preamps and A/Ds	8.3	17.0
Scan Control Unit (SCU)	6.0	12.0
Process Control Unit (PCU)	9.0	18.0
Scan Motor, Encoder, and Tach	5.3	10.0
Flip-In Motor and Scan Mirror Encoder	0.4	6.0
Chopper	0.8	2.0
Power Distribution Electronics	18.0	36.0
Calibration Sources	1.2	5.0
Refrigerator:		
Electronics	11.0	22.0
Compressors	42.0	178.0
Displacers	2.0	8.0
10% Margin	11.0	
TOTAL POWER + 10% Margin	115.0	*

* By sequential activation of subsystems, the peak power at start-up will be limited to 220 W.

2.3.5 Commands

The IRLE instrument uses three types of commands: (1) power commands, (2) discrete commands, and (3) serial commands. The power commands provide external power to the instrument in the proper sequence. Discrete commands allow direct manual control over basic instrument functions while the serial commands provide for instrumental calibration and operational verification.

2.3.5.1 Power Commands. The power commands are required to sequentially power the IRLE instrument so that the spacecraft peak power requirements are not exceeded. Once completely powered, the IRLE instrument will automatically enter the normal operational mode and begin making measurements. The power commands used for this purpose are:

1. Compressors/displacers ON
2. Compressors/displacers OFF
3. Calibration sources, chopper ON
4. Calibration sources, chopper OFF
5. Electronic power ON
6. Electronic power OFF

Power commands are also used to place the instrument in survival mode and to provide redundant cover. The power commands used for these purposes are:

7. Survival power ON
8. Survival power OFF
9. Redundant cover ON
10. Redundant cover OFF

There are a total of 10 power commands.

2.3.5.2 Discrete Commands. Discrete commands are designed to provide manual system control, bypassing the normal system control of the IRLE instrument. These commands allow manual scan operation of the instrument, initiate resets, and provide safety overrides. The discrete commands are not used during normal operation of the IRLE instrument.

The discrete scan commands allow the automatic system control over the scan mode to be replaced by one of three manual scan modes. Other system functions will remain unchanged. A discrete scan command is also provided to return the system to full automatic scan control.

The discrete scan commands are:

1. Start auto scan mode
2. Start acquisition (long) scan mode
3. Start adaptive (short) scan mode
4. Move to space calibrate position
5. Move to full-aperture calibrate position

The acquisition scan command initiates a repeated scan of the same length used for earth limb acquisition. Its length is based on preset limit switches. The adaptive or short scan command initiates a repeated short scan which is also based on preset limit switches. These short scan limit switches are preset for approximately 13.63 to 25.17 deg, which includes the most likely earth limb position of about 20.15 deg.

The space calibrate command causes the scan mirror to move to the space calibrate position (about 15.3 deg) and stop. The full-aperture calibrate command causes the scan mirror to move to the full-aperture calibrate position (about 110.15 deg) and stop.

Discrete reset commands allow individual sections of the IRLE system control to be reset manually without causing a system reset. A master system reset is also provided. The discrete reset commands are:

6. Master system reset
7. Sample control reset
8. Digital filter reset
9. Scan control reset
10. System control reset

The master system reset command causes a complete system restart, including reloading all microprocessor programs, a new calibration sequence, and a new earth limb acquisition. A downlink report is then made of the IRLE instrument status and data acquisition is resumed.

The subsystem reset commands cause a reload of the appropriate microprocessor program, a checkout sequence, and a downlink status report. Since the individual subsystems can operate independently, only the subsystem being reset is affected. The downlink IRLE instrument data, however, will be interrupted. A scan control reset command also initiates a new earth limb acquisition.

Safety overrides and contingency control are also provided by this set of commands. The discrete/contingency commands are:

11. Safety override #1
12. Safety override #2
13. Safety override #3
14. Contingent #1
15. Contingent #2
16. Contingent #3

The scan control discrete commands remove all digital control over the scan electronics and substitute a fixed analog control. The reset discrete commands are implemented through the appropriate microprocessor reset inputs. There are a total of 16 discrete commands.

2.3.5.3 Serial Commands. The serial commands provide the normal method of exceptional IRLE instrument operation. These commands are used only occasionally for adjusting instrument parameters and for verification of instrument operation. Each of the serial commands is 32 bits long including appropriate system parameters and timing information.

Scan control serial commands 1 through 5 implement the same functions as the discrete scan control commands. The primary difference is that the serial command functions are implemented under control of the appropriate microprocessor. The short scan limits can be set by the short scan serial command. Scan status is reported through the housekeeping channels.

1. Start auto scan mode
2. Start acquisition (long) scan
3. Start adaptive (short) scan
4. Move to space calibrate position
5. Move to full-aperture calibrate position

Calibration control serial commands 6 through 13 provide individual control of the calibration mirrors, preamplifier calibration, and A/D calibration. These commands contain imbedded bits to override normal system control of the functions. Status is reported through the housekeeping channels.

6. IFC mirror #1 IN
7. IFC mirror #1 OUT
8. IFC mirror #2 IN
9. IFC mirror #2 OUT
10. IFC mirror #3 IN
11. IFC mirror #3 OUT
12. Preamp & A/D calibrate ON
13. Preamp & A/D calibrate OFF

Verification and calibration serial commands 14 through 24 provide individual control over the indicated function. These commands contain imbedded bits to override normal system control of the functions. Status is reported through the housekeeping system.

14. Compressor/displacer #1 ON
15. Compressor/displacer #1 OFF
16. Compressor/displacer #2 ON
17. Compressor/displacer #2 OFF
18. Flip-in BB ON
19. Flip-in BB OFF
20. Flip-in tungsten lamp ON
21. Flip-in tungsten lamp OFF
22. Full-aperture BB ON
23. Full-aperture BB OFF
24. Special header

There are a total of 24 32-bit serial commands.

The IRLE instrument has a command uplink capacity of 48 commands per orbit which corresponds to 192 bytes per orbit. The serial command structure is capable of uploading IRLE instrument parameters or programs. For example, six orbits allow an 1152-byte program to be uploaded.

2.3.6 Summary of IRLE Instrument Parameters

The IRLE instrument parameters are summarized in Table 2-3-4.

Table 2.3-4. Summary of IRLE Instrument Parameters

Name	Infrared Limb Experiment
Heritage	Nimbus 6 & 7 (LIMS,LRIR), UARS (ISAMS)
Atmospheric Region	Forward limb
Geophysical Features	Temperature, O_3, NO, NO_2, H_2O, OH, NLTE
Wavelength	1.5 to 17.0 μm
Resolution	.180 to 2.4 μm
Etendue	1.2 x 10^{-3} cm^2ster
Instrument FOV (vertical & horizontal)	0.04 x 0.57 deg (2 x 28 km)
Pointing	110-deg Zenith angle, in orbit plane
Avoidance	35 deg vertical, 25 deg horizontal (1/2 angle)
Scan Range	4.6 deg (225 km) adaptive mode; 13 deg (635 km) acquisition mode
Scan Time	18.4 sec
Detector	HgCdTe & InSb
Detector T	75 ± 5 K
Sensor Operating Temp.	280 ± 10 K
Refrig. Operating Temp.	280 ± 10 K
Other Elec. Operating Temp.	293 ± 20 K
Mass	72 kg
Power	115 W (including 10% margin)
Integration Time	0.083 sec
Bits per Word	16
No. of Data Channels	9
Data Rate	2528 b/s
Duty Cycle	100%
Data Storage	37.9 Mbytes/day

2.4 CONTAMINATION

The ability of the IRLE instrument to reject radiation outside the field of view depends on keeping the optics free of contamination. The critical optical elements are those that precede the chopper, the scan mirror, the primary mirror, and the secondary mirror. IRLE will be assembled, aligned, and tested under Class 100 clean room conditions. A contamination door is provided to seal the optical cavity when the instrument is not in test or deployed in space. Whenever the assembled instrument is not under Class 1000 or better clean room environment, the instrument will be bagged and sealed under a dry nitrogen purge.

Only proven low-outgassing material will be used in the IRLE instrument. The scan drive and flip-in mechanism will use low-outgassing lubricants and will be designed in accordance with practices successfully employed on previous missions. The refrigerator components are hermetically sealed units with low-outgassing material. The contamination door uses a double-sealed ordnance mechanism which has been extensively tested and has demonstrated no observable contamination.

2.5 RADIOMETRY

2.5.1 Noise Equivalent Radiance

The noise equivalent radiance (NEN) is given by

$$NEN = \frac{(A_d \, \Delta f)^{1/2}}{\eta_o \, \eta_c \, A \, \Omega \, D^*}$$

where

A_d = area of detector = (0.03cm)(0.2cm) = 6.00×10^{-3} cm^2 †

† The .03 cm detector width is larger than the .015 cm detector field stop width to allow for fabrication tolerances and a space between the front surface of the detector and the detector field stop. This space is required to accommodate stress-relief loops in the wires coming off the front surface of the detector. Using the full detector width in the NEN calculation is slightly pessimistic because the detector field stop is cold so that the area of the collecting background photons is nearly equal to the area of the detector field stop.

Δf = noise equivalent electrical bandwidth = 1.85 Hz †

η_o = optical efficiency = $(\rho_{mirror})^4(\rho_{lens})^2(\tau_{filter})$
$= (0.98)^4(0.88)^2(0.70) = 0.50$

η_c = chopper efficiency = 0.29 (assuming triangular wave form)

A = Area of elliptical entrance aperture
$= \pi$ (10cm/2) (20cm/2) = 157 cm^2

Ω = Field-of-view solid angle = (0.75 mrad)(10 mrad)
$= 7.50 \times 10^{-6}$ sr

D^* = Average dee-star over the spectral band of each channel with a 300-Kelvin background temperature, a 75-Kelvin detector temperature, and a cold filtered detector with an f/1 optical cone.

$$NEN = \frac{[(6.0\times10^{-3})(1.85)]^{1/2}}{(0.50)(0.29)(157)(7.50\times10^{-6})D^*}$$

$$= \frac{617}{D^*} \quad \left[\frac{W}{cm^2\ sr} \right]$$

---

† Noise equivalent bandwidth was computed as follows:

Time per scan = 4.6 deg/0.25 deg per sec
= 18.4 sec/scan.

Number of resolution elements =
4.6 deg/{(57.3 deg/rad)$(0.75\times10^{-3}$ rad)}
= 107 elements.

Integration time =
(18.4 sec/scan)/{(2 samples/element)(107 elements)}
= 86 msec.

Since the system rise time is set equal to the integration time,
$f_{3dB} = 1/(2\pi\ 86\times10^{-3}) = 1.85$ Hz.
For the many-pole digital filter, $\Delta f \approx f_{3dB} = 1.85$ Hz.

NEN values for each channel computed, using this equation and state-of-the-art D^* values, are tabulated in Table 2.5-1. EG&G Judson provided the D^* values for the photoconductive HgCdTe detectors of channels 1 through 7, while Cincinnati Electronics provided the D^* values for the InSb detectors of channels 8 and 9. These D^* values include preamplifier noise, feedback resistor noise, and photon noise from a 300-Kelvin background cold filtered detector to f/1 with the detector at 75 Kelvin. As discussed in the detector module section of this report, the D^* values for channels 1 through 4 may be slightly optimistic for a 75-Kelvin detector temperature. For these channels, it would be advantageous to operate the detectors at 65 Kelvin.

Table 2.5-1. NEN Values Computed from D^* Values

Channel	$\Delta\lambda$ (μm)	D^* 10^{10} ($cmHz^{1/2}W^{-1}$)	NEN 10^{-9} ($Wcm^{-2}sr^{-1}$)
1. CO_2 (N)	14.99-15.58	8	7.7
2. CO_2 (W)	13.70-16.53	5	12
3. CO_2 (W)	13.70-16.53	5	12
4. O_3	9.05-10.46	6	10
5. H_2O	6.52-7.15	9	7
6. NO_2	6.14-6.35	9	7
7. NO	5.12-5.60	9	7
8. CO_2 (4.3)	4.19-4.36	84	0.7
9. OH	1.5-1.8	200	0.3

The effective NEN value for the wideband CO_2 channels, channels 2 and 3, must be made slightly larger than the NEN value computed from D^* in order prevent saturation when measuring the maximum expected signal. The IRLE digital data system has 16 bits, so the maximum signal that can be measured is 2^{16} times the level of the least significant bit (LSB). The maximum expected signal levels and 2^{16}NEN for each channel (based on data obtained on the SPIRE and LIMS programs) are tabulated in Table 2.5-2. For the two wideband CO_2 channels, the maximum signal is greater than 2^{16}NEN. Therefore, for these two channels the LSB must be set to a level greater than NEN to prevent saturation. The signal level at which the LSB is set is defined as NEN_{sys}. Values for NEN_{sys} are also tabulated in Table 2.5-2. NEN_{sys} is set equal to NEN for all channels except channels 2 and 3.

Table 2.5-2. NEN_{sys} Values Dictated by Dynamic Range Requirements

Channel	$2^{16}NEN$ 10^{-6} ($Wcm^{-2}sr^{-1}$)	Signal Max 10^{-6} ($Wcm^{-2}sr^{-1}$)	NEN_{sys} 10^{-9} ($Wcm^{-2}sr^{-1}$)
1. CO_2 (N)	505	250	7.7
2. CO_2 (W)	786	1000	18
3. CO_2 (W)	786	1000	18
4. O_3	655	400	10
5. H_2O	459	7	7
6. NO_2	459	2	7
7. NO	459	0.2	7
8. CO_2 (4.3)	46	2	0.7
9. OH	20	0.1	0.3

2.5.2 Internal Flight Calibrator Radiance Levels

Four internal flight calibration sources are provided: a full-aperture 305-Kelvin full-aperture blackbody and three flip-in mirror calibrators. One of the flip-in mirrors fills 25 percent of the IRLE entrance aperture, while the other two mirrors fill 3 percent of the IRLE aperture. A 315-Kelvin source is collimated by both a 25- and a 3-percent-area mirror. The second 3-percent-area mirror is used to collimate a 600-Kelvin source that is used to calibrate the OH channel. The radiance levels of the full-aperture calibration source and the 315-Kelvin 25-percent-area flip-in mirror calibration sources are compared to the saturation levels of each channel in Table 2.5-3.

The full-aperture calibration source provides near full-scale calibration points for channels 1, 6, 7, and 8. The 315-Kelvin 25-percent-area calibration source provides near full-scale calibration points for channels 2, 3, 4, and 5. The 315-Kelvin 3-percent-area source provides calibration points for channels 1 through 8 that ranged from 1/15 (channel 4) to 1/114 (channel 6) of full scale. The 600-Kelvin 3-percent-area calibration source provides the OH channel a radiance of 4×10^{-6} $W/cm^{-2}/sr$ in the passband of the OH channel; that is, it provides the OH channel with a calibration point at one-fifth of full scale.

Table 2.5-3. Radiance Level Comparisons of 305-Kelvin Full-Aperture Calibrator and 315-Kelvin 25-percent-Aperture Calibrator to Sensor Saturation Level

Channel	Saturation Level 10^{-6} ($Wcm^{-2}sr^{-1}$)	25% Aperture Cal Source 10^{-6} ($Wcm^{-2}sr^{-1}$)	Full-Aperture Cal Source 10^{-6} ($Wcm^{-2}sr^{-1}$)
1. CO_2 (N)	505	112	403
2. CO_2 (W)	1180	550	1980
3. CO_2 (W)	1180	550	1980
4. O_3	655	443	1520
5. H_2O	459	158	506
6. NO_2	459	44	138
7. NO	459	64	195
8. CO_2 (4.3)	46	8	23
9. OH	20	-	-

2.5.3 Chopped Background

The magnitude of the chopped background radiance is given approximately by

$$N_{background} = 2 \epsilon N_{blackbody}$$

where

ϵ = mirror emissivity ≈ 0.02

$N_{blackbody}$ = radiance of a blackbody at the temperature of the mirrors.

This equation follows from the fact that there are three mirrors in front of the chopper and the emissivity of the backside of the chopper equals that of the mirrors. The chopped radiance computed from this equation with an optics temperature of 290 Kelvin is tabulated for each channel in Table 2.5-4.

Table 2.5-4. Chopped Radiance with 290 K Optics

Channel	Chopped Radiance 10^{-6} ($Wcm^{-2}sr^{-1}$)
1. CO_2 (N)	14
2. CO_2 (W)	67
3. CO_2 (W)	67
4. O_3	47
5. H_2O	26
6. NO_2	4
7. NO	5
8. CO_2 (4.3)	0.5
9. OH	-

3. IRLE MODULE DESCRIPTIONS

3.1 OPTICS MODULE

The optical module consists of the telescope, scan mirror assembly, flip-in mirror assembly, chopper, and full-aperture blackbody calibration source.

3.1.1 Telescope

3.1.1.1 Optics

3.1.1.1.1 Optical System Design. The optical system, which was designed by Don Robinson of NASA Langley, is shown schematically in Figure 3.1-1. It is an unobscured, off-axis, reimaging, three-mirror, one-lens design. There are actually four mirrors in the telescope, but only three mirrors have power. The fourth mirror is the external scanning mirror. The field stop and chopper are located at the first focal plane, which is formed by the primary and secondary mirrors. This focal plane is reimaged at the detector array by the tertiary mirror and the lens. Reimager designs reduce stray light because they block all stray light that cannot pass through the first field stop. The system aperture stop and the filters are located inside the dewar. The aperture stop also functions as the optical cold shield resulting in the minimum possible background flux.

The off-axis design was selected because it permits orders of magnitude better rejection of off-axis radiance than on-axis designs. When making earth limb measurements, the earth is a very bright source, just outside the field of view, that must be rejected. In addition, an off-axis design can be calibrated with greater assurance because there is no central obscuration. However, off-axis designs do require more space and are therefore heavier.

The optical prescription is tabulated in Table 3.1-1 in Super-Oslo format. The thickness of each filter has been selected such that all channels focus at the same detector plane. The filter thickness for each channel and the substrate material from which it is made are tabulated in Table 3.1-2.

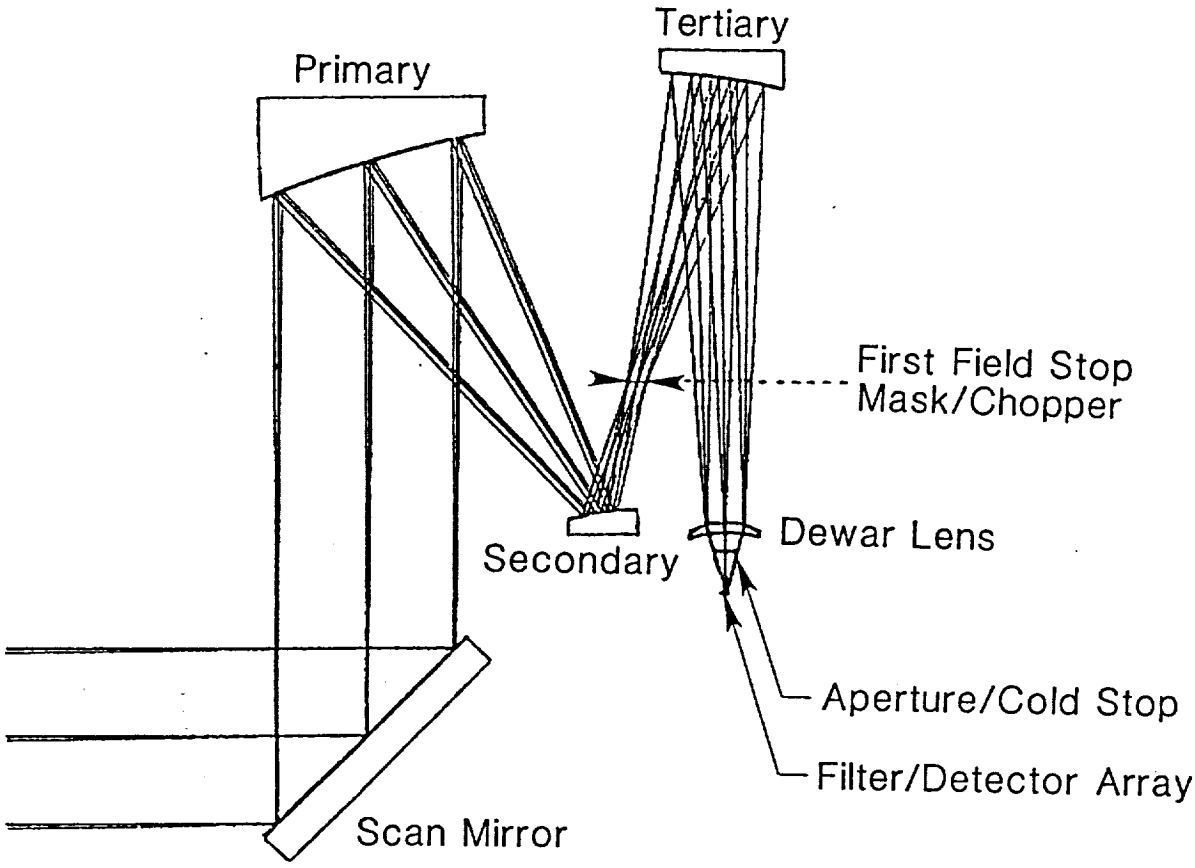

Figure 3.1-1. IRLE Instrument Optical Layout

Table 3.1-1. Optical Prescription

SRF	Radius		Thickness		Aperture		Glass	
1	---	S	2.37548E-13		50.000000	S	Air	
2	---		---		80.000000		Reflect	*
3	---		-350.000000		50.000000	S	Air	*
4	500.000000		220.000000		225.000000		Reflect	*
5	102.857143	S	-71.400000		50.000000		Reflect	*
6	---		-175.000000		4.931974	S	Air	*
7	282.685930	V	---		75.000000		Reflect	*
8	---		253.674789	V	26.131297	S	Air	*
9	---		---		10.107108	S	Air	*
10	---		---		10.107108	S	Air	*
11	34.030683	V	6.000000		20.000000		IRTR6	
12	56.688365	S	6.174889	S	20.000000	P	Air	
13	---		---		6.928778	A	ASTOP	
14	---		25.687500	V	6.928778	S	Air	**
15	---		1.200000	P	2.022288	S	Silica C	**
16	---		0.100000		1.863598	S	Air	
17	---		---		1.844498	S	Air	

* Special and aspheric data:

2	DT	1.000000	TLA	-45.000000				
3	DT	1.000000	TLA	-45.000000				
4	CC	-1.061490	DCY	150.000000				
5	CC	-8.802334	DCY	-0.054238				
6	DCY	0.054238						
7	CVX	0.003617	CC	0.123044	DT	1.000000	DCY	5.431950
7	TLA	1.100761						
8	DT	-1.000000	DCY	-5.431950	TLA	-1.100761		
9	DT	1.000000	TLA	0.388181				
10	DCY	50.000000						

** These values are for OH channels. The thickness of each filter is adjusted so that all channels have a common focal plane.

Table 3.1-2. IRLE Filter Thicknesses and Substrate Materials

Channel	Thickness (mm)	Substrate Material
1. CO_2 (N)	0.6375	Germanium
2. CO_2 (W)	0.6375	Germanium
3. CO_2 (W)	0.7575	Germanium
4. O_3	0.5662	Germanium
5. H_2O	0.7475	Germanium
6. NO_2	0.7718	Germanium
7. NO	0.9375	ZnSe or Ge
8. CO_2 (4.3)	1.0875	Sapphire
9. OH	1.2000	Fused Silica

3.1.1.1.2 Optical Fabrication. All mirrors that precede the chopper (the scan mirror, primary mirror, and secondary mirror) are superpolished and maintained contamination-free. Light scattered from these mirrors into the system will be chopped in the same manner as signals. During limb measurements, the brightness of the earth directly illuminates the scan mirror and can partially illuminate the other two mirrors. Therefore, the fraction of light scattered by these mirrors must be very small, hence they must be superpolished. Superpolishing is done on electroless nickel that covers the mirror substrates. Electrolytic gold, which is more rugged than vacuum-deposited gold and can be cleaned without damage, is applied after superpolishing. The substrates for all mirrors, except the scan mirror, are aluminum. The scan mirror is made of beryllium to provide the necessary low mass for rapid movement. The lens is made of CdTe to provide the flat spectral transmission across the 1 to 18 μm wavelength band.

3.1.1.1.3 First Order Parameters. The system focal length is 200 mm and the entrance aperture is elliptical with a minor diameter of 100 mm and a major diameter of 200 mm. The minor diameter is in the plane of Figure 3.1-1. These and other first-order telescope parameters are tabulated in Table 3.1-3.

Table 3.1-3. Telescope First-Order Parameters

System Focal Length: 200 mm
System Aperture: 100 x 200 mm ellipse
Aperture Collecting Area: 157 cm^2
Effective Circular Aperture Diameter: 141 mm
Focal Length at First Field Stop: 600 mm
Focal Length at Detector: 200 mm
Demagnification from Field Stop to Detector Array: 3X
Wavelength Range: 1.5 to 18 μm

3.1.1.1.4 Image Quality. The geometrical spot size, geometrical image of a point source, and Airy disk size (the central lobe of the diffraction pattern of an aberration-free optical system) for the nine channels are given in Table 3.1-4. The table indicates that the IRLE instrument in the Y direction is diffraction limited for channels 1 through 4 and nearly diffraction limited for channels 5 through 9.

Since the narrow dimension of the detector, 0.15 mm, is in the Y direction, imaging quality in the Y direction is more important than in the X direction. The detector width is at least five times greater than the spot in the Y direction for all nine channels.

Table 3.1-4. Geometrical and Diffraction-Limited Spot Sizes

Channel	GEOMETRICAL SPOT		DIFFRACTION-LIMITED SPOT	
	RMS Y RADIUS (mm)	RMS X RADIUS (mm)	Y RADIUS (mm)	X RADIUS (mm)
1. CO_2(N)	0.020	0.032	0.037	0.019
2. CO_2(W)	0.020	0.032	0.037	0.019
3. CO_2(W)	0.020	0.032	0.037	0.019
4. O_3	0.016	0.037	0.024	0.012
5. H_2O	0.027	0.035	0.017	0.008
6. NO_2	0.027	0.033	0.015	0.008
7. NO	0.019	0.031	0.013	0.007
8. CO_2(4.3)	0.015	0.037	0.010	0.005
9. OH	0.011	0.010	0.004	0.002

The effect of the telescope on system performance is best described by the modulation transfer function (MTF). The telescope MTF for each of the nine IRLE channels at an object spatial frequency of 0.25 cy/km, a period of 4 km, is tabulated in Table 3.1-5. IRLE is specified to provide data for spatial periods equal to or greater than 4 km. These telescope MTF values are dominated by the instantaneous field of view MTF values shown if Figure 2.3-1.

Table 3.1-5. Telescope MTF at Object Spatial Frequency of 0.25 cy/km (4-km Spatial Period)

Channel	MTF
1. CO_2 (N)	0.82
2. CO_2 (W)	0.83
3. CO_2 (W)	0.83
4. O_3	0.91
5. H_2O	0.83
6. NO_2	0.83
7. NO	0.92
8. CO_2 (4.3)	0.95
9. OH	0.97

3.1.1.1.5 Stray Light Performance. When the spacecraft is oriented correctly, no direct rays from the sun can enter the telescope aperture because the IRLE instrument is completely shaded by the spacecraft. In addition, no sun-illuminated satellite surfaces are in view of the telescope aperture. As described in the following paragraphs, reflected sunlight from the earth in IRLE's passbands is much less than the thermal radiance from the earth. Therefore, the major stray light challenge for IRLE is to reject thermal radiation from the earth. That is, IRLE must reject a very bright earth just outside its field of view. When IRLE is looking at a tangent height of 40 km, the earth is only 0.8 deg off axis.

Estimates of the nonrejected earth radiance (NRER) versus tangent height in the 8 to 14 μm spectral band for both on- and off-axis reimager telescope designs are given in Figure 3.1-2. These estimates assume that the earth has a temperature of 280 Kelvin and an emissivity of 0.8. Estimates are given for both pristine clean mirrors (BRDF equals 1E-4 at 1 deg) and mirrors at the expected operational cleanliness level (BRDF equals 1E-3 at 1 deg).

These NRER estimates were prepared by Sensor Systems Group, Inc. (SSG) using a mathematical model proposed by Jerome M. Dowling of The Aerospace Corporation. SSG has demonstrated, by the construction and testing of many low-scatter telescopes, that this modeling technique gives accurate results when the foreoptics are directly illuminated by the earth as they are for IRLE. For this situation, the scattering from a properly defined baffle is much less than the scattering from the directly illuminated foreoptics; that is, NRER is dominated by the BRDF of the foreoptics and not by the baffle. Robert Breault of Breault Research Organization has also confirmed that when the foreoptics of a telescope are directly illuminated and the baffle is properly designed, scattering is determined by the BRDF of the foreoptics and not by the baffle.

NRER is a function of the IRLE channel because the earth emits a different amount of radiance in each channel passband. The ratio of the NRER for each channel to the NRER of the 8 to 14 μm spectral band equals the ratio of the earth radiance in that channel to the earth radiance in the 8 to 14 μm spectral band. These ratios are tabulated in Table 3.1-6. The NRER for each channel can be determined by multiplying the curves in Figure 3.1-2 by the ratios given in Table 3.1-6. For example, the NRER radiance of channel 4 at a tangent height of 100 km with an on-axis reimaging telescope with a BRDF of 10^{-3} is

$$(3 \times 10^{-8})(3 \times 10^{-1}) = 9 \times 10^{-9}\ \mathrm{Wcm^{-2}sr^{-1}}.$$

This NRER radiance value is nearly equal to the NEN of channel 4; therefore, there is no design margin for these conditions. The NRER at lower tangent heights is much greater than NEN, but the expected O_3 emission is also greater.

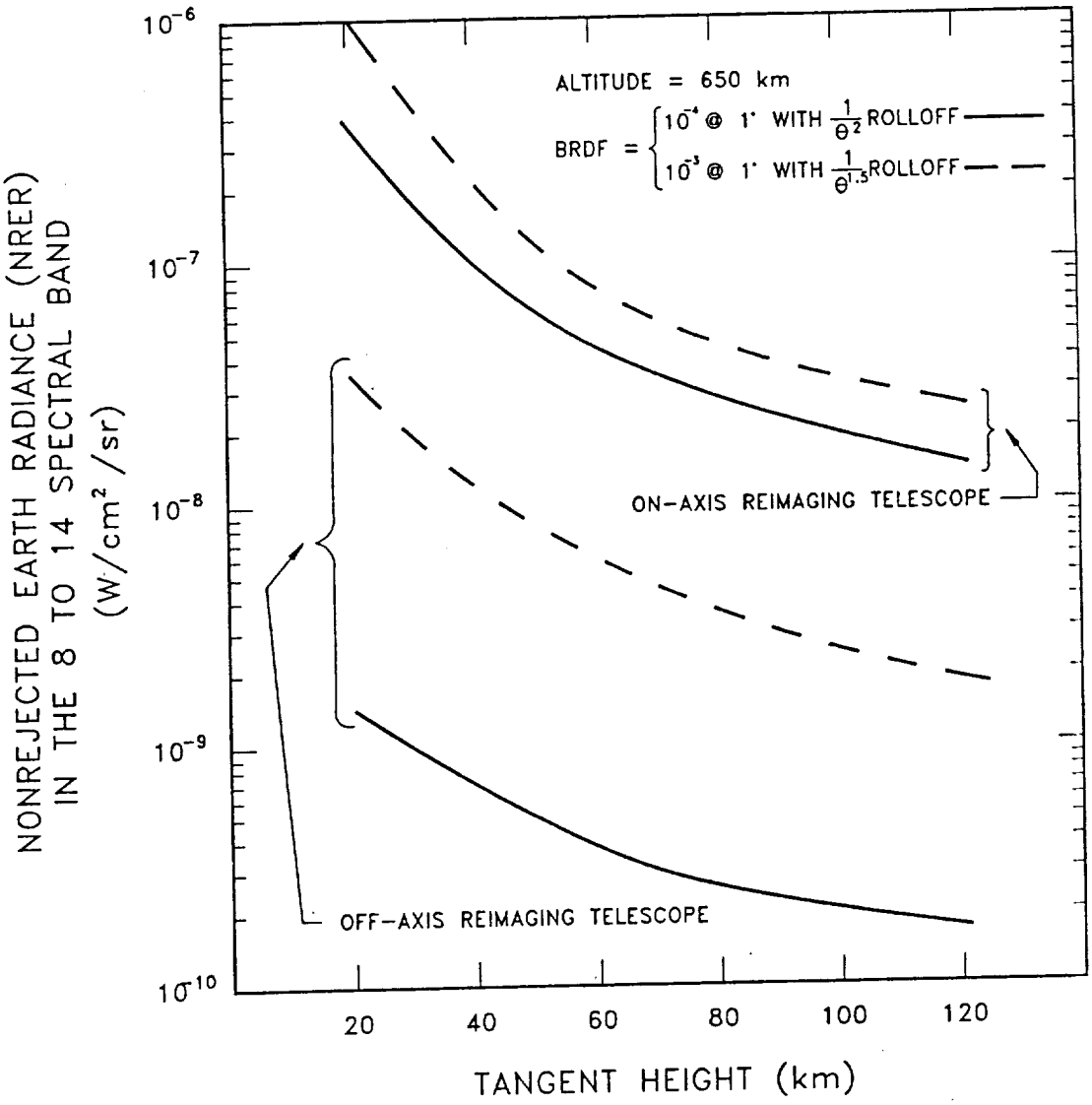

Figure 3.1-2. NRER Comparison of On-Axis and Off-Axis Telescopes

Table 3.1-6. Ratio of NRER in Each Channel to NRER in 8- to 14-μm Spectral Band

Channel	Ratio
1. CO_2 (N)	8×10^{-2}
2. CO_2 (W)	4×10^{-1}
3. CO_2 (W)	4×10^{-1}
4. O_3	3×10^{-1}
5. H_2O	7×10^{-2}
6. NO_2	2×10^{-2}
7. NO	2×10^{-2}
8. CO_2 (4.3)	2×10^{-3}
9. OH	1×10^{-10}

In addition to thermal radiation from the earth, the telescope must reject sunlight reflected from the earth. The ratio of the sunlight radiance in each channel passband that is reflected from the earth, assuming a reflection coefficient of 0.3, to the thermal radiance emitted by the earth in the 8 to 14 μm spectral band is tabulated in Table 3.1-7. The nonrejected reflected sunlight radiance for each channel can be found by multiplying the curves in Figure 3.1-2 by the ratios in Table 3.1-7. For example, the nonrejected reflected sunlight radiance for channel 9, the OH channel, at a tangent height of 100 km with an on-axis telescope with a BRDF of 10^{-3} is

$$(3 \times 10^{-8})(6 \times 10^{-2}) = 1.8 \times 10^{-9} \text{ Wcm}^{-2}\text{sr}^{-1}.$$

This value is a factor of 6 larger than the NEN of channel 9.

Table 3.1-7. Ratio of Sunlight Radiance in Channel Passbands Reflected from Earth (Assuming 0.3 Reflection Coefficient) to Thermal Radiance Emitted by Earth in 8 to 14 μm Spectral Band

Channel	Ratio
1. CO_2 (N)	$9x10^{-5}$
2. CO_2 (W)	$4x10^{-4}$
3. CO_2 (W)	$4x10^{-4}$
4. O_3	$1x10^{-3}$
5. H_2O	$2x10^{-3}$
6. NO_2	$1x10^{-3}$
7. NO	$4x10^{-3}$
8. CO_2 (4.3)	$3x10^{-3}$
9. OH	$6x10^{-2}$

Thus, an on-axis design looking at a tangent height of 100 km sees an NRER equal to the NEN with channel 4; it sees a reflected sunlight radiance equal to 6 times the NEN with channel 9. These rejection results led to selection of an off-axis telescope design rather than an on-axis design.

3.1.1.2 Baffle. As previously described, the NRER is determined by the BRDF of the foreoptics rather than by the baffle because the foreoptics are directly illuminated by the earth. IRLE looks at the earth as part of the scan cycle, so it is impossible to prevent direct illumination of the foreoptics.

The optical baffle and the graphical construction used to select the location of the knife edges are shown in Figure 3.1-3. The plane of this drawing contains the centerline of the baffle and the center of the earth. This graphical construction yields the minimum number of knife edges that prevent light from scattering into the aperture from the baffle tube. The minimum number of knife edges results in the minimum scattering coefficient for the baffle. The baffle scattering coefficient is proportion to the ratio of the area of the knife edges to the area between the baffles.

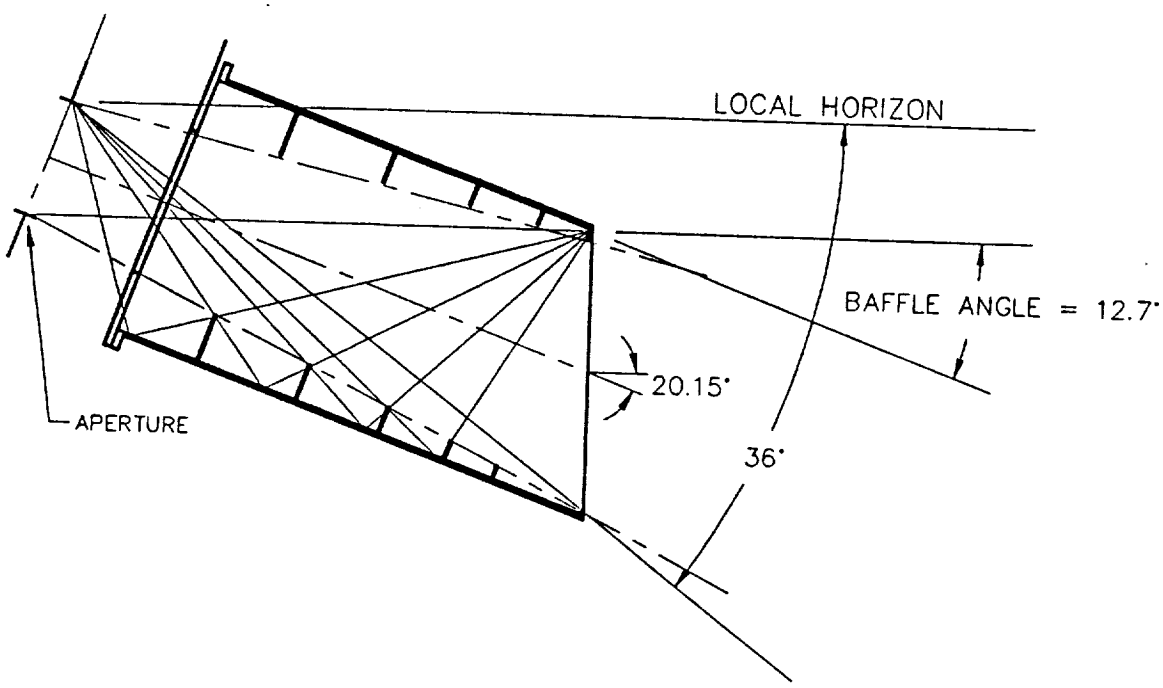

Figure 3.1-3. Optical Baffle Layout

The aperture identified in Figure 3.1-3 is the image formed at the scan mirror of the system aperture. The baffle length is approximately 450 mm. The baffle end is cut at an angle in order to maximize the baffle length on the earth side under the constraints that IRLE must not extend beyond the instrument plate and must not obscure the view of other MELTER instruments. On the earth side, no rays at an angle greater than 16 deg to the baffle axis are admitted by the system aperture; on the top side, this angle is 20 deg. The baffle axis is 20.15 deg below the local spacecraft horizon. Thus, no rays from the earth making an angle greater than 36 deg with the local horizon are admitted by the entrance aperture. Even though the system aperture is elliptical, the end of the baffle tube is nearly circular because the beam spread is much greater for the small dimension than for the large dimension of the ellipse. The small dimension is shown in the plane of Figure 3.1-3.

The baffle is cylindrical and painted on the inside with absorbing black paint. The baffle structure encloses the flip-in mirror assembly, but mechanical support for this assembly is provided by supports from the telescope structure. Mechanical support for the contamination cover at the end of the baffle is provided by connection to the IRLE structure. These external supports allow a lightweight, 2 kg, yet relatively long baffle.

3.1.2 Scan Mirror Assembly

The scan mirror assembly, shown in Figure 2.2-3, consists of a scan mirror, a dc torque motor, a tachometer, and an angle encoder. An analysis of the scan mirror assembly was performed by James Miller of NASA Langley. His results demonstrate the feasibility of the design and establish first-order estimates of mass, size, impulse torque, and power.

The scan mirror is made of lightened beryllium to facilitate rapid movement. Its surface is superpolished to minimize optical scattering because the NRER for IRLE is determined primarily by the scatter properties of this mirror. The scan mirror is elliptically shaped with a minor diameter of 176 mm and a major diameter of 220 mm. These dimensions allow for a 20 mm margin around the clear aperture of the mirror and a maximum mechanical angle of 50.2 deg between the mirror normal and the telescope axis. The scan mirror

is 25.4 mm thick, has a mass of 0.64 kg, and a moment of inertia, with the axis of rotation at its face, of 0.001 kg m^2 (0.195 in.-oz sec^2).

The angular resolution requirement of the line of sight is assumed to be half the angular width of one detector element (one half of 0.75 mr). The required mechanical resolution of the scan mirror is 0.188 mr, half the line of sight resolution requirement. This mechanical resolution requirement implies that the angular shaft encoder must produce at least 33,510 counts per revolution. An angular encoder that meets this requirement has not yet been identified. The closest candidate, the RI 36K/40 incremental spacecraft angular encoder made by Itek Measurement Systems, Inc., has an angular resolution of 9000 counts per revolution. The mass, 1.36 kg, and moment of inertia, 3.9E-3 in.-oz sec^2, of this encoder were used as first-order estimates for this analysis. The selection of the encoder must be revisited during the preliminary design phase.

The maximum torque, maximum encoder rate, peak current, peak power, and peak impulse torque all occur when the scan mirror is moved as rapidly as possible from the top of the adaptive scan to the space-look position. It is assumed that this motion takes place in the time it takes to measure two data samples (2 x 86 ms) and that the velocity profile is triangular. The maximum required motor torque is 15.016 in.-oz, and the maximum encoder rate is 5601 counts per second. This maximum torque computation assumed a frictional torque of 5 in.-oz, a motor-encoder-tachometer moment of inertia of 1.0E-2 in.-oz sec^2, and a torque safety margin of 2. The selected torque motor, the TQ34W-1 brushless wide-angle dc torque motor made by Aeroflex Laboratories, Inc., has a continuous torque rating of 25 in.-oz. This motor has a mass of 0.368 kg, a moment of inertia of 4.2E-3 in.-oz sec^2, an angular excursion of 120 deg, and a torque sensitivity of 18.3 in.-oz per amp. This torque sensitivity yields a peak current of 0.3 amps. Assuming a 28 V supply, this peak current corresponds to a peak power requirement of 8.4 W. The average power requirement of the torque motor is 4.7 W. The peak impulse torque is 0.002 N·m sec.

samples. This computation assumes that motor current was limited to 1.5 times the normal scan current.

The selected tachometer, the TG34W-12 brushless dc tachometer made by Aeroflex Laboratories, Inc., is the mate to the torque motor.

3.1.3 Flip-In Mirror Assembly

The in-flight calibration flip-in mirror assembly, shown in Figure 2.2-3, consists of three mirrors mounted on a plate, a stepping motor, and a shaft encoder. During each calibration sequence, these three mirrors are introduced in turn into the optical beam. The direction of the mirror assembly alternates on each calibration scan. The two smaller mirrors are 25 mm in diameter and made of aluminum. The third mirror is 71 mm in diameter and made of beryllium. The mirrors are mounted on a 90 mm radius about the assembly center of rotation and are separated by 60 deg with the large mirror located between the two smaller ones. The flip-in mirror assembly has a mass of 0.216 kg and a moment of inertia of 0.248 in.-oz sec^2.

It is assumed that the tangential position of the flip-in mirrors must be accurate to 1 mm. This implies that the angular shaft encoder must produce at least 565 counts per revolution. This requirement can be satisfied by the spacecraft angular encoder model RI 1.0K/20 supplied by Itek Measurement Systems. It has an angular resolution capability of 1000 counts per revolution. This unhoused incremental encoder has a mass of 0.136 kg and a moment of inertia of 1.0E-3 in.-oz sec^2.

As indicated in the scan profile in Figure 2.1-2, the flip-in calibration sequence is a 5-step process. First, the flip-in mirror assembly remains in the space-look position (flip-in mirrors are removed from the optical beam) for two sample periods. Then each flip-in mirror is inserted into the optical beam for two sample periods. Finally, the flip-in mirrors are removed for another two sample periods. This accounts for 10 sample periods; each sample period is 86 ms. Since the whole calibration sequence must be completed in 2.9 sec, there remains six sample periods for each motion.

The average angular velocity is 116 deg/sec, 60 deg divided by 6 sample periods. The peak velocity is 155 deg/sec and the angular acceleration is 1200 deg/sec^{-2} when it is assumed that the velocity profile is trapezoidal with acceleration and deceleration each taking 25 percent of the available motion time. A triangular velocity profile was also considered, but the stepper motor, described in paragraph 3.1.4) produced insufficient torque for this profile. The 155 deg/sec peak velocity requires a maximum encoder rate of 244 counts/sec.

The maximum required motor torque is 11.58 in.-oz. This computation was made assuming a frictional torque of 2.5 in.-oz, a motor and encoder inertia of 1.0E-3 in.-oz sec^{-2}, and a torque margin factor of 1.5. This torque requirement can be satisfied by the combination of a Type 8 stepper motor and a Type 9-2D high-capacity spur gearhead supplied by MPC Products Corporation. This stepper motor-gearhead combination produces an estimated output torque of 12.2 in.-oz at the maximum velocity of the flip-in mirror assembly.

The impulse torque produced by performing a single 60 deg motion is 0.007 N·m sec. The impulse torque produced by performing a single 1 deg motor step is 0.003 N·m sec.

The peak stepping motor power is 5.2 W with an average power of 0.182 W, assuming the space-look positions and the limb scan positions are insensitive to movements of less than one motor step. The estimated mass is 0.30 kg, excluding support structure, bearings, and shaft.

3.1.4 Chopper and First Field Stop

As shown in Figure 3.1-1, the first field stop and chopper are located between the secondary mirror and the tertiary mirror of the telescope. The dimensions of the first field stop are given in Figure 3.1-4. A 3-to-1 demagnification exists between the field stop and the detector plane. The long dimensions of the field stop openings are perpendicular to the telescope meridional plane, the plane which contains the optical axis. The meridional plane is unique for an off-axis telescope; it is the plane of the optical layout drawing shown in Figure 3.1-1.

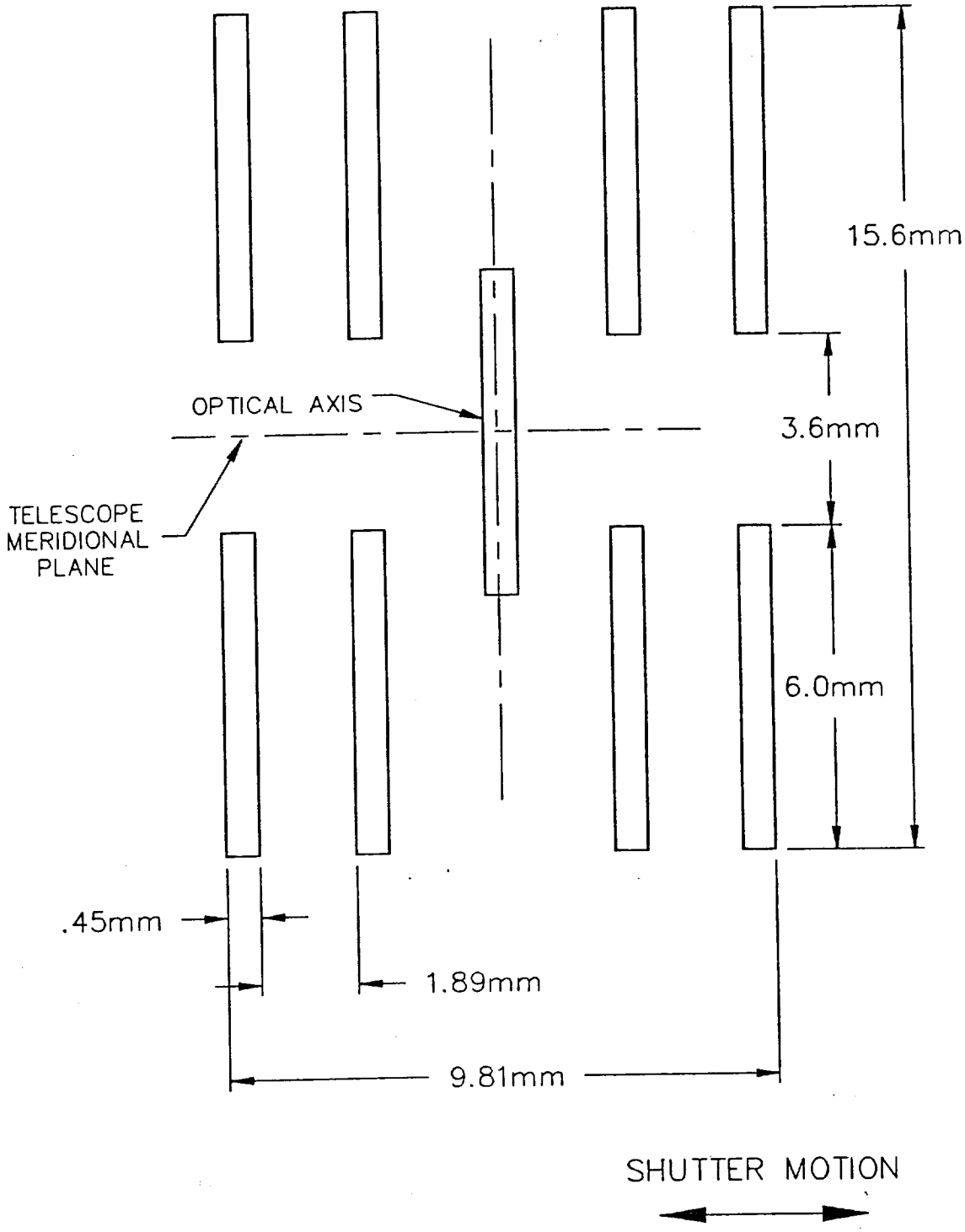

Figure 3.1-4. First Field Stop Dimensions

An optical-mechanical schematic drawing of the chopper is shown in Figure 3.1-5. The chopper is a tuning-fork or "picket fence" chopper that has operated for 3 years on the Solar Mesospheric Explorer (SME). The chopper will be made by Philamon, who also made the SME chopper.

A picket-fence chopper has a shutter opening for each detector element, so the required relative motion between the two shutter blades is only the width of the detector element instead of the width of the entire detector array as is the case for a conventional chopper. Minimizing the amplitude of the shutter motion results in minimizing the stress in the chopper and thus maximizes chopper reliability. The required motion between the two shutters is only 0.45 mm, which is half Philamon's ultraconservative design limit for the peak-to-peak motion of one tine. For ultraconservative long-life designs, Philamon uses the rule of thumb that the peak-to-peak amplitude of one tine should not exceed 610 mm divided by the chopping frequency. Using the 700 Hz chopping frequency of IRLE, this rule yields a limit of 0.87 mm for the peak-to-peak motion of one tine. Since the total chopper motion can be provided by one tine, one shutter can be made stationary and function as the field stop. This approach allows the chopper to be placed at the focal plane instead of behind the focal plane as is required when a separate field stop is used.

To provide sufficient strength, the shutter edges are both crimped outward from their facing surfaces. If a separate field stop is used, there must be clearance between the field stop and this crimped edge. If the chopper is used behind the focal plane, the chopper holes must be larger to account for defocusing which requires a larger relative motion between the shutters. However, in this case, both shutters move so the motion of each tine is only half the total required relative motion. The chopper can provide ample motion for either approach. The final selection will be made during the preliminary design phase.

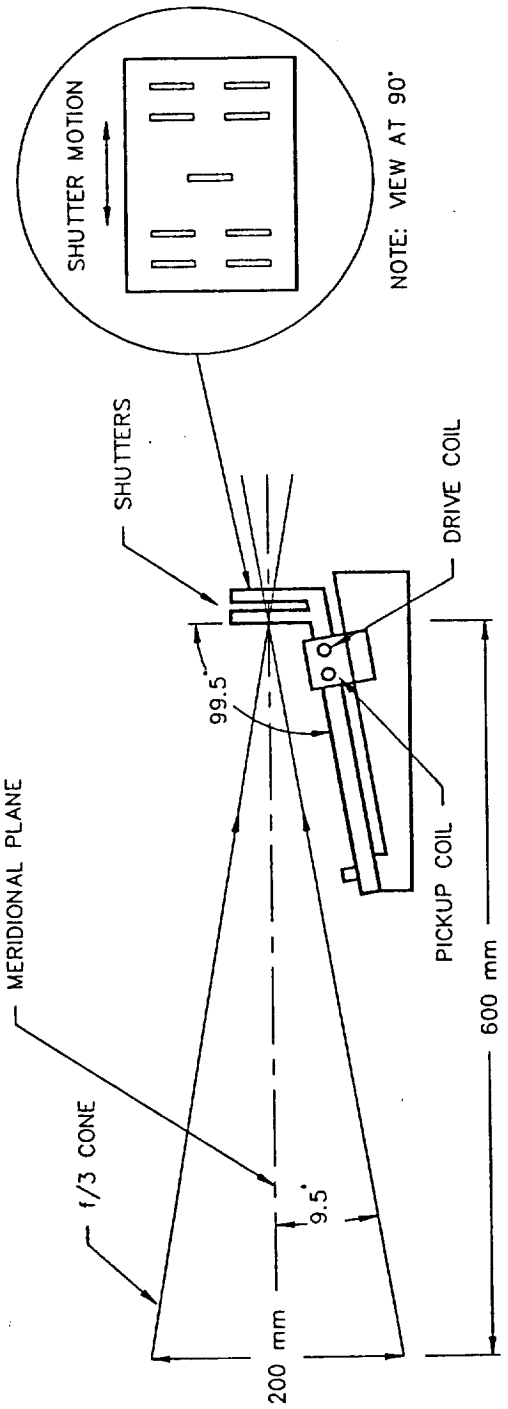

Figure 3.1-5. Chopper Optical-Mechanical Schematic

The 99.5-deg angle between the chopper tines and the shutters minimizes the angular variation of the shutter openings, caused by the radial motion of the tine ends, under the constraint that the length of the shutters must be minimized. If the angle between the chopper tines and the shutters could be made 90 deg, there would be no angular variation in the direction of the shutter openings. However, a 90-deg angle and the requirement that the chopper body must not obstruct the optical beam would require extremely long shutters which would twist. With a 99.5-deg angle between the tines and shutter, the cross-coupling of the radial tine motion into angular variation of the shutter openings is negligible. In the SME chopper, this angle is 102 deg. The optical beam is f/3 in the plane of Figure 3.1-5. The long dimension of the entrance aperture is also shown in Figure 3.1-5.

The shutters are 0.127 mm thick stainless steel. The sides facing the light will be painted black to absorb light, while the sides seen by the detectors will have a low-emissivity surface to minimize background radiation. The openings in the shutter will be chemically milled to an accuracy of 1/10th the shutter thickness. If this accuracy should prove inadequate, the openings can be stamped, requiring a tooling charge of approximately $40,000. It is questionable whether this extra accuracy could be maintained once the shutters are painted black. In contrast, chemical milling only costs $7,500.

Since the shutter is a single-point failure, a breadboard chopper will also be constructed and life tested until launch. Philamon prefers to avoid the use of redundant drive and pick up coils. Redundant coils require extra connections which, in their opinion, actually cause reduced rather than increased reliability. Tests on similar Philamon choppers have shown a frequency variation of only 1 part per million over an 8-year period and a frequency change of only 0.27 Hz over a 77 to 338 Kelvin temperature range. The chopper requires an estimated average current of 30 ma at 28 V for an average power of 0.84 W. The estimated masses of the chopper head and the chopper electronics are 0.06 and 0.03 kg, respectively. The chopper electronics are hermetically sealed in a package volume of approximately 33 cm^3. Figures 3.1-6 and 3.1-7 show side and rear views, respectively, of a Philamon chopper similar to the IRLE chopper.

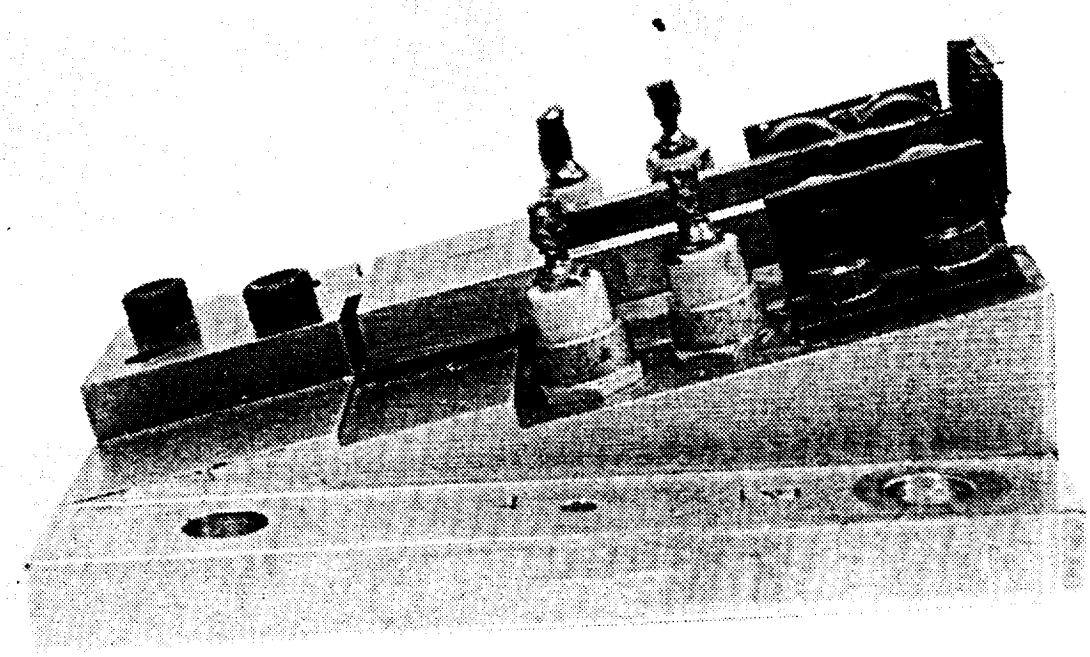

Figure 3.1-6. Philamon Chopper Side View

ORIGINAL PAGE
BLACK AND WHITE PHOTOGRAPH

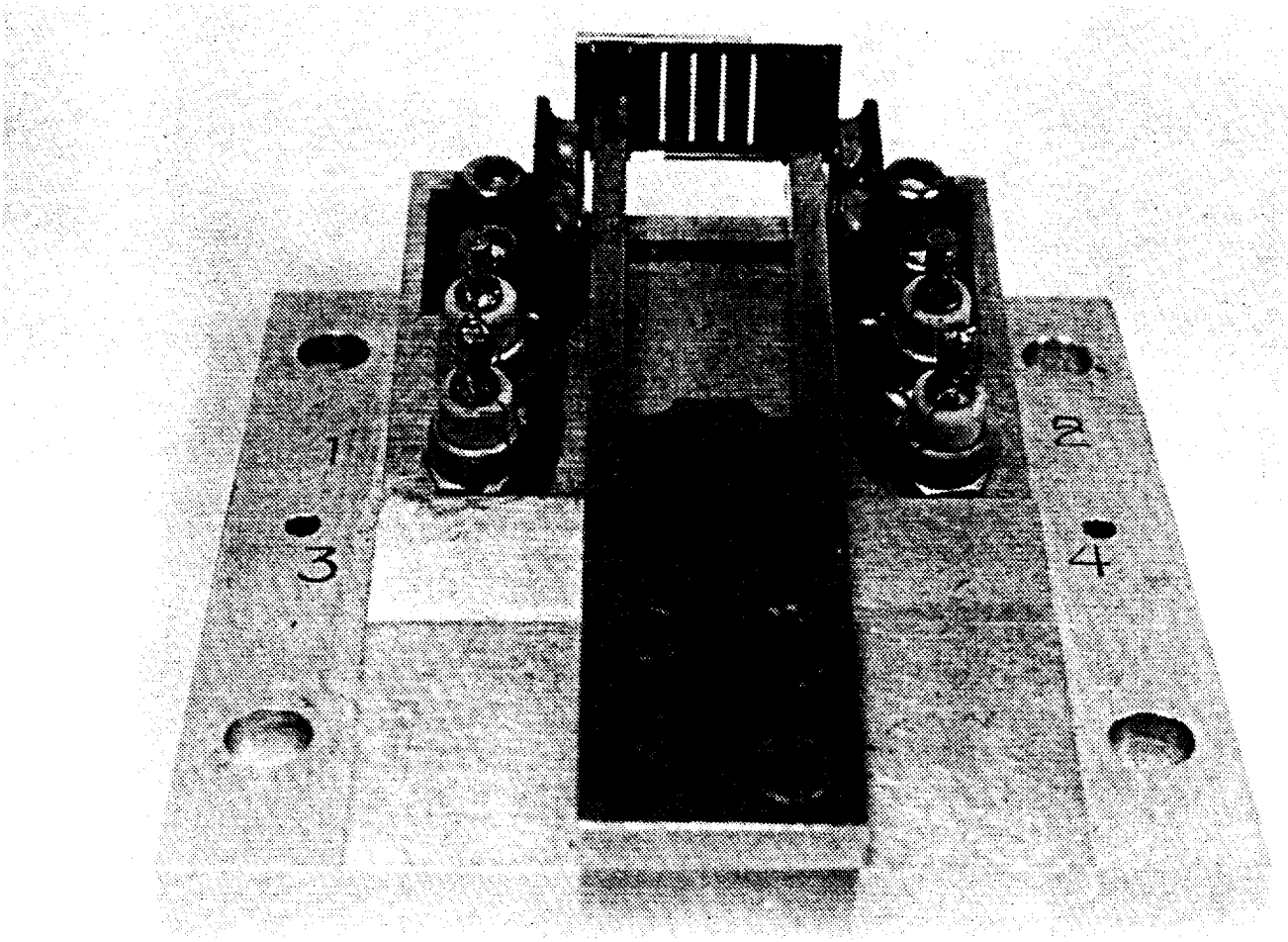

Figure 3.1-7. Philamon Chopper Rear View

3.1.5 Full-Aperture Blackbody

The full-aperture blackbody is an elliptically shaped plate of 13 mm thick aluminum, slightly larger than the 100 by 200 mm entrance aperture. Hundreds of holes are numerically drilled on the emitting side to improve the emissivity for wavelengths beyond 12 μm. The emitting surface is painted black for high emissivity, while the edges and back surface are gold coated for low emissivity. The blackbody is heated by means of Dale power resistors spread over a channel cut in the back side of the blackbody. The blackbody temperature is monitored by an array of platinum resistance thermometers (PRT) that are accurate to 0.1 Kelvin. Since the temperature difference between the extended blackbody and its surroundings is less than 20 Kelvin, temperature gradients between the thermometers and the emitting surface will be small. Therefore, it is estimated that the temperature of the emitting surface is known to 0.2 Kelvin. The estimated mass of the extended blackbody is 0.5 kg. The estimated average power required is 2 W.

3.1.6 Contamination Cover

The contamination cover release, hinge, spring, and latch components are an adaption of the HALOE telescope door subsystem. The HALOE door opener uses two redundant ICI Americas, Inc. P/N 228-3000F piston retractors especially packaged to provide a double seal for "blow-by". This pin-puller configuration has been extensively tested by NASA in a vacuum chamber over a range of temperatures. The vacuum chamber atmosphere was monitored by a gas chromatograph to search for blow-by. No blow-by was observed. The HALOE door subsystem provides positive lock in the closed position, spring opening, and positive latch in the open position.

3.2 DETECTOR MODULE

The detector module, shown in Figure 3.2-1, consists of the detector array, optical filter array and second field stop, optical cold shield, thermal switches, detector dewar, and displacers. The displacers, which are the two cylindrical bodies bolted on either side of the detector dewar, are part of the cryocooler covered in paragraph 3.3. The optical details of the detector module are shown in Figure 3.2-2.

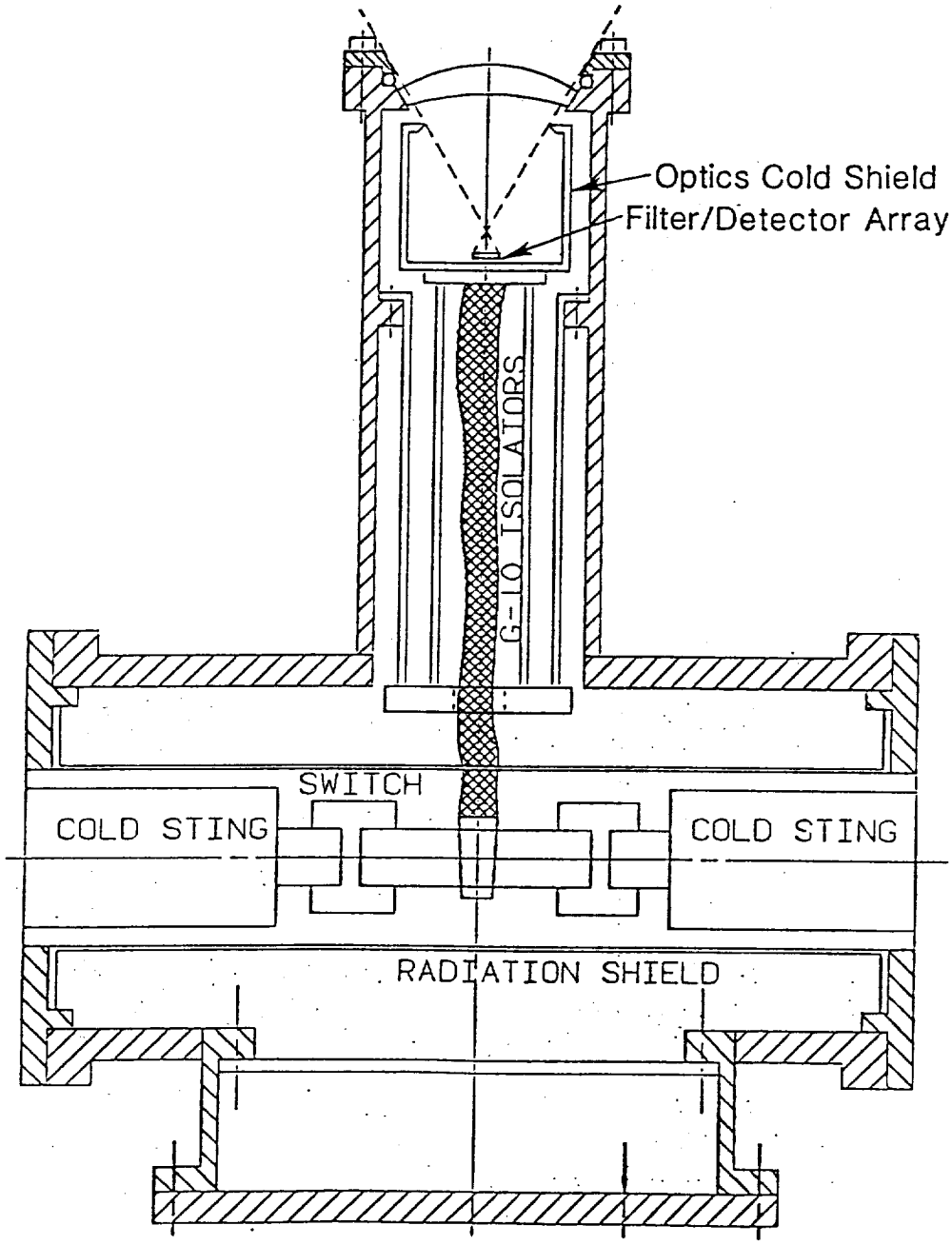

Figure 3.2-1. Detector Module

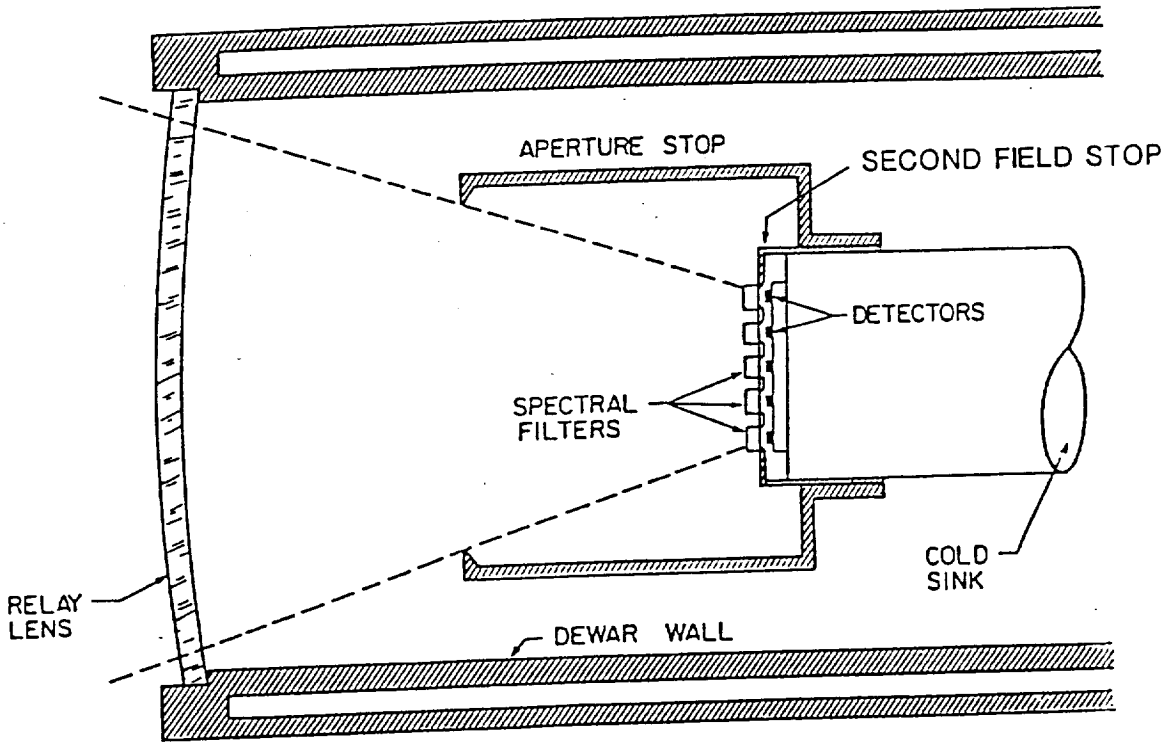

Figure 3.2-2. Optical Portion of Detector Module

3.2.1 Detector Array

3.2.1.1 Detector and Second Field Stop Layout. The second field stop, located directly over the detectors, defines the sensor field of view. The second field stop dimensions are in Figure 3.2-3. The detectors are wider than the field stop opening to allow for fabrication tolerances and image spread. Image spread results from the requirement that detectors be located at least 0.15 mm behind the field stop to allow for detector defocus necessary to make room for stress-relief loops in the bonding wire from the detectors. Since the f-cone in the narrow detector dimension is f/2, 0.15 mm was added to the 0.15 mm field stop width for a total detector width of 0.30 mm. The long detector dimensions were not increased because the f-cone spread (f/1 in this dimension) is much less than the detector length. Since the second field stop is cold, the effective width of the detector-collecting background photons is only the width of the field stop opening.

3.2.1.2 Detector Performance. State-of-the-art detector performance was ascertained from discussions with five detector vendors: Honeywell Electro-Optics Division, Judson, Santa Barbara Research Center (SBRC), Cincinnati Electronics, and Epitaxx, Inc. The D^* values predicted by Judson for channels 1 through 7 and those predicted by Cincinnati Electronics for channels 8 and 9 are tabulated in Table 3.2-1. These D^* values are computed for a detector temperature of 75 Kelvin, a 300 Kelvin background that is cold shielded to an f/1 cone and also cold filtered, a 700 Hz chopping frequency, and a maximum detector power dissipation of 10 mW. These D^* values also include preamplifier noise and Johnson noise in a 300 Kelvin feedback resistor. Channels 1 through 7 are photoconductive HgCdTe detectors while channels 8 and 9 are photovoltaic InSb detectors. Honeywell, Judson, and SBRC are possible sources for the HgCdTe detectors, while Judson, SBRC, and Cincinnati Electronics are possible sources for the InSb detectors. Epitaxx supplies a new detector, InGaAs, which is an alternate candidate for the channel 9 detector. InGaAs appears to have D^* values greater than 4E12 with a room temperature cutoff wavelength of 1.65 μm. However, when this detector is cooled, its cutoff shifts to shorter wavelengths. At 77 Kelvin, a typical InGaAs detector will have a cutoff wavelength of 1.55 μm which is too short for the OH channel.

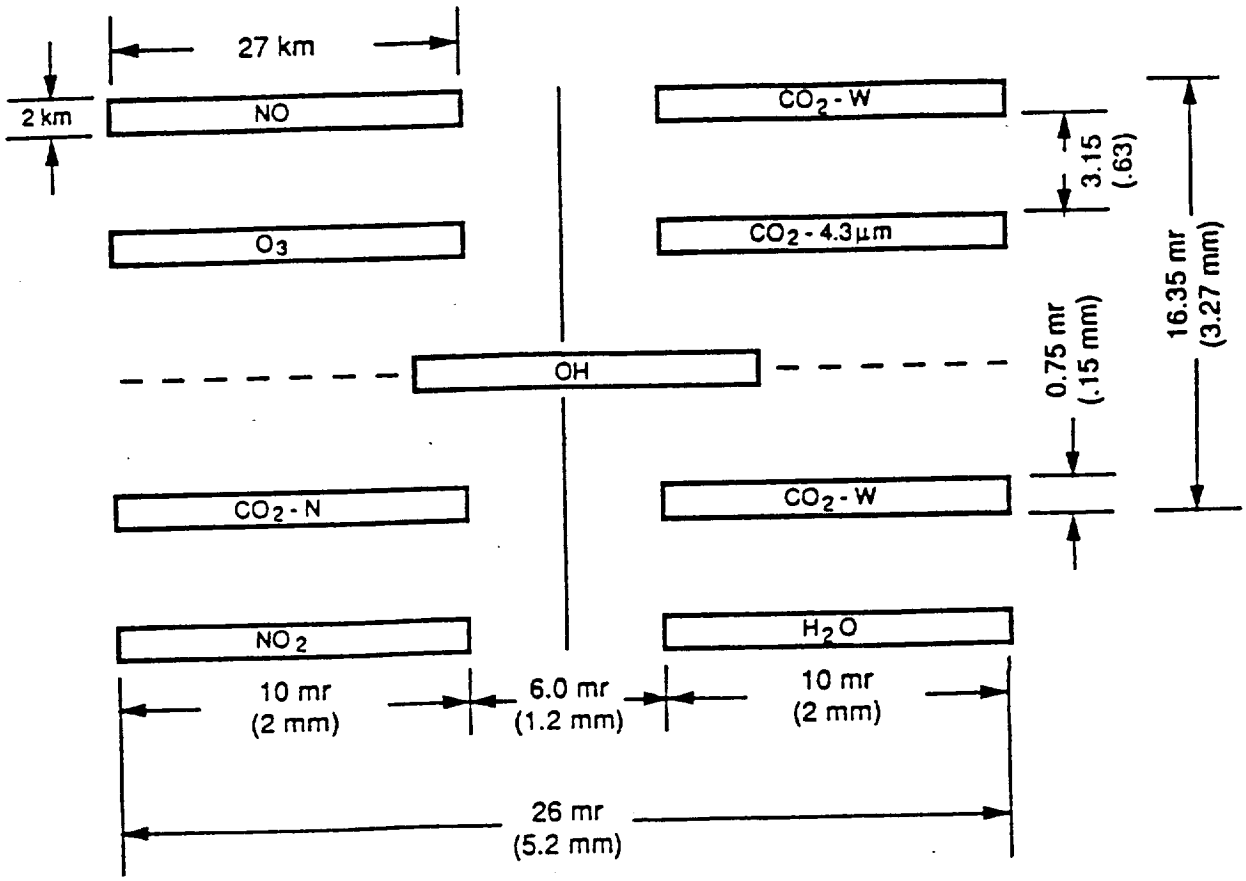

Figure 3.2-3. Second Field Stop

Table 3.2-1. D^* Values Predicted by Judson and Cincinnati Electronics

Channel		$\Delta\lambda$ (μm)	Detector Material	D^* 10^{10} ($cmHz^{\frac{1}{2}}W^{-1}$)
1.	CO_2 (N)	14.99-15.58	HgCdTe (PC)	8
2.	CO_2 (W)	13.70-16.53	HgCdTe (PC)	5
3.	CO_2 (W)	13.70-16.53	HgCdTe (PC)	5
4.	O_3	9.05-10.46	HgCdTe (PC)	6
5.	H_2O	6.52-7.15	HgCdTe (PC)	9
6.	NO_2	6.14-6.35	HgCdTe (PC)	9
7.	NO	5.12-5.60	HgCdTe (PC)	9
8.	CO_2 (4.3)	4.19-4.36	InSb (PV)	84
9.	OH	1.50-1.80	InSb (PV)	200

The long wavelength channels (channels 1, 2, and 3) determine the required focal plane temperature. At 80 Kelvin, HgCdTe detectors become thermal limited at a wavelength of 15 μm. Values for D^* as a function of temperature, computed by Honeywell using their computer model, are tabulated in Table 3.2-2.

Table 3.2-2. D^* Values as Function of Temperature Predicted by Honeywell Computer Model with 1 nV/$\sqrt{Hz}$ and 10 mW Detector Dissipation Limit

Channel		$\Delta\lambda$ (μm)	Temperature (K)	D^* 10^{10} ($cmHz^{\frac{1}{2}}W^{-1}$)
1.	CO_2 (N)	14.99-15.58	65	7.5
	CO_2 (N)	14.99-15.58	80	2.4
2&3.	CO_2 (W)	13.70-16.53	65	5.2
	CO_2 (W)	13.70-16.53	70	3.9
	CO_2 (W)	13.70-16.53	80	1.9
4.	O_3	9.05-10.46	65	6.3
	O_3	9.05-10.46	80	4.7
6.	NO_2	6.14-6.35	65	14.1
	NO_2	6.14-6.35	80	10.3

This Honeywell data indicates that it would be desireable to operate the long wavelength channels at 65 Kelvin, the focal plane temperature that was used in LIMS. Decreasing the HgCdTe detector temperature for the long wavelength channels increases the long wavelength cutoff. For example, the cutoff increases by 1.5 μm as the detector temperature decreases from 80 to 65 Kelvin. The long wavelength cutoff of the detector should be long enough to extend beyond the long wavelength edge of the filter so that it remains outside the filter passband for any temperature variations.

Despite the advantages of operating the detectors at 65 Kelvin, the coolers are only capable of maintaining a focal plane temperature of 70 Kelvin. The nominal detector temperature was set at 75 Kelvin because this temperature requires 4 W less compressor power and because it also allows some design margin. The detector temperature should be studied further in the next phase of the IRLE program.

The HgCdTe photoconductive detectors will use three types of HgCdTe material: long, standard, and short. Channels 1, 2, and 3 require long wavelength material which is not ordinarily available and may need to be specially manufactured. Channel 4 requires standard HgCdTe material, while channels 5, 6, and 7 require short wavelength material which the detector vendors typically have on hand.

The chopping frequency was set as low as the 1/f noise of the HgCdTe detectors would allow. The decrease in chopper amplitude with the increase in chopper frequency, as well as the increase in the required sampling frequency with chopper frequency, made it imperative to keep the chopping frequency as low as possible. However, detailed detector studies may show that it is necessary to increase the chopper frequency to 1 kHz to obtain adequate detector yields.

The resistivity of the HgCdTe detectors is estimated at 60 ohms per square which, when multiplied by the aspect ratio (2.0 mm/0.30 mm), yields a resistance of 400 ohms. The bias current must be kept low to minimize 1/f noise. The estimated bias current is 5 mA; this current through the 400 ohm detector resistance results in a power dissipation of 10 mW per HgCdTe detector.

The D^* values for channels 5, 6, and 7 could be increased by allowing greater detector power dissipation which increases responsivity. This option will be investigated in the next phase of the IRLE program.

3.2.2 Optical Filter Array

The spectral properties of the IRLE filters are provided in Table 3.2-3. The wideband CO_2, narrowband CO_2, and O_3 filters are all identical to the LIMS filters. The H_2O and NO filters have the same passbands as the LIMS filters but are blocked to out-of-band transmissions of 10^{-4} rather than to 10^{-3}. Based on the LIMS experience and the results of SPIRIT III analyses, the blocking levels given in Table 3.2-3 should be adequate. However, these blocking levels will be confirmed during the preliminary design phase by integrating the product of the spectral radiance and the filter transmission over the out-of-band region and comparing the result to the NEN of the channel.

There is some concern that the actual out-of-band blocking of the filters may be less than the measured out-of-band blocking because the filters in IRLE are placed within a few mils of the detector. Stierwalt, at NOSC, has shown with measurements of filters made for the LIMS mission (he may not have tested the filters actually flown on LIMS) that the out-of-band blocking due to interference coatings can be degraded by orders of magnitude when the filters are placed within 10 mils of the detector. Stierwalt has postulated that the close proximity of the filter to the detector causes the detector to collect rays scattered into large angles. These large-angle rays are not collected in a conventional filter measurement setup. However, the LIMS filters were actually better than specified, so that even with the one to two order degradation that Stierwalt found, the out-of-band transmission blocking was still less than 10^{-3} for all channels except the CO_2 wideband and CO_2 narrowband channels. For these two channels, the out-of-band transmission was less than 3E-3. One approach to this problem is to make the out-of-band blocking specification considerably better than the three orders required so that degradation will not occur below the three orders. Another approach is to use absorbing blockers which do not suffer degradation when placed near the detector. Based on the LIMS results, this problem is considered manageable.

TABLE 3.2-3 Spectral Properties of IRLE Filters

CHANNEL	5% CUT-ON		CUT-ON SLOPE (%)	5% CUT-OFF		CUT-OFF SLOPE (%)	PEAK TRANS-MISSION (%)	BLOCK-ING LEVEL	LONG WAVE BLOCK LIMIT μm	COMPARISON TO LIMS FILTER
	POINT cm^{-1}	TOLER-ANCE (%)		POINT cm^{-1}	TOLER-ANCE (%)					
1. CO_2(N)	680	±1.0	≤3	635	±1.0	≤2.9	≥75	10^{-3}	22.4	IDENTICAL
2. CO_2(W)	760	±1.0	≤2.4	580	±1.0	≤2.9	≥65	10^{-3}	24.4	IDENTICAL
3. CO_2(W)	760	±1.0	≤2.4	580	±1.0	≤2.9	≥65	10^{-3}	24.4	IDENTICAL
4. O_3	1157	±1.0	≤2.4	940	±1.0	≤2.9	≥80	10^{-3}	15.5	IDENTICAL
5. H_2O	1560	±1.0	≤2.6	1380	±1.0	≤2.9	≥70	10^{-4}	12.5	PASSBAND IDENTICAL*
6. NO_2	1645	±0.5	≤2.0	1565	±0.5	≤2.0	≥75	10^{-4}	12.5	PASSBAND IDENTICAL*
7. NO	1990	±1.0	≤2.0	1750	±1.0	≤2.0	≥75	10^{-3}	10.0	NONE
8. $CO_2$4.3	2410	±1.0	≤2.0	2270	±1.0	≤2.0	≥75	10^{-3}	10.0	NONE
9. OH	6735	±1.0	≤2.5	5825	±1.0	≤2.5	≥75	10^{-3}	10.0	NONE

* LIMS Blocking = 10^{-3}

The filter thicknesses and substrate materials are tabulated in Table 3.1-2. Other physical filter parameters are tabulated in Table 3.2-4.

Table 3.2-4. Filter Physical Parameters

Parameter	Value
Size	0.694 by 3.04 mm (+0.000, -0.0254 mm)
Clear Aperture	0.51 by 2.83 mm (-0.000 mm)
Thickness	(See Table 3.1-2)
Thickness Tolerance	±0.06 mm
Thickness Matching	±0.03 mm
Optical Finish	quarter wave at 6328 nm

The filters are mounted in a bezel that will be held at approximately 75 Kelvin, which greatly reduces the thermal radiation from the detectors. Thermal radiation from the filters is discussed in paragraph 2.5. Heaters are installed in the filter bezel to drive off any contamination that may collect on the filters.

3.2.3 Optical Cold Shield

The cold shield is located in the detector dewar where it is cooled to approximately 80 Kelvin. The cold shield is shown in Figure 3.2-4 located between the detector plane and the CdTe dewar window. The cold shield also functions as the system aperture stop. This combination of functions minimizes the background radiation by limiting the detector's view inside the telescope to the low-emissivity optical surfaces. The cold shield aperture is elliptical with major and minor diameters of 27.6 and 13.8 mm, respectively. Figure 3.2-4 shows the major axis. The cold shield is located approximately 27 mm in front of the detectors. The f/number of an equivalent circular aperture is 1.38.

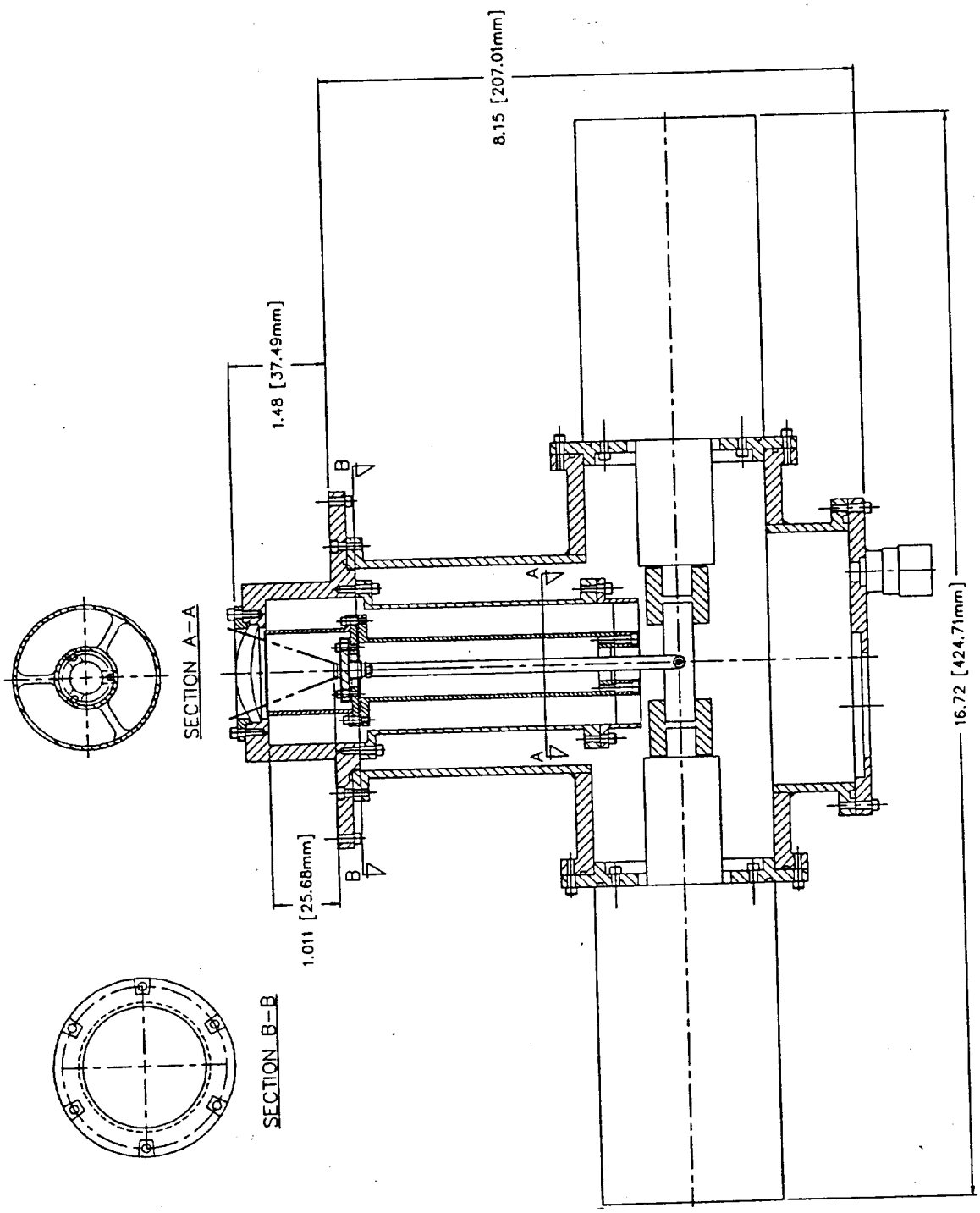

Figure 3.2-4. Detector Dewar Mechanical Layout

3.2.4 Detector Dewar

3.2.4.1 Requirements. The required functions of the detector dewar are to provide:

a. Thermal linkage between the coolers and the detectors. It is desireable to minimize the temperature drop between the detector and cooler cold sting. A $\Delta T \leq 3$ Kelvin is baselined for this design.

b. Capability to thermally switch either of the two coolers out of the system in the event of a cooler failure.

c. Stable mechanical support for the detector. The cold detectors should not move in any direction relative to warm mounting surfaces more than approximately .03 mm.

d. Excellent thermal isolation between cold components and warm structural mounts to keep the thermal load within the capability of the mechanical coolers. Total dewar thermal load should be $\leq$600 mW to meet cooler capabilities, power constraints, and temperature requirements.

e. Operational capability in the lab at atmospheric pressure as well as in the vacuum of space. This requirement necessitates a vacuum shell for the dewar.

f. Contamination protection of the focal plane components.

3.2.4.2 Proposed Design. The proposed design for the detector dewar is shown in Figure 3.2-4. The vacuum shell consists of two intersecting aluminum cylinders. One cylinder (horizontal in Figure 3.2-4), surrounding the cold stings of the cooler displacers, is attached directly to the displacer mounting flanges. Vacuum seal is provided by o-rings. A thermal switch is located between each displacer cold sting and the cold link to the detector. The other cylinder (vertical in Figure 3.2-4), with the window lens mounted in a flat surface at the upper end, contains the detectors, filters, and a flexible copper strap connecting the thermal switches to the detector mounting plate. A cold shield is

attached to the cold detector mounting plate, extending nearly to the window and surrounding the detectors and filters. The detector mounting plate is supported by two concentric tubes made of glass-epoxy composite (G-10) material. This arrangement provides both a long heat path (approximately 152 mm) between warm and cold surfaces and excellent mechanical stability.

Wires connecting the cold detector to external electronics will exit from the dewar through a vacuum connector in the flat surface at the bottom of the vertical vacuum shell cylinder. Vacuum port connections are also located on this surface.

3.2.4.3 Thermal Switches. The design for the thermal switches has not been finalized. Bimetallic shrink-fit mechanical type switches developed by Lockheed serve as the baseline. Other options currently under evaluation include gas gap types, heat pipe diodes, and a proprietary switch under development by the British Aerospace Corporation (BAC). The switches must fit inside the small space available inside the dewar, be extremely reliable, and limit the heat leak into the dewar from a failed cooler to approximately 100 mW.

3.2.4.4 Flexible Cold Link Between Switches and Detector. It is desirable to minimize the surface area of the flexible cold link to reduce radiant heat from the warmer surrounding walls while maximizing the cross-sectional area to reduce thermal impedance. Preliminary properties are:

a. Length	10 cm = 4.17 in.
b. Thermal Conductivity	450 W/m-K
c. Allowable ΔT	1 K
d. Assumed heat load	250 mW
e. Required cross-sectional area	5.56×10^{-5} m^2 = .086 $in.^2$
f. Mass	.05 kg = .11 lb

3.3 CRYOCOOLER

3.3.1 Cooler Selection

Selection of the cooler for the IRLE instrument is primarily driven by the mission requirements for extended life, low weight, low power, and detector temperatures of approximately 70 Kelvin. The miniature Stirling-cycle cryogenic cooler developed by Oxford University and produced by BAC is the only system currently available that will meet these requirements. Although this cooler system has not yet been flown in space, it is being space qualified for the Improved Stratospheric and Mesospheric Sounder Instrument (ISAMS) to be flown on the NASA Upper Atmospheric Research Satellite. A laboratory model cooler has recently completed 3 years of continuous operation at full capacity with no measurable degradation in performance.

3.3.2 Cooler Description and Performance

The BAC-built cryocooler consists of a compressor and a displacer, as shown in Figure 3.3-1, together with the control electronics (not shown). The compressor is connected to the displacer by a flexible copper tube. The instrument design must allow for maintaining this connection during procedures including installation and mounting. Performance curves provided by BAC, shown in Figure 3.3-2, indicate that a single cooler operating at full capacity (20 W net power input to compressor) with a heat rejection temperature of 280 Kelvin will provide 600 mW of cooling at a cold sting temperature of 66 Kelvin. Using two coolers will reduce the heat lift requirements for each cooler to about 50 percent of the full capacity value. The performance values given in Figure 3.2-2 are based on a nominal length of 30 cm for the tubing that connects the compressor and displacer. As the instrument layout and design are further refined, it will be important to minimize the length of this tubing to the extent possible.

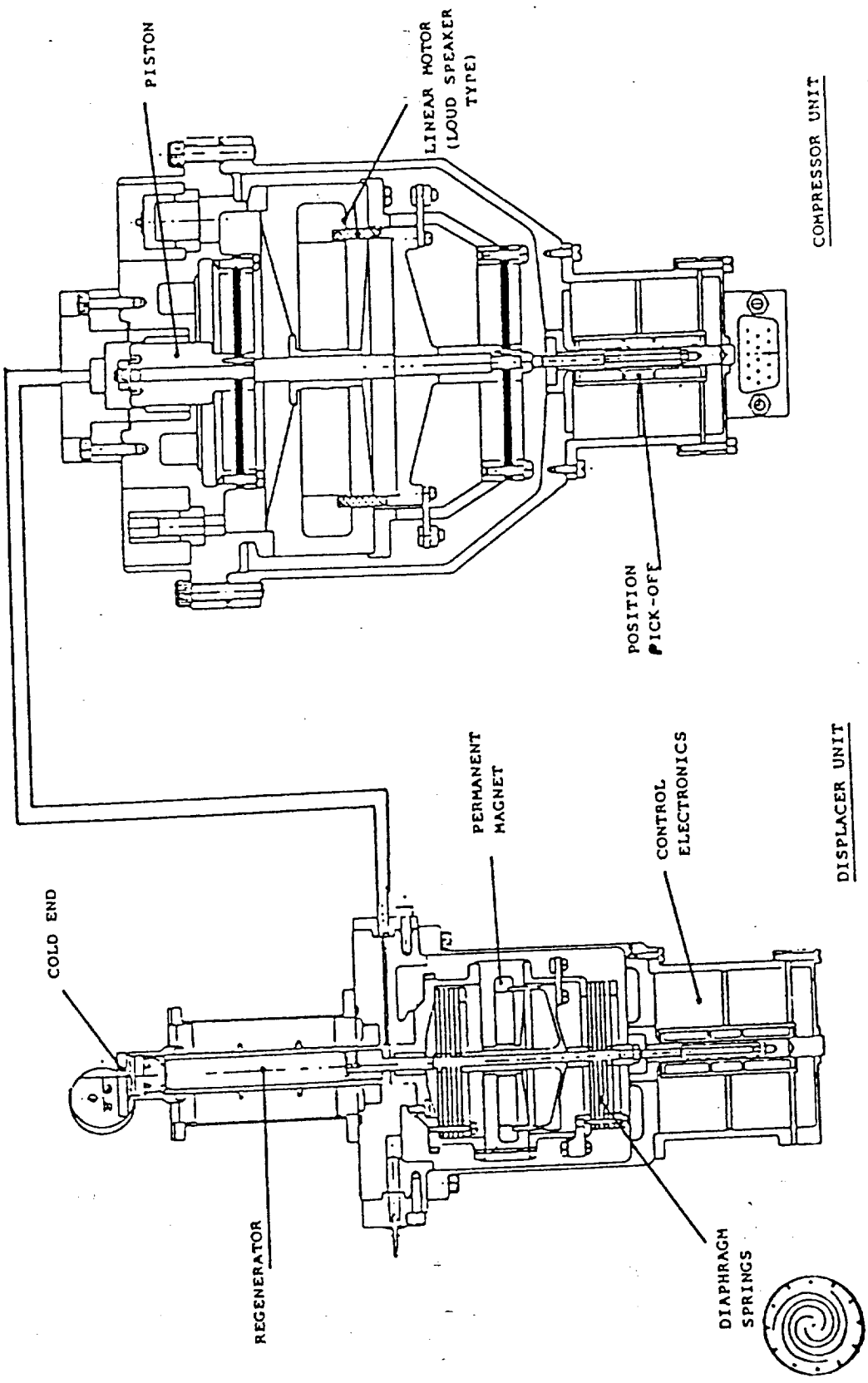

Figure 3.3-1. British Aerospace Stirling-Cycle Cooler

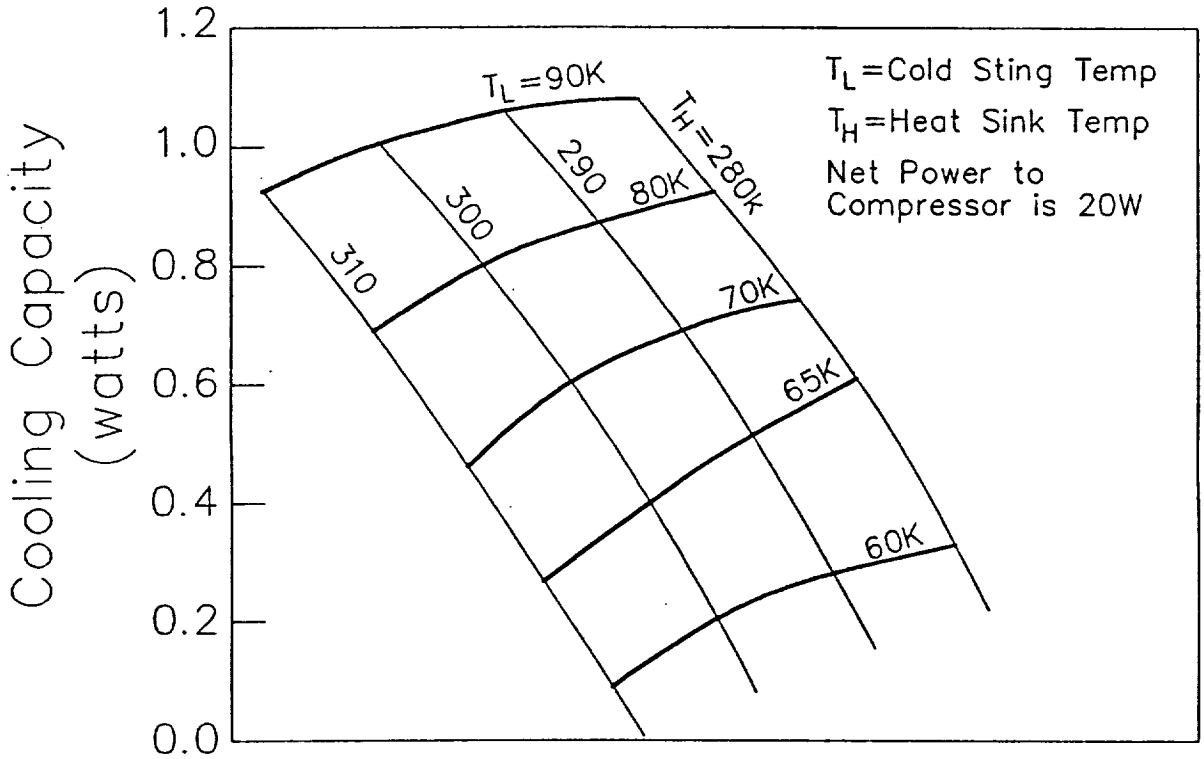

Figure 3.3-2. Cooling Capacity of Single Cooler as a Function of Cold Sting Temperature and Heat Sink Temperature

3.3.3 Probable Life Expectancy of Coolers

BAC provides the following values for the probability of achieving a given operating life before failure.

Life (years)	3	5	7	10
Reliability				
Mechanical	.982	.970	.959	.942
Electronics	.989	.982	.975	.964

BAC engineers suggest that life expectancy can be enhanced considerably by running the cooler at 50 percent capacity. Exact values for enhancing life expectancy while operating at reduced capacity are not yet determined.

3.3.4 Vibration and Momentum Compensation

Cooler mechanisms are operated by linear drive motors and generate sinusoidal vibrations at a frequency near 40 Hz. The compressor has a moving mass of .145 kg with a peak-to-peak displacement of 8 mm. Corresponding values for the displacer are .04 kg and 2.6 mm. Peak compressor momentum is calculated as follows:

$$x = .004 \sin \omega t$$

$$dx/dt = .004\ \omega \cos \omega t$$

$$\text{maximum velocity} = .004(40)(2\pi) = 1.0053 \text{ m/s}$$

$$\text{peak compressor momentum} = .145 \text{ kg}(1.0053 \text{ m/s}) = .146 \text{ N}\cdot\text{s}$$

$$\text{rms momentum} = .146/\sqrt{2} = .103 \text{ N}\cdot\text{s}$$

The results and corresponding values for the displacers are:

	Moving Mass (kg)	Displacement (mm)	Momentum Peak (N·s)	Momentum rms (N·s)
Compressor	.145	8	.146	.103
Displacer	.040	2.6	.013	.009

Uncompensated momentum can be reduced to less than 1 percent of these values by mounting two compressors and two displacers head to head and running 180 deg out of phase.

3.3.5 Cooler Power Requirements

Assuming that each cooler operates at 50 percent capacity with a cold sting temperature of 65 Kelvin, it may be estimated from Figure 3.3-3, as provided by BAC, that the net power requirement for each compressor is about 15.5 W. The compressor drive motor is expected to operate at 68 percent efficiency giving a total input power to each compressor of 22.8 W. This value results in a detector temperature of 70 Kelvin instead of the final design temperature of 75 Kelvin. Running the detectors at 75 rather than 70 Kelvin reduces the total power for the two compressors by about 4 W. BAC engineers estimate the power input to the electronics controlling both coolers to be 11 W. Each displacer draws about 1 W for a total cooler system power requirement of about 60 W. Voltage requirements are:

a.	Compressors	28 V dc ± 7
b.	Displacers	7 V dc ± .35
c.	Electronics	±15 V dc ± .75

3.3.6 Cooler Heat Dissipation

The heat dissipation from cooler components would be identical to the power requirement except that about 6 W are transferred from each compressor to each displacer. The expected heat loads are:

a.	Compressors	17 x 2 = 34 W
b.	Displacers	7 x 2 = 14 W
c.	Electronics	11 W

3.3.7 Temperature Stability

The intermittent nature of the Stirling-cycle cooler results in small cyclic variations in the cold sting temperature (thermophonics). These variations are expected to be reduced to acceptable levels at the detector by the thermal inertia inherent in the cold link between cold sting and detector. Variations are also expected in heat sink temperature as the spacecraft orbits through changing incident albedo on radiating surfaces. Temperature variation of approximately .3 Kelvin in the heat sink on the warm side of the cooler is expected to be attenuated by a factor of 5 on the cold sting.

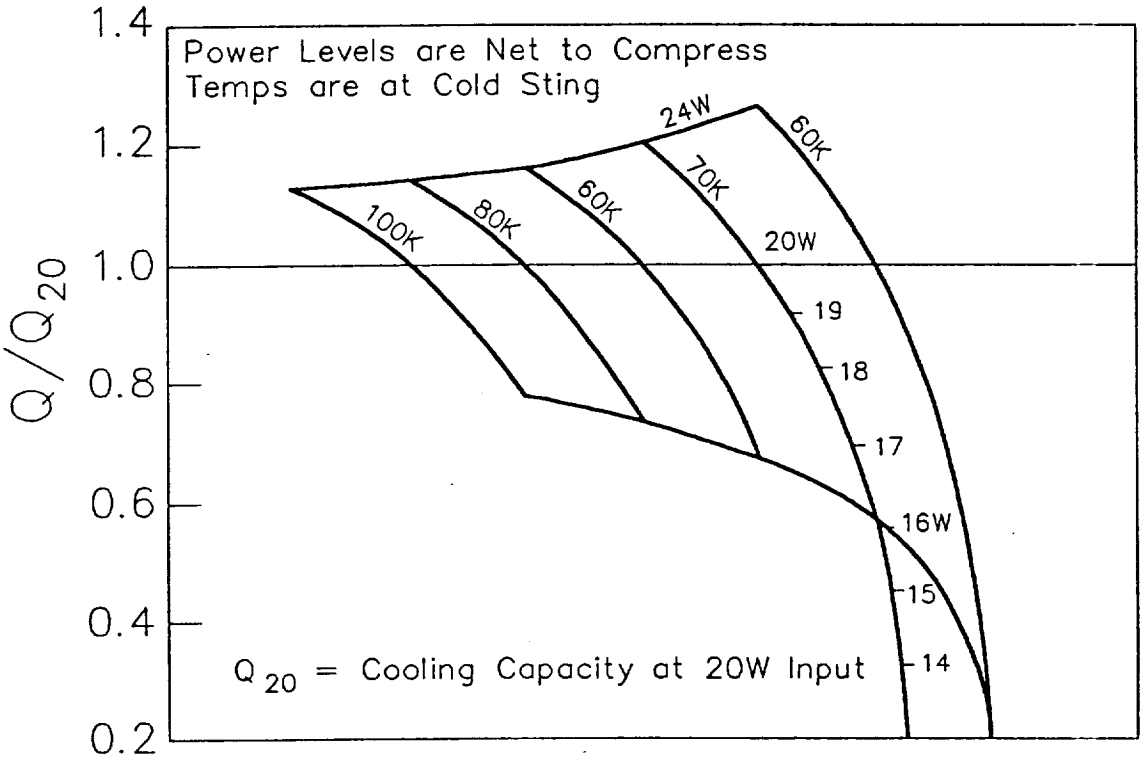

Figure 3.3-3. Cooling Capacity of Single Cooler as a Function of Cold Sting Temperature and Compressor Net Power

For example, a temperature increase of .3 Kelvin at the warm side will result in a temperature increase of about .06 Kelvin at the cold sting. Temperature variations on the warm side are discussed further in paragraph 3.4.

3.3.8 Cooler Redundancy

The baseline design calls for two compressors and two displacers, together with the capability to thermally disconnect a nonoperative compressor-displacer unit. In the event of a component failure in either compressor-displacer unit, that unit would be shut down and the mission continued with the other compressor-displacer. It is expected that the heat leak into the dewar from a disabled cooler can be limited to 150 mW or less. The single cooler could be expected to maintain a cold sting temperature of about 74 Kelvin with a heat lift of 750 W while operating at full capacity. (Corresponding detector temperature would be about 77 Kelvin). Vibration levels from the single uncompensated cooler can be expected to increase by a factor of about 100. Redundant electronics could be implemented, but this approach would increase weight and power requirements.

3.3.9 Cooler Mass

Component masses are:

a.	Compressors	3.0 x 2 = 6.0 kg
b.	Displacers	0.9 x 2 = 1.8 kg
c.	Electronics	= 4.6 kg
	TOTAL	12.4 kg

3.4 THERMAL CONTROL

3.4.1 Justification for Two Radiators

Two radiators, thermally isolated from each other and operating at different temperatures, are baselined to cool the IRLE instrument package. The basis for the selection of this approach follows.

a. Cooler performance is improved as the heat rejection temperature is reduced. It is desireable to operate the refrigerator radiator at the lowest temperature possible.

b. Lower radiator temperatures may be achieved by increasing radiator area (and weight) or by reducing the heat load.

c. The electronics packages, releasing considerable heat, operate satisfactorily at higher temperatures.

d. Diverting the electronics heat load to a separate radiator operating at higher temperature results in a lower temperature refrigerator heat sink and weight reduction.

3.4.2 Radiator Heat Loads

3.4.2.1 Instrument Heat. The IRLE instrument components are assigned to radiator A and radiator B as follows.

Radiator A (area = 0.20 m^2)

Component	Heat Load (W)
Power Dist.	18
PCE	15
A/D	8.3
10% margin	4.1
TOTAL	45.4

Radiator B (area = 0.49 m^2)

Component	Heat Load (W)
Cooler	
Compressors	34
Displacers	14
Electronics	11
Telescope	
Scan Mtr and Tach	5.3
Aperture	3
Calibration	2.5
Chopper	.8
Flip-In Mirror	.4
10% margin	7.1
TOTAL	78.1

Increasing detector temperature from 70 to 75 Kelvin decreases the heat load on radiator B by 4 W.

3.4.2.2 Earthshine and Albedo. The radiators are mounted on the sun-shaded end of the instrument platform; therefore, under normal operating conditions, they will never be exposed to direct sunlight. Assuming a 3 o'clock, 600 km, 98.6 deg sun-synchronous orbit, the computer model Simplified Space Platform Thermal Analyzer (SSPTA) predicts that earthshine flux incident to the radiator will be about 56.4 W/m^2 and is nearly constant. Albedo incident flux, a function of both position in orbit and time of year, will vary from zero to 80 W/m^2, averaging about 24.5 W/m^2. Typical results are shown in Figure 3.4-1.

Assuming that the selective surface absorptivities for the longer wavelength earthshine and the shorter wavelength albedo are .75 and .20 respectively, the absorbed heat flux on the radiators from these sources becomes 42.3 W/m^2 from earthshine and an average of approximately 4.9 W/m^2 from albedo for a total of 47.2 W/m^2.

3.4.3 Radiator Average Temperatures

At equilibrium

instrument heat + earthshine + albedo = heat emitted

It is assumed that a total emissivity of .75 or greater may be maintained on the radiating surfaces over the entire mission.

Therefore, for radiator A

$$45.4\ W + 47.2\ \frac{W}{m^2}(0.2\ m^2) = (0.75)(0.2)(5.67)(T_A \times 10^{-2})^4$$

or

$$T_A = 283\ K$$

The average temperature of radiator B is similarly calculated from

$$78.1\ W + 47.2\ (0.49) = 0.75(0.49)(5.67(T_B \times 10^{-2})^4$$

$$T_B = 264\ K$$

Thus, Radiator B is expected to operate at a temperature nearly 20 Kelvin lower than radiator A.

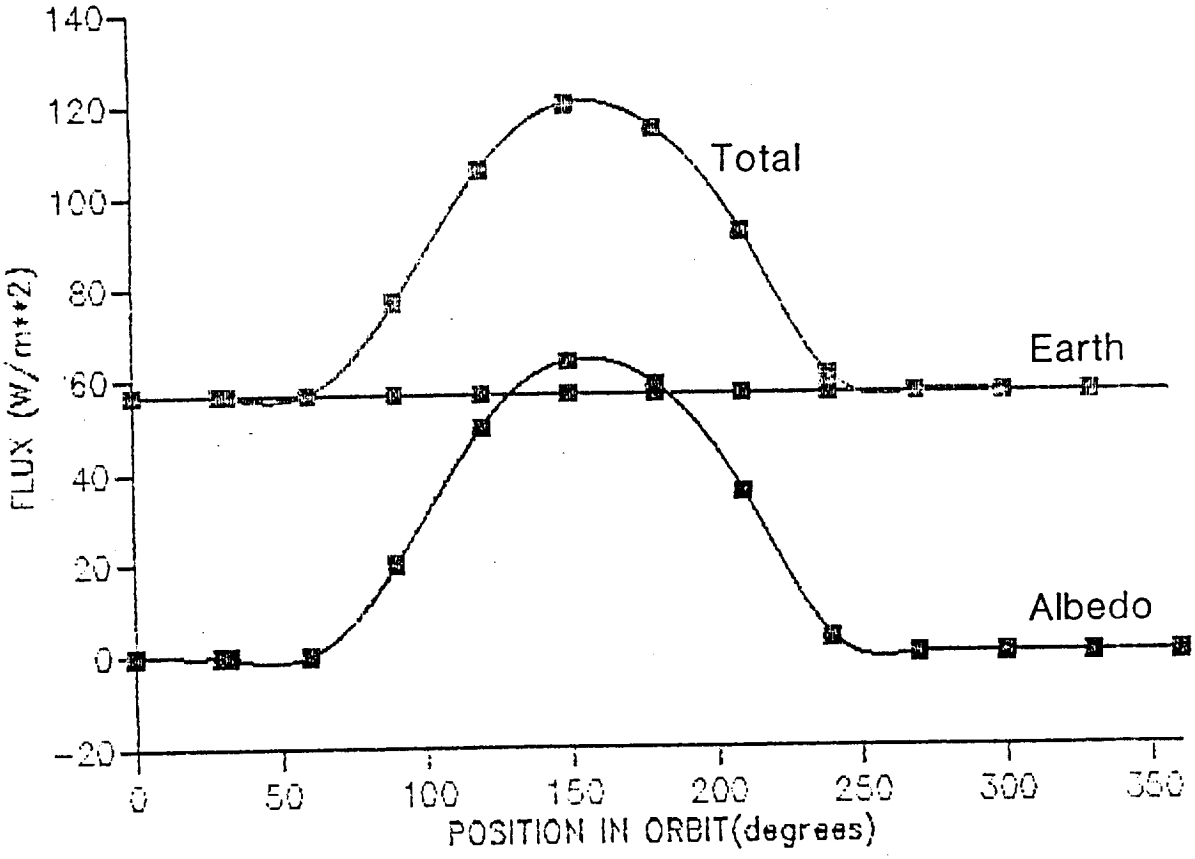

Figure 3.4-1. Earthshine and Albedo Flux Variance

3.4.4 Variation in Radiator Temperature

The radiator temperature will vary due primarily to changes in albedo heat flux (see Figure 3.4-1). The amplitude of the variation may be reduced by:

a. Coating the radiator with a material having a low spectral absorptivity for solar radiation.

b. Increasing the thermal inertia of the system to which the radiator is thermally connected.

A simple lumped capacity model based on the following parameters was used to evaluate the magnitude of the radiator temperature variation.

Radiator area	.49 m^2
Lumped mass	27.0 kg
Radiator	8.6 kg
Compressors & displacers	7.8 kg
Electronics package	4.6 kg
Mounting plates	6.0 kg
Instrument heat load	78.1 W
Radiator absorptivity	
Earthshine	.75
Albedo	.20
Radiator emissivity	.75

(Earthshine and albedo as predicted by SSPTA. See paragraph 3.4.2.2 and Figure 3.4-1.)

The results, shown in Figure 3.4-2, indicate that radiator B and the components to which it is thermally connected should not experience temperature variation amplitudes greater than about .3 Kelvin. The period of this variation is approximately 90 minutes about once each orbit.

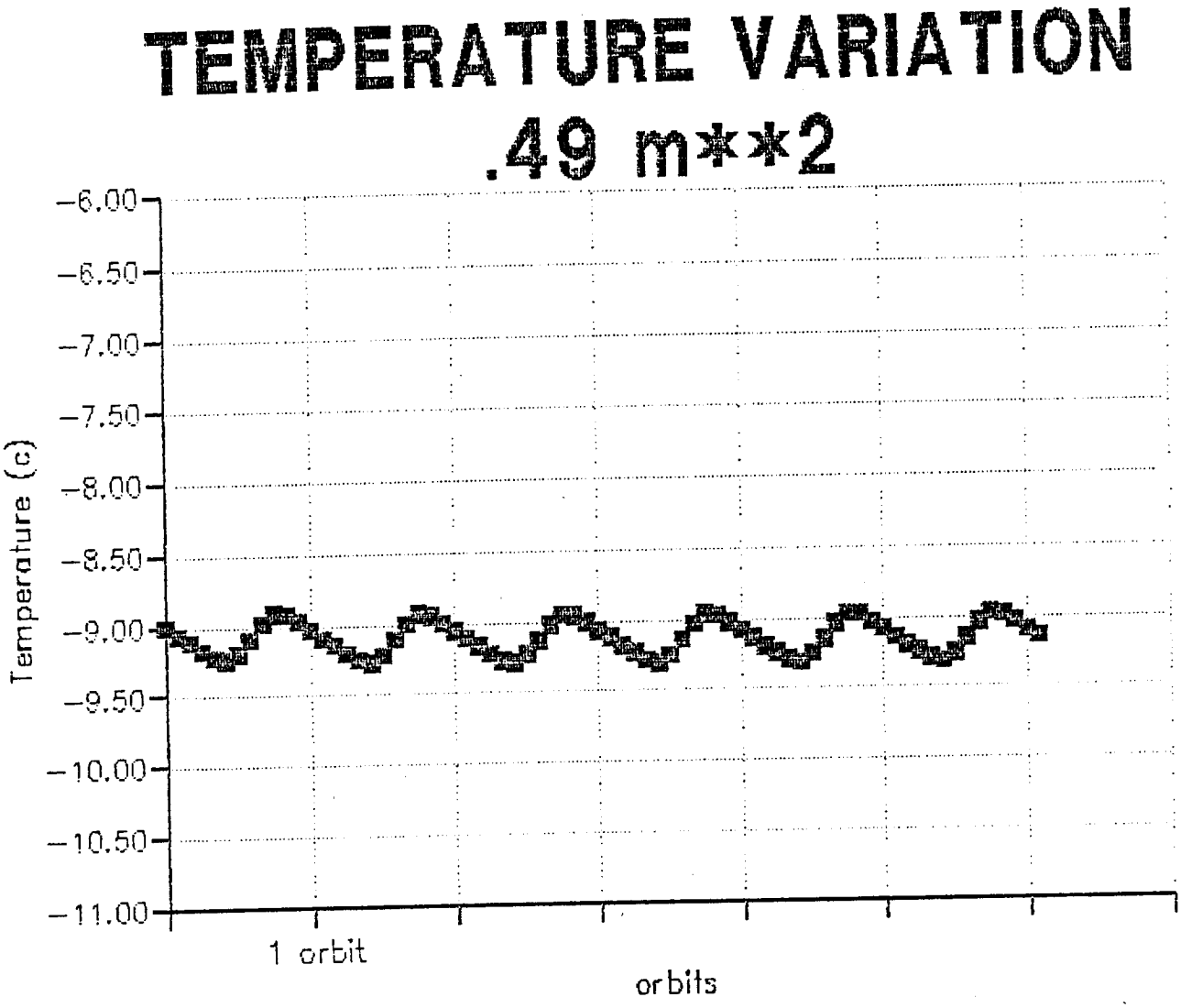

Figure 3.4-2. Temperature Variation

3.4.5 Radiator and Thermal Linkages Radiator Mass

The severe weight constraints on the IRLE instrument design have driven assumptions made for mass calculations. The radiators are assumed to be 1/4-in. thick aluminum plate which will require stiffening and extra material placed at thermal connections to avoid hot spots. The radiators may thus be thinner than 1/4 in. in some places and thicker than 1/4 in. in other places. Assuming a 1/4-in. average thickness, the following results:

$$M_A = 2770 \times .20\ m^2 \times .25\ in \times .0254\ in/in^2 = 3.52\ kg$$

$$M_B = 2770\ kg/m^3 \times .49\ m^2 \times .25\ in \times .0254\ m/in = 8.62$$

$$M_A + M_B = 12.14\ kg = 26.7\ lb$$

3.4.6 Survival Heat

The radiators are located on the IRLE instrument such that they are always exposed to earthshine and thus, in the event of a power failure, temperatures will not drop to levels expected for radiators pointing to deep space.

The equilibrium temperature for the IRLE system with no instrument power is calculated as

$$\text{earthshine} + \text{albedo} = \epsilon\sigma T^4$$

or

$$47.2 = .75(5.67)(Tx10^{-2})^4$$

The no-power temperature based on this calculation is about 183 Kelvin. Survival temperature for all refrigerator components, including electronics thermally linked to radiator B, are specified as -45 to 85°C (228 to 358 K). The other electronics packages thermally linked to radiator A have a specified survival temperature range of -55 to 125°C (218 to 398 K).

Survival heater requirements are estimated as follows:

$$\text{survival heat} = \epsilon A \sigma T^4 - (\text{earthshine} + \text{albedo})$$

For radiator A

$$Q_{survival} = .75(.20)(5.67)(2.18)^4 - 47.2(.2)$$
$$= 19.21 - 9.44 = 9.8 \text{ W}$$

For radiator B

$$Q_{survival} = .75(.49)(5.67)(2.28)^4 = -47.2(.49)$$
$$= 56.31 - 23.13 = 33.2 \text{ W}$$

Heating elements will be placed at appropriate locations on component mounting surfaces.

3.5 ELECTRONICS

3.5.1 Signal Processing Method

One of the primary electronics design goals is to preserve 16-bit accuracy on all nine signal channels. This goal is accomplished by a combination of careful analog design and early conversion of the signals to digital form. Conversion of the IRLE radiometric data to digital form at the output of the preamplifiers minimizes linearity, noise, and environmental problems. The synchronous demodulation and low-pass filtering are then performed digitally. This procedure is accomplished in three steps: sampling, demodulation, and filtering.

3.5.1.1 Signal Sampling. The first step in the IRLE digital signal processing is to sample the analog signal at the output of the low-pass filter preamplifiers. Sampling the signal introduces aliasing; that is, it folds the signal spectrum at integer multiples of half the sampling frequency so that in the sampled spectrum all spectral components occur at frequencies less than half the sampling frequency. The effects of aliasing can be made negligible by a judicious choice of the sampling frequency with respect to the chopping frequency and by low-pass filtering the analog signal before sampling. For a chopping frequency of 700 Hz and a sampling frequency of 2975 Hz, the first harmonic after the fundamental that occurs at the chopping frequency in the sampled

spectrum is number 16. But the amplitude of this harmonic is zero because the chopped waveform has half-wave symmetry which requires that the amplitude of all even harmonics equal zero. The next harmonic to occur at the chopping frequency is number 33. The amplitude of this harmonic is at least 61 dB less than the fundamental because for half-wave symmetry the harmonic amplitude decreases as $1/n^2$ where n is the harmonic number. A 2-pole low-pass filter in the preamplifier with a corner frequency of 3500 Hz will provide an additional 33 dB attenuation of harmonic number 33. Thus, the total attenuation is 94 dB, which is just 2 dB short of the 96 dB corresponding to the 16-bit dynamic range of IRLE. If this 2 dB deficit is judged to be important, a sampling frequency of 3300 Hz could be chosen. For this sampling frequency the first odd harmonic after the fundamental to occur at the 700 Hz chopping frequency is number 63. This harmonic is at least 72 dB down from the fundamental, thus the low-pass filter need only supply 24 dB attenuation at 44.1 kHz to reach the total 96 dB attenuation that corresponds to the 16-bit dynamic range of IRLE.

3.5.1.2 Synchronous Demodulation. The second step in IRLE digital signal processing, synchronous demodulation, is accomplished by changing the sign of the sampled detector signal at the proper time, which is determined by the chopper reference signal and the time delay of the detector and preamplifier. The chopper reference signal is squared up by a phase-lock loop and then digital delay circuits for each signal channel delay the squarewave by the amount appropriate for that particular channel. The state of this delayed squarewave is examined whenever a signal sample is obtained. If the state of this delayed squarewave is low, the signal sample is negated; but if the state of this waveform is high, then the signal sample is not negated. This process is performed on a real-time basis.

3.5.1.3 Digital Low-Pass Filtering. The third step in IRLE digital signal processing, digital low-pass filtering, obtains the final output data. This step uses a high-speed microprocessor, a TI TMS320 model. The rectified digital detector samples are stored in a two-port memory buffer through one of the ports. When the selected number of samples are stored in this memory, the TMS320 accesses the data through the second port and performs the digital convolution with the selected filter weights. The result of this convolution is then sent to the IRLE system control as an output digital data value.

The IRLE digital filter will have a bandwidth of about 4 Hz. The nearest harmonic that it must reject is at 175 Hz for a sampling frequency of 2975 Hz and at 100 Hz for a sampling frequency of 3300 Hz. This rejection requirement can easily be met by a digital filter.

The final output data rate of the IRLE instrument is 12 samples per second per channel. A 256 weight digital filter would require 3072 samples per second per channel. The sampling frequencies of 2975 Hz and 3300 Hz previously chosen will result in a filter output data rate of 11.62 and 12.89 samples per second per channel, respectively, using a 256 weight filter.

Because of the high amount of over sampling (about 128 times), it is possible to extend the resolution of the digital filter beyond the 16 bits used in the input data. However, this approach would require the digital filter microprocessor to carry more than 16 bits in its computations.

3.5.2 Electronic Functional Groups

The IRLE instrument electronics are divided into five functional groups: (1) preamplifiers, (2) digital signal processor, (3) scan and flip control, (4) system control and housekeeping, and (5) power distribution.

3.5.2.1 Preamplifiers. Two types of preamplifiers are used: a bipolar operational amplifier (op-amp) input stage is used for the low-resistance HgCdTe detectors, while a JFET op-amp input stage is used for the high-resistance InSb detectors.

The HgCdTe detector preamplifier is shown in Figure 3.5-1. A bipolar op-amp, the LT1028, is used for the first stage because of its low-input noise voltage (1 $nV/Hz^{1/2}$) and because its current noise is negligible due to the low resistance (less than 1 kΩ) of the HgCdTe detectors.

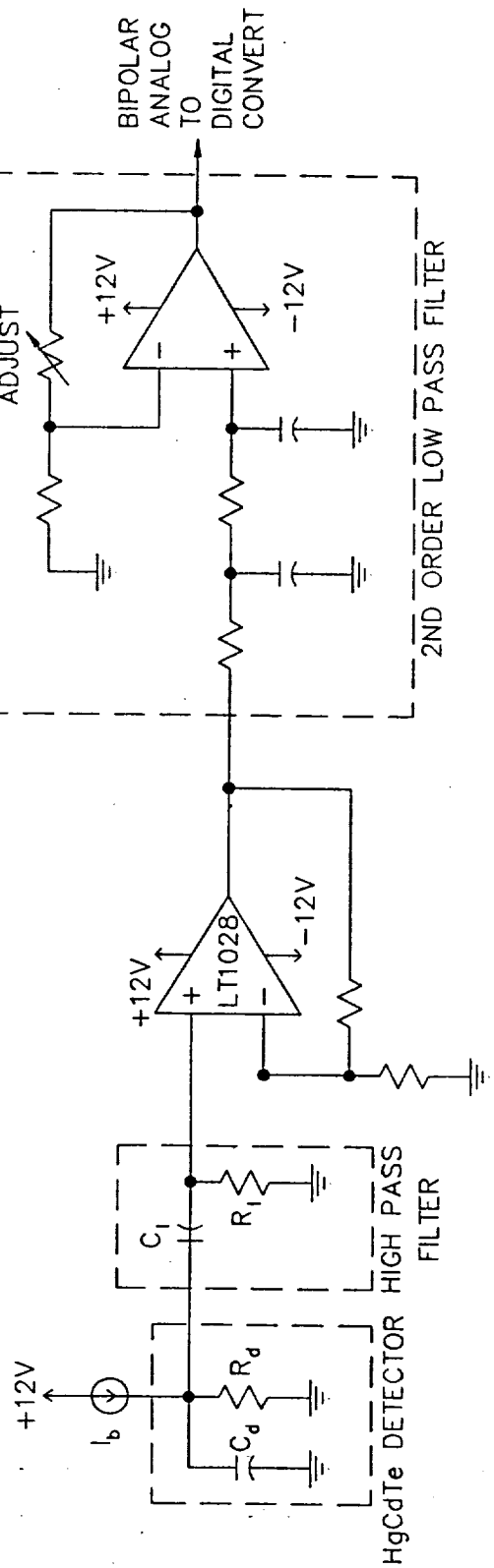

Figure 3.5-1. Preamplifier for HgCdTe Detectors

The input noise voltage component dominates the current noise component and the Johnson noise components even with the feedback resistor at ambient temperature. The entire preamplifier can be run warm since the input capacitance of long leads is not significant. The dc offset is removed by the high-pass circuit formed by R_1 and C_1 at the input of the first stage. This circuit can be located here because of the low resistance of the HgCdTe detectors. The second-order low-pass filter prevents aliasing due to sampling as described in paragraph 3.5.1.1. This filter also has adjustable gain so that the signal level can be matched to the input requirements of the bipolar A/D converter.

The InSb detector preamplifier is shown in Figure 3.5-2. The first stage of this preamplifier uses a JFET op-amp rather than a bipolar op-amp because the noise current must flow through the extremely large resistance of the InSb detector (greater than 10 MΩ). The Burr Brown OPA 111 JFET op-amp, which has an input noise current of only 0.5 $fA/Hz_{1/2}$ and an input noise voltage of 8 $nv/Hz^{1/2}$, was selected for the input stage of this preamplifier.

The input stage of the InSb detector preamplifier is a double-compensated amplifier design. Compensation is necessary because the large detector resistance requires a feedback resistor of approximately 10^8 Ω to obtain significant gain in the first stage. The small amount of stray capacitance associated with the feedback resistance creates a pole that is significant at the 700 Hz chopping frequency. To overcome the uncertainty of the location of this pole, a capacitor C_L is added to dominate the stray capacitance associated with R_L. The pole associated with C_L is canceled by the zero associated with C_C; the result is a frequency compensated feedback network. However, frequency compensating the feedback network results in amplifier instability. This instability results because the amplifier transfer function equals $-R_f/Z_d$, where R_f is the dc resistance of the feedback network and Z_d is the parallel combination of the detector resistance R_d, the detector capacitance C_d, and any stray capacitance at the amplifier input. Thus, Z_d introduces a zero into the amplifier transfer function. For frequencies above this zero, the gain rolls up at 20 dB per decade so that at the point where the gain curve intersects the op-amp gain curve the rate of closure is 40 dB and instability results. Instability is corrected by adding C_S, which adds a pole that limits the rate of closure to 20 dB per decade.

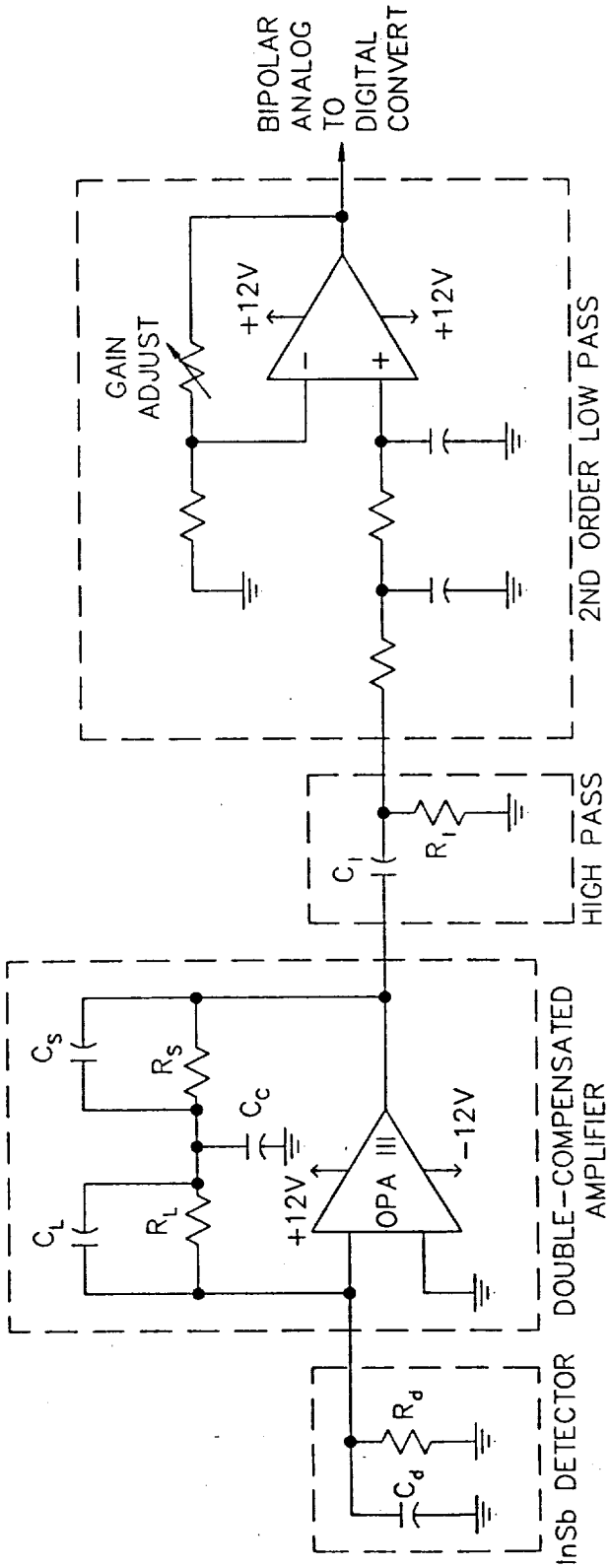

Figure 3.5-2. Preamplifier for InSb Detectors

In the InSb detector preamplifier, the low-pass circuit is located after the input stage because of the large resistance of the InSb detector. This circuit removes the dc offset. The second-order low-pass filter prevents aliasing due to sampling as explained in paragraph 3.5.1.1. This filter also has a gain adjustment for matching the signal level to the bipolar A/D converter.

3.5.2.2 Digital Signal Processor. The function of the digital signal processor (DSP) electronics group is to sample, synchronous rectify, and low-pass filter the detector signal from each of the nine detector channels. A block diagram of the DSP is shown in Figure 3.5-3. The detector and the detector preamplifier/filter are part of the detector module.

Each of the nine detector signals is individually sampled with a Crystal 16-bit low-power A/D as shown at the left of Figure 3.5-3. This avoids the crosstalk, noise, and accuracy problems associated with an analog mux. The start of conversion (SOC) input of each A/D is connected in parallel to the timer output of NSC 810 #2. This timer counts down the 4 MHz clock to provide the correct sampling frequency. Since all channels are sampled at the same time, temporal correlation between the channels is preserved.

The end of conversion (EOC) output of each A/D is connected individually to one of the digital inputs of ports A and B of NSC 810 #2. This connection allows the NSC 800 microprocessor, shown at the middle right of Figure 3.5-3, to sense an EOC for each channel A/D.

The 16 digital outputs of each channel are respectively connected together to form a 16-bit data bus. These outputs are tristate controlled by the chip select (CS) input of each A/D. Only one A/D will have control of the 16-bit data bus at a time.

The digital synchronous rectifier block, shown at the top middle of Figure 3.5-3, has as input the A/D 16-bit data and outputs 16-bits of data to I/O ports A and B of NSC 810 #1, shown to the right of the figure. The 16-bit output of the digital synchronous rectifier is either identical to the input or the negative of the input as selected by the synchronous sign generator.

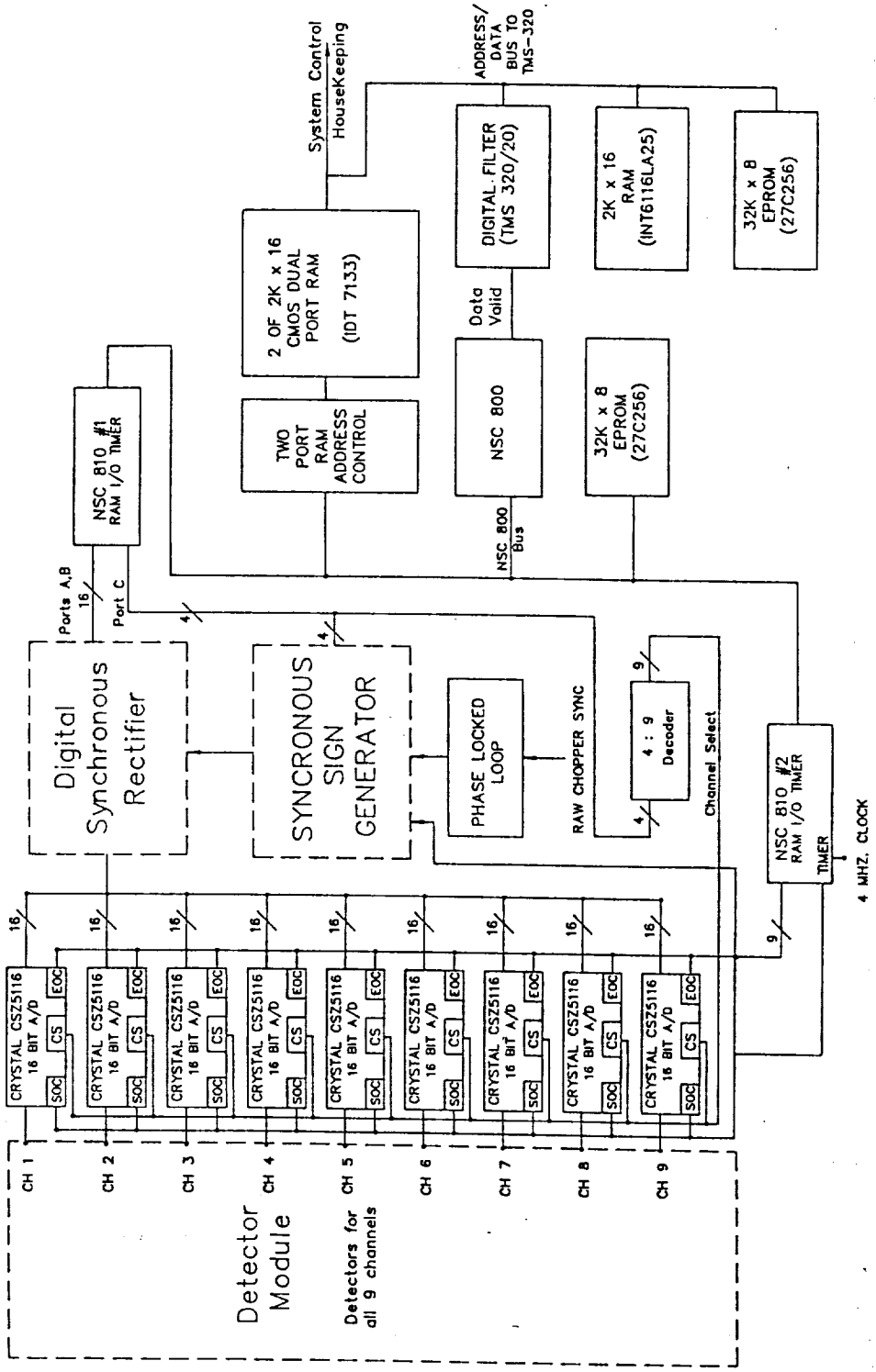

Figure 3.5-3. Digital Signal Processor

Detail of the digital synchronous rectifier is shown in Figure 3.5-4. The circuit shown forms a 64 K x 16 EPROM. The 16-bit input data is applied to the address lines of the composite EPROM. Each 16-bit memory location is programmed to contain the negative (in two's complement form) of the address used to select it. This negated data is input to a 16-bit tristate buffer and the non-negated data is input to a second 16-bit tristate buffer. The respective buffer outputs are connected in parallel forming the 16-bit synchronous rectified data bus.

The synchronous sign generator, shown at the bottom of Figure 3.5-4, determines whether to select the direct of negated data. The input to this circuit is a digital pulse generated at the start of each half cycle of the chopper by a phase-locked loop. Each time one of these pulses occurs, an 8-bit binary counter is started counting a 4 MHz clock. This counter will count to zero in 64 μs in increments of 0.25 μs and stop until the next start pulse is applied. The 8-bit binary count is input to the following time delay latch.

Nine of the flip-flops within the time delay PAL device (one for each detector channel) will be programmed to toggle when a predetermined count occurs on the 8-bit counter. The output of each flip-flop is the delayed synchronous demodulation signal required to synchronously rectify the respective detector channel data. The final function performed is to store (in a 9-bit latch) the state of the synchronous demodulation signal for each channel at the time of the A/D SOC. One of the channels is selected by a 9:1 mux (controlled by a 4-bit channel select signal) to control the sign selection of the respective detector channel data.

As shown in Figure 3.5-3, the phase-locked loop block generates the digital pulses required to control the synchronous sign generator. The phase-locked loop input is the raw chopper sync.

The NSC 800 microprocessor, shown at the middle right of Figure 3.5-3, performs the sample control. Connected to this microprocessor by an NSC 800 bus are the two NSC 810s, a 32 K x 8 EPROM (for program storage) and the 2-port RAM used to store the rectified data samples. On initialization, all flip-flops are reset and the NSC 800 presets both 810s to the proper configuration. The timer of 810 #2 is preset to generate the correct sampling frequency.

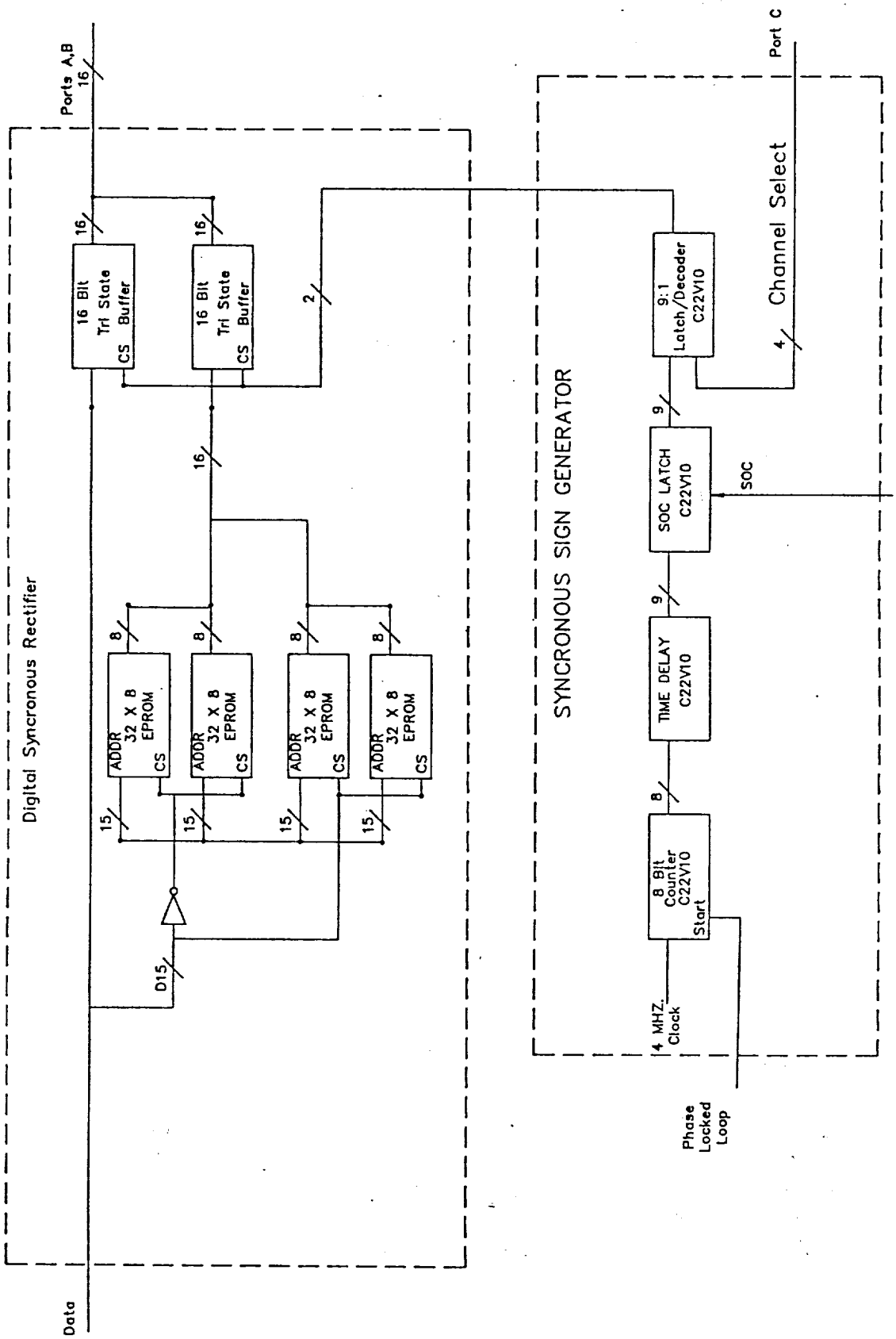

Figure 3.5-4. Digital Synchronous Rectifier and Sign Generator

One operational cycle of the NSC 800 is as follows.

1. Wait for an EOC on channel 1 (through 810 #2).
2. Output channel 1 address through port C of 810 #1. This inputs the channel 1 A/D 16-bit output into the digital synchronous rectifier input. It also selects the channel 1 sign bit from the synchronous sign generator. By the time this instruction is complete, the synchronously rectified data for the first sample of channel 1 is present at ports A and B of 810 #1.
3. Read the input data from 810 #1 and store it in the 2-port RAM in the section reserved for channel 1.
4. Repeat steps 1 through 3 for each of the other channels.

At a sampling frequency of 3300 kHz, about 34 μs per channel are available to complete the above operations. This provides 136 T-states for the NSC 800 which should be adequate.

The 2-port RAM is organized in nine sections (one section per channel) with two buffers per section. When the NSC 800 fills one buffer, it automatically begins filling the second buffer. When the second buffer is full, the first buffer is used. This double-buffer organization allows the digital filter to work with one buffer while the other buffer is being filled with data.

The digital filter is implemented using a TI TMS82020. Connected to the TMS320 is the 2-port RAM (for data access), a high-speed 2 K x 16 RAM (for program execution), and a 32 K x 8 EPROM (for program storage).

When a buffer for channel 1 is filled, the TMS320 performs a filter convolution with data from that buffer and outputs the 16-bit result to the system control microprocessor. The TMS320 then moves to the same buffer of each of the other channels and repeats the process. A direct communication link between the NSC 800 and the TMS320 is provided for the necessary handshaking.

3.5.2.3 Scan and Flip-In Mirror Controller. The scan and flip-in mirror control electronics group contains the control systems necessary to implement the analog electronic drive for the scan mirror and the stepping controller to drive the flip-in mirrors. This package also contains a microprocessor which automatically sets the limb scan limits based on data from the CO_2 channels.

A block diagram of the scan and flip-in mirror control is shown in Figure 3.5-5. At the right of this figure is a velocity feedback servo circuit designed to provide the current drive for the scan mirror torque motor. An 8:1 analog at the input to the servo circuit provides a selection of constant velocity voltages. The velocity voltage is selected under control of the NSC 800 microprocessor through 810 #3.

The NSC 800 is connected to two 810s, a 2 K x 8 static RAM for storage of CO_2-wide limb data and scan limit constants, and a 32 K x 8 EPROM for program storage. The calibrate and cage signals from the scan encoder are input into 810 #3, and the same signals from the flip-in encoder are input into 810 #4. The scan encoder fine marker signal is input into the 810 #3 counter, and the flip encoder fine marker is input into the 810 #4 counter. The scan mirror velocity is controlled by 810 #3, and the flip-in mirror stepping motor controller is controlled by 810 #4.

NSC 810 #4 also receives a 16-bit value for the CO_2-wide detector channel each time the signal processing digital filter performs the computation. The corresponding scan position is read from the counter of 810 #3. During and initialization sequence, the limb position will be determined from this data and appropriate short scan limits set.

During normal operation, the NSC 800 is programmed to read the scan fine marker counter, compare the value against the scan limits, and select the appropriate scan voltage. The scan mirror position data is not output.

During a calibration sequence when the flip-in mirror is activated, 810 #4 provides the proper control signals to the flip stepping motor controller. Proper mirror position is verified by the flip fine marker counter in 810 #4.

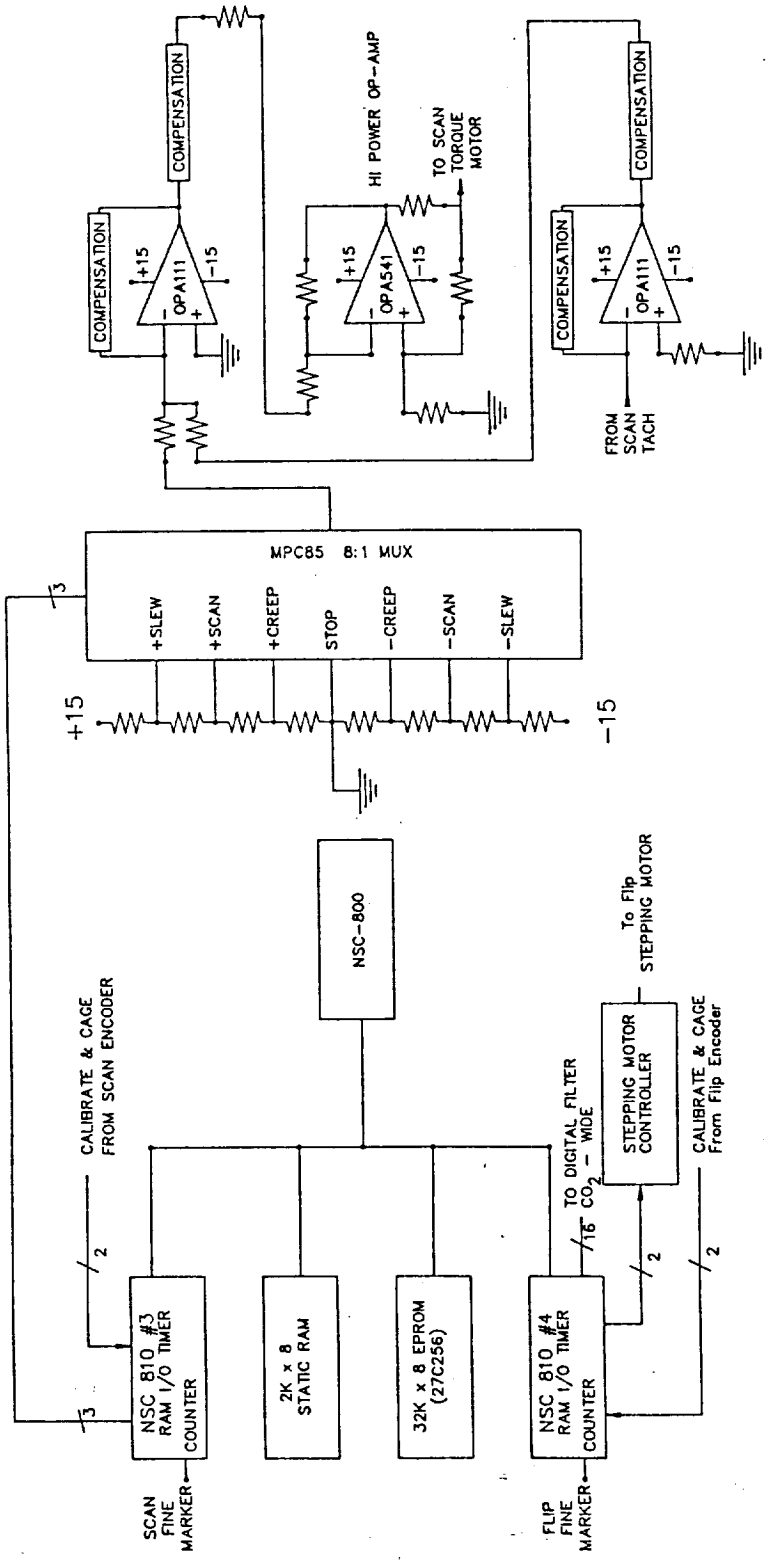

Figure 3.5-5. Scan and Flip-In Mirror Controller

3.5.2.4 System Control and Housekeeping. The system control and housekeeping electronics group contains the interface between the IRLE payload and the spacecraft 1553 bus. This interface will receive the serial commands uploaded through the spacecraft and provide the downlink path for the IRLE scientific data. This package contains the housekeeping data acquisition circuits and a link to the digital signal processor package. For the IRLE instrument, the SIRT module will be used to communicate with the spacecraft bus. This section describes an alternative communication method in the event that the SIRT module is not completed on schedule.

The system control and housekeeping electronics are shown in Figure 3.5-6. It includes an NSC 800 microprocessor, a 32 K x 8 EPROM for program storage, a 2 K x 8 RAM for data buffering and interprocessor commands, an NSC 810 for interfacing with the digital filter, a 1553 microprocessor interface module, and a 1553 RTU for connection to the spacecraft 1553 bus. It also contains an NSC 810 for digital housekeeping data and a 12-bit A/D for analog housekeeping data.

The primary function programmed into the NSC 800 is to receive 108 16-bit data points each second (12 for each channel) and place them on the spacecraft bus. Other functions include acquiring both digital and analog housekeeping data and including it on the spacecraft bus.

The NSC 800 program will also receive commands from the spacecraft bus. The commands will be either implemented by the program or passed on to another IRLE microprocessor controller. The communication between microprocessors is implemented by placing the 2 K x 8 RAM memory in common with all microprocessors, using the STD bus standards. Buffers in this memory are reserved for the necessary handshaking and command communication.

The housekeeping requirements are not currently well defined. A spacecraft standard 1553 bus interface and housekeeping module may be used. The system control electronics will require modifications to accommodate these changes.

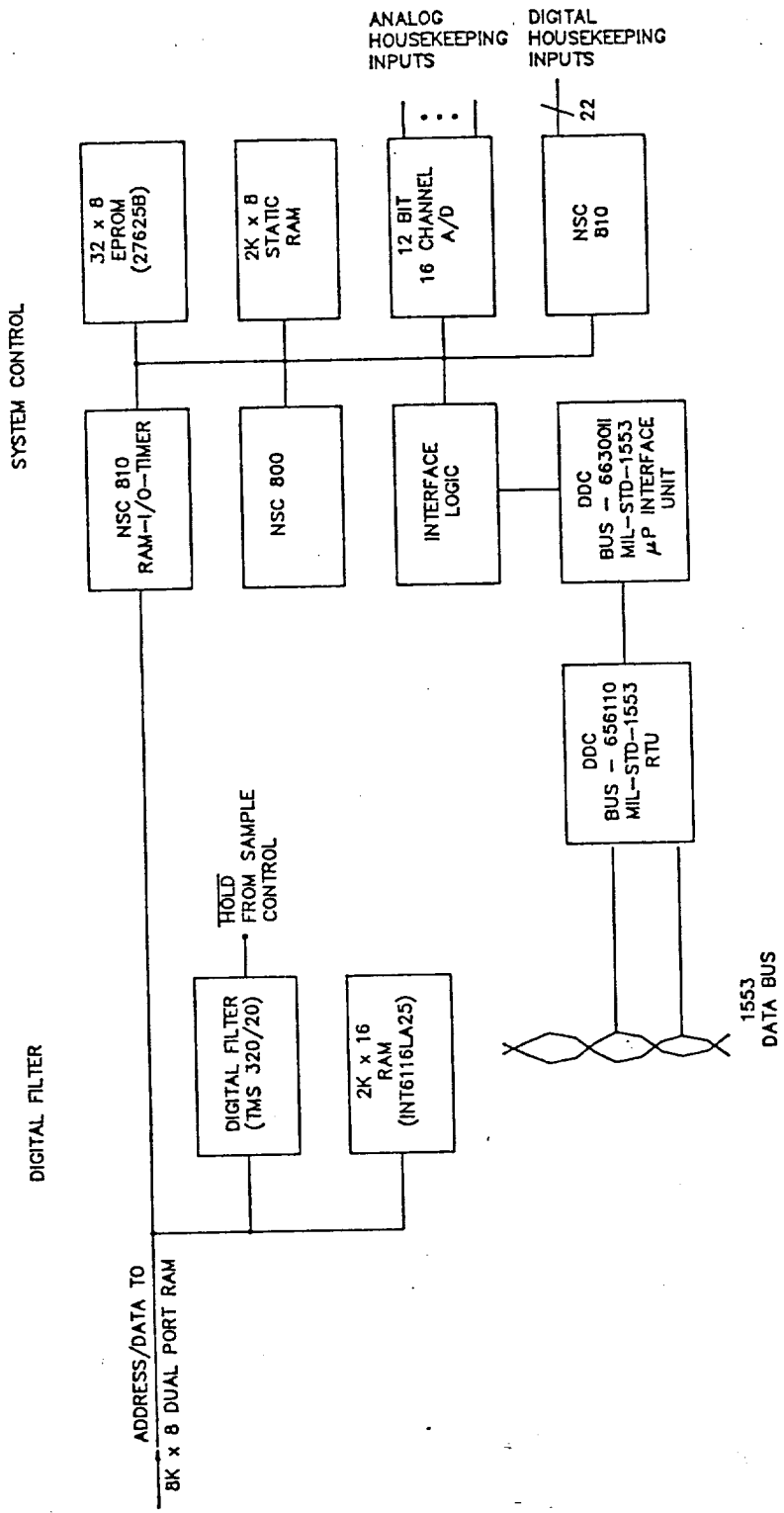

Figure 3.5-6. System Control and Housekeeping

3.5.2.5 Power Distribution Electronics. The power distribution electronics (PDE) system provides the dc power levels required by the IRLE modules. The major design requirement for this system is that its noise must be small enough to allow IRLE to make 16-bit measurements. This stringent requirement results in extra power dissipation and extra weight. The basic PDE system design will be the same as that used on the SPIRIT I sensor, which demonstrated a 16-bit measurement capability. The SPIRIT II PDE system has been constructed using this same basic design, and it is planned to use this system on the SPIRIT III and EDX sensors.

The PDE system is shown in Figure 3.5-7. The spacecraft power is first preregulated to minimize voltage swings and hence minimize power loss in the converters. Power for the survival heaters, and the mechanical action of the refrigerator, is taken from the output of the regulator. This power can be switched on or off by means of a relay attached to the control bus. Power for the rest of the system is supplied to a shielded, low-noise dc-to-ac converter which operates at a frequency of 2500 Hz. The resulting ac power is supplied to five ac-to-dc power supply modules where it is rectified, filtered, and regulated to provide isolated dc outputs. Each ac-to-dc module, except the one supplying the system controller, can be switched on or off by a relay attached to the control bus. Each signal channel has its own isolated power supplies; each supply has its own transformer secondary. The signal channel grounds will be tied together at only one point near the A/D converters.

The PDE system requires an input of 104.1 W; 29.9 W are dissipated internally and 74.2 W are supplied at its output. Thus, the overall efficiency of the PDE is 71 percent and its total mass is 5 kg.

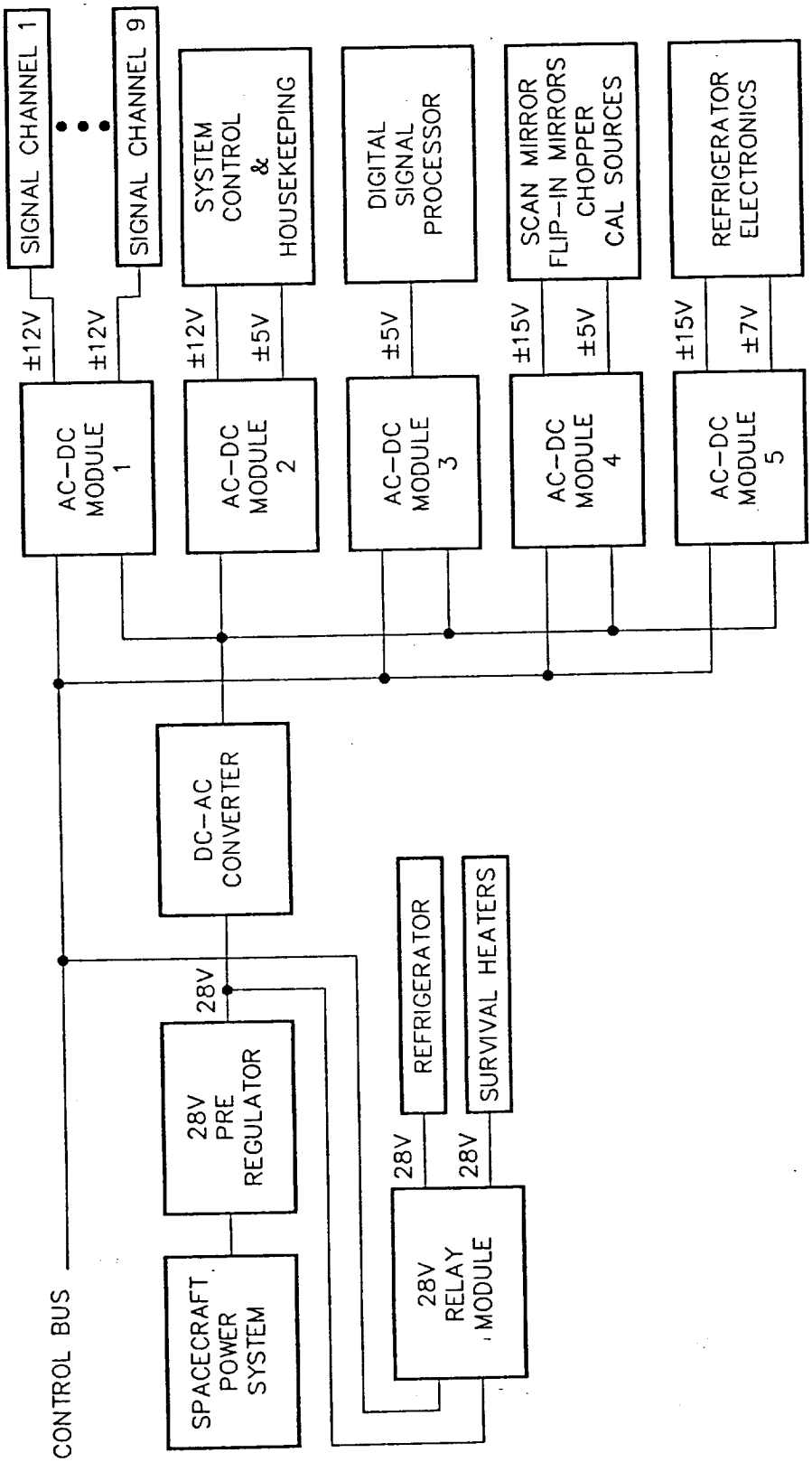

Figure 3.5-7. Power Distribution System Block Diagram

3.5.3 Packaging

All electronics, with the exception of the detector preamplifier/filters, will be mounted in a common STD bus cardcage. By selecting this standard card, connector, and bus structure, commercial extenders and other debug cards may be used. Communication between control microprocessors is also possible using the standard bus definitions. HPIB and other computer interface cards may be easily installed to facilitate engineering checkout and calibration.

The critical nature of the detector electronics will require mounting in individually shielded compartments. These compartments will be mounted in a custom box located as close to the detectors as possible.

3.6 SOFTWARE

3.6.1 Flight Software

The flight software will consist of programs for the following microprocessors:

a. Sample control microprocessor
b. Digital filter microprocessor
c. Scan control microprocessor
d. System control and housekeeping microprocessor
e. 1553 bus RTU
f. NSC 810 I/O interface

Items a, c, and d are NSC 800 microprocessors which are software equivalent to the Zilog Z80. Item b is a TI TMS32020. Items e and f are not microprocessors but programmable devices for which handler modules must be developed.

The sample control software is basically a tight loop transferring data from the synchronous rectifier to the proper location in the 2-port memory. Because of the timing constraints, this software must be written in assembly language for the Z80. The software is expected to be relatively short.

The digital filter software is also a tight convolution loop and must be written in assembly language for the TMS320. The software is expected to be relatively short.

The scan control software is of medium complexity and will involve some tight real-time modules which must be written in Z80 assembly language. The higher level control will be written in C.

The software for the system control microprocessor will be complex because of the large number of functions to be performed. The digital filter data and housekeeping data acquisition modules must be interrupt driven and written in assembly language. The 1553 bus module must be written in assembly language. The remaining control functions will be written in C.

3.6.2 Ground Support Software

Three types of ground support software will be written: control, data recording, and data analysis. Control software provides the required control functions for IRLE, and data recording performs the required data acquisition and storage functions. Both data control and data recording software will be written using the software package called OASSIS; this software will run on the I-TOCC computer system discussed in Section 4. Portions of this software will also be used by the Mission Operations Control Center (MOCC) computer system. Data analysis software will be used for calibration and instrument checkouts. This software will be written mostly in C, and it will run on 386 PC computers described in Section 4.

The control software modules include:

a. A real-time interactive display of the IRLE instrument status. Windows for display of limb, housekeeping, and other instrument status data will be included. A window for uplink command selection will also be included.
b. HPIB interface module.
c. 1553 bus interface module.
d. Remote instrument control modules to remotely perform the functions of the scan and system control microprocessors.

The data recording software modules include:

a. Data recording program including data obtained from the 1553 bus and the HPIB. This module will include an appropriate real-time interactive windowed display.
b. HPIB interface module.
c. 1553 bus interface module.
d. High-speed optical disk interface module.

The data analysis modules include:

a. A complete radiometric calibration module.
b. A data output module displaying radiometric and housekeeping data on screen and output to hard copy.
c. IRLE instrument operational checks.

3.7 IRLE STRUCTURAL/VIBRATION ANALYSIS

3.7.1 IRLE Structural Analysis

Two major components were considered for detailed structural analysis: (1) the "shroud" or suspension/thermal isolation system, and (2) the top radiator/telescope support plate. The shroud will be constructed of a carbon/graphite composite material. This material will be extremely thin (.040 in.) and must therefore be stiffened to prevent buckling and excess vibration.

Structural analysis includes stress and deflection calculations. The finite element package NASTRAN was used to provide these and vibration results. Basic geometry, center of mass locations, and external loading information must be input to obtain these results.

3.7.2 Material Properties

Design properties for carbon/graphite composite and aluminum are given for 300 Kelvin:

a. 6061-T6 Aluminum - Young's Modulus: 10.0 x 10^6 psi
Poissons' Ratio: .33
Thermal Expansion: 23. x 10^{-6} /K
Yield Strength: 40.3 ksi
Thermal Conductivity: 120 W/m-K

b. Carbon/Graphite - Assumed quasi-isotropic $[0/60/-60]_{sym}$ lay-up
Young's Modulus: 10.0×10^6 psi
Poissons' Ratio: .30
Ultimate Strength: >50 ksi
Thermal Conductivity: 3 W/m-K

3.7.3 Shroud Stresses/Deflections

Since no actual load environments have been prescribed at this time, a 10 g static load has been chosen. This acceleration was applied in the X coordinate direction separately and then simultaneously in the X, Y, and Z directions. The masses of the optical system and aluminum top plate were rigidly attached to the shroud top and then accelerated. Stress contours and deflection patterns are shown in Figures 3.7-1 through 3.7-4.

	Maximum Stress:	Maximum Deflection:
10 g X	846 psi	1.69×10^{-3} in.
10 g XYZ	1870 psi	2.99×10^{-3} in.

Stress levels are well below ultimate strength of the composite. Maximum stresses are found at the base of the shroud where it attaches to the rocket bulkhead. Stresses are also concentrated mainly in the corners of the triangular shroud. This condition gives rise to two major points of concern for design: (1) Corners must be well rounded to avoid stress concentrations, and (2) Shroud fixity to the bulkhead must be designed to provide for thicker material in this area and prevent stress concentrations or pull-out.

3.7.4 Top Plate Stresses and Deflections

A simplified analysis of the aluminum radiator/support plate was performed and showed no immediate problems. Final design of stiffening for this plate will be forthcoming.

A .25 in. 6061-T6 Aluminum plate, simply supported around the outer edge and supported by columns on the interior edge, was assumed. A mass of 100 lb was attached to the plate and accelerated axially by 1 g (see Figures 3.7-5 through 3.7-7). The stresses and deflections are linear and may be interpolated for larger loadings.

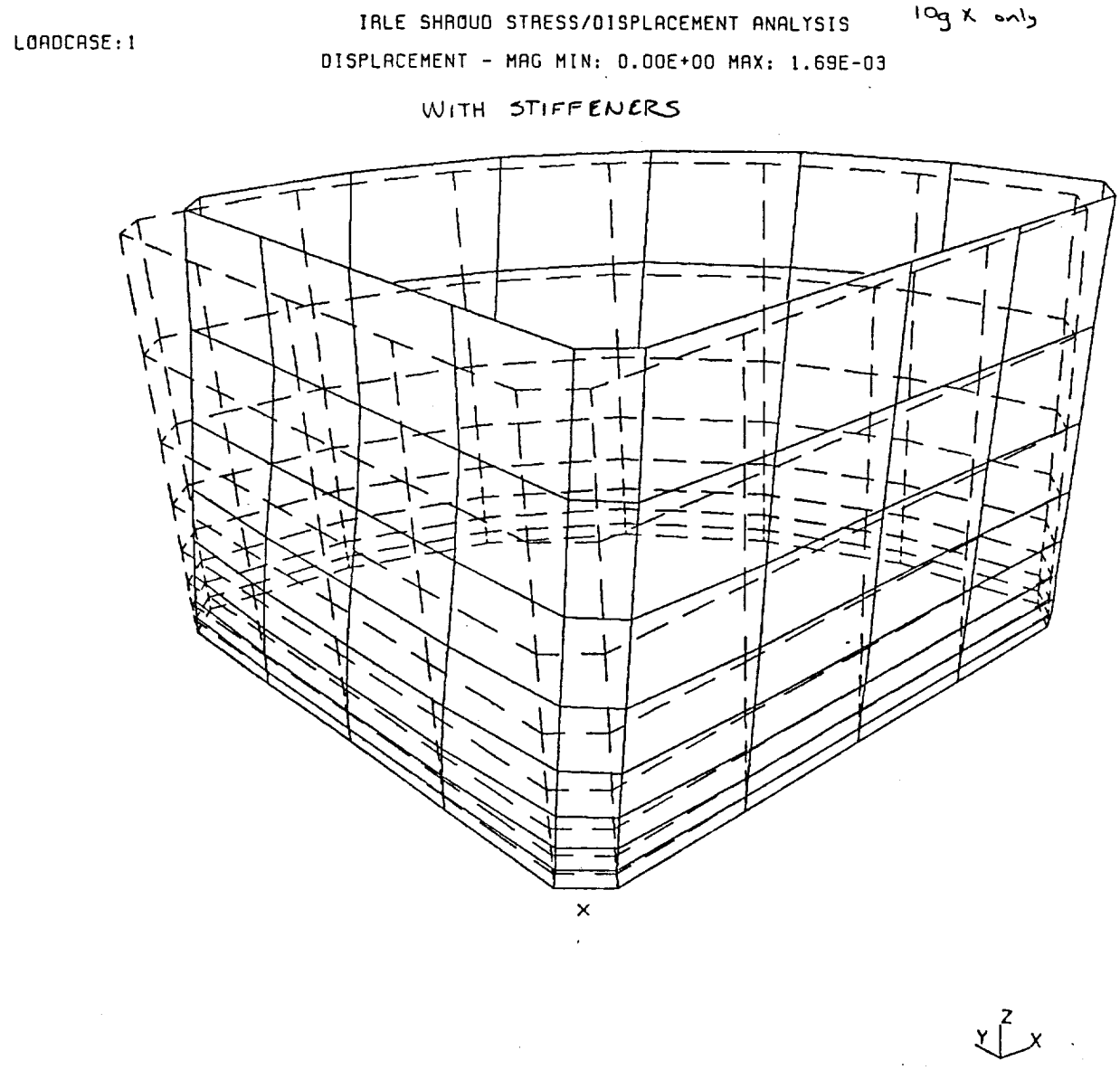

Figure 3.7-1. IRLE Shroud Deflection Analysis (10 g X Only)

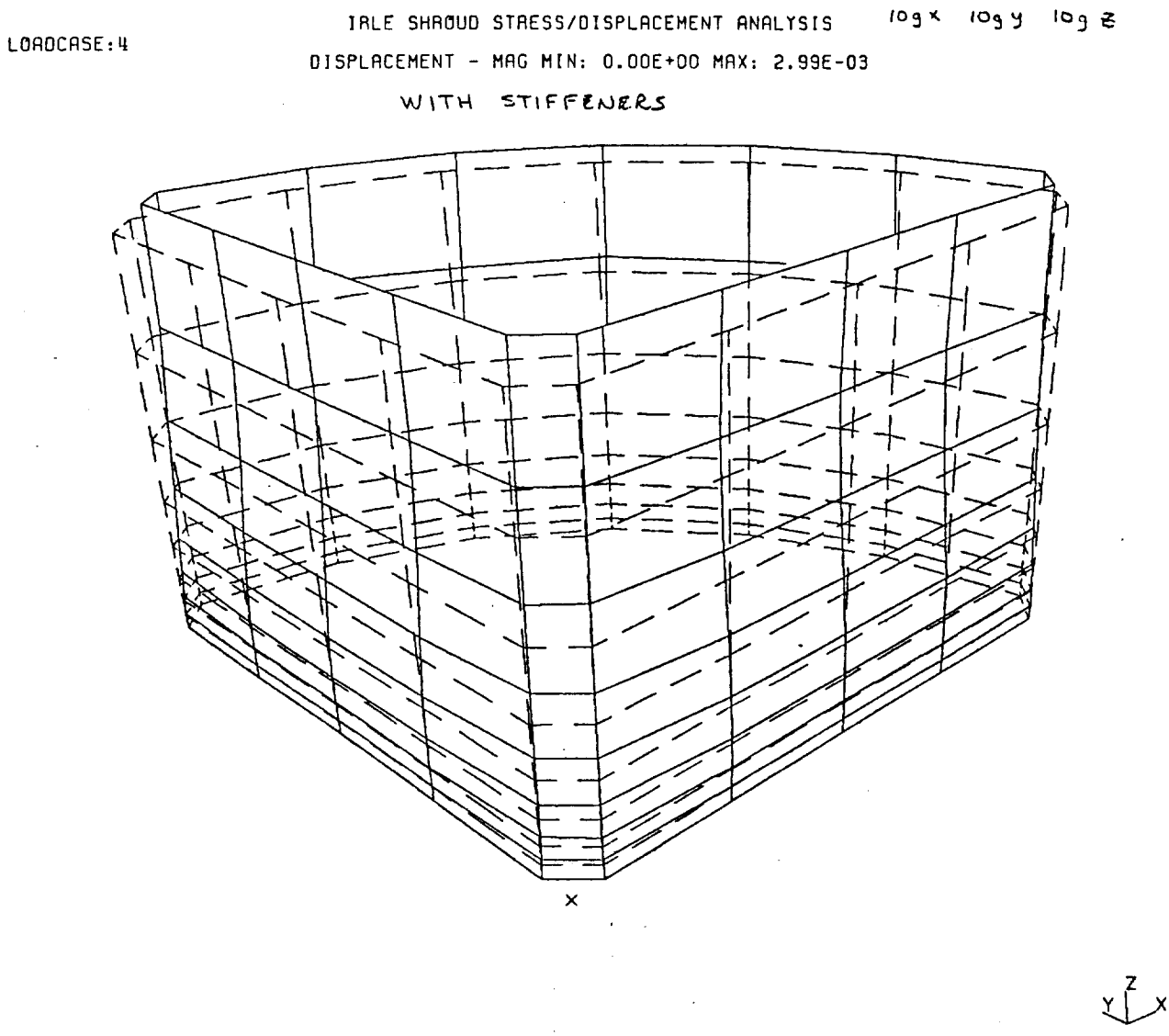

Figure 3.7-2. IRLE Shroud Deflection Analysis (10 g XYZ)

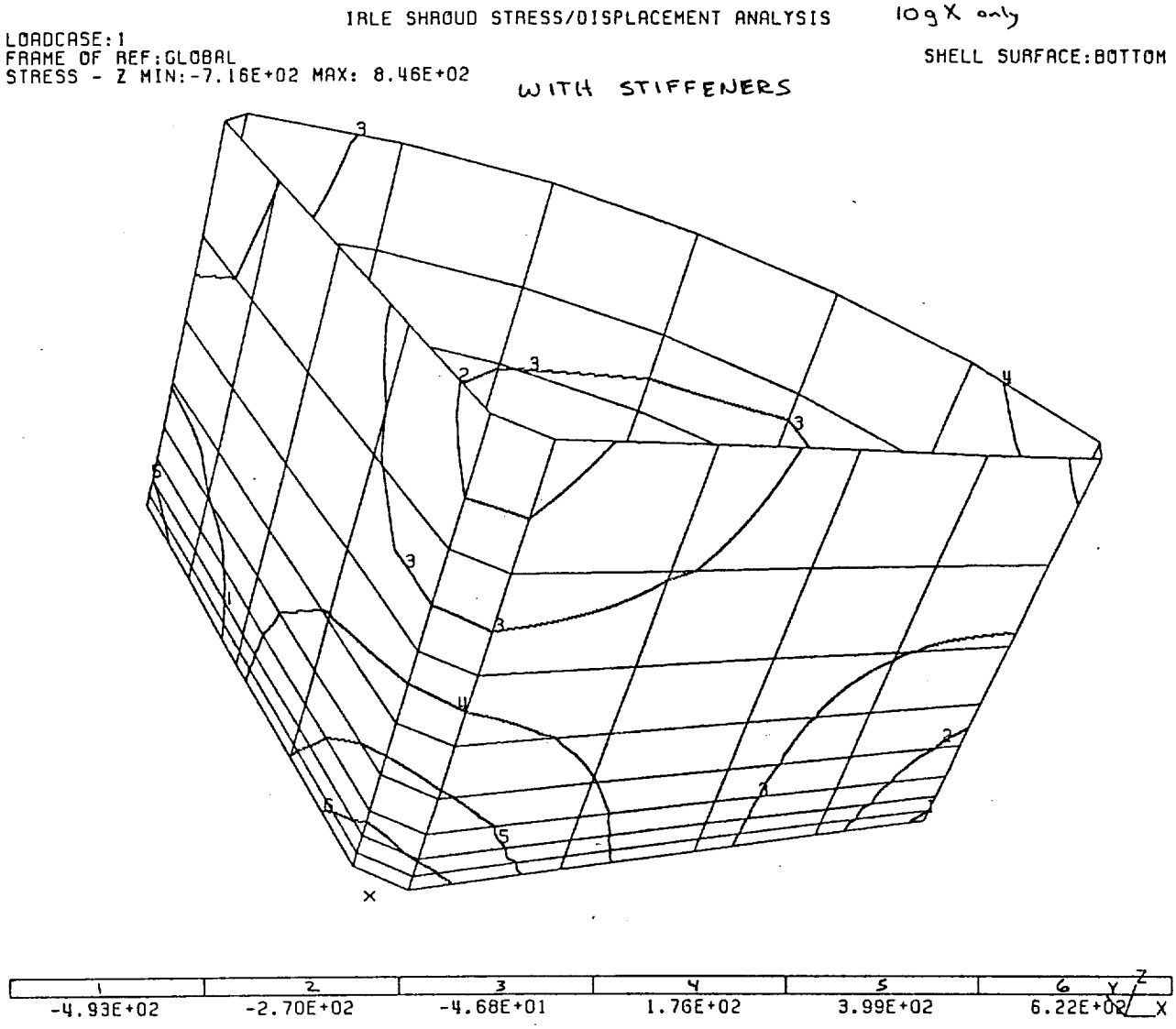

Figure 3.7-3. IRLE Shroud Stress Analysis (10 g X Only)

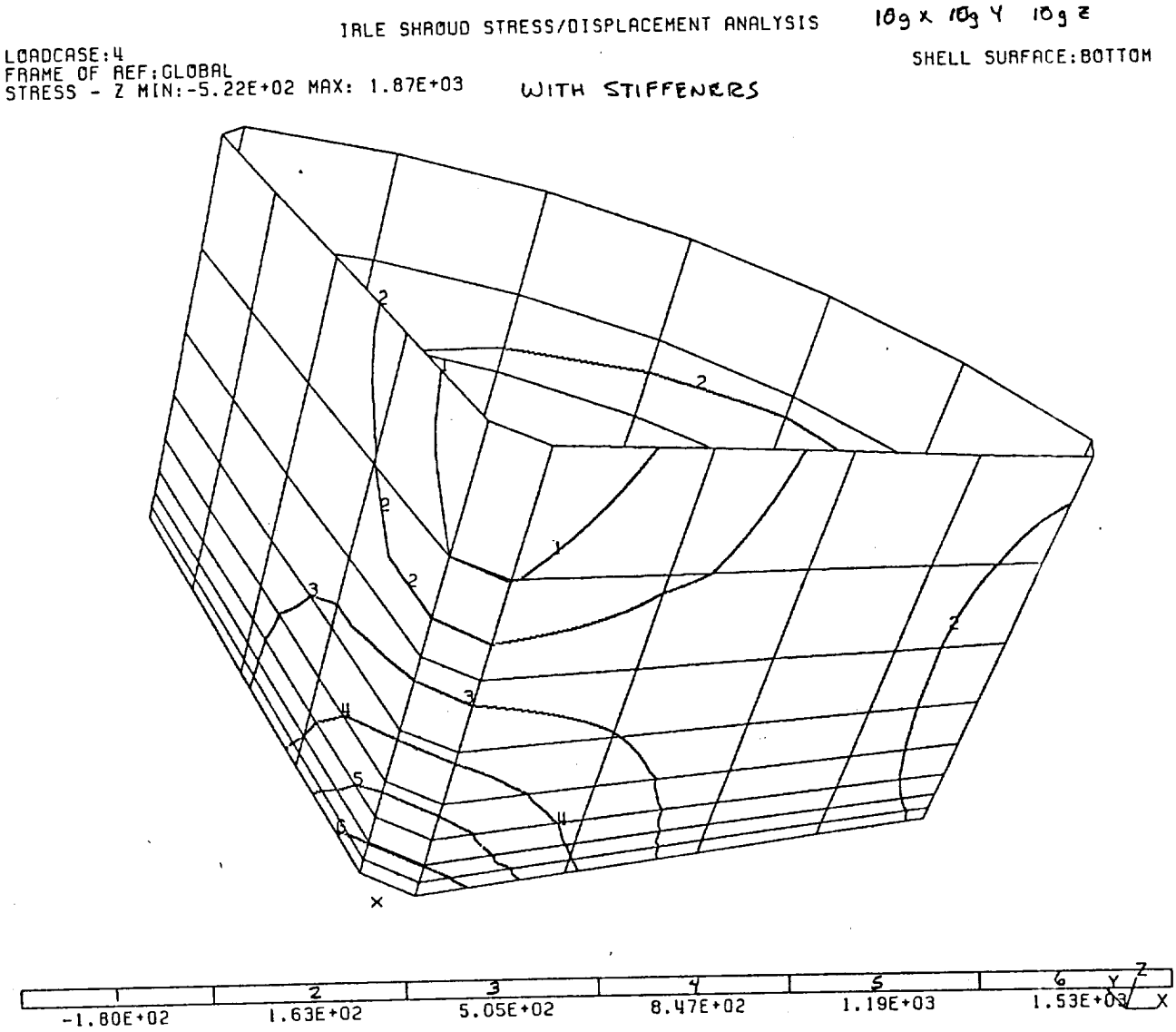

Figure 3.7-4. IRLE Shroud Stress Analysis (10 g XYZ)

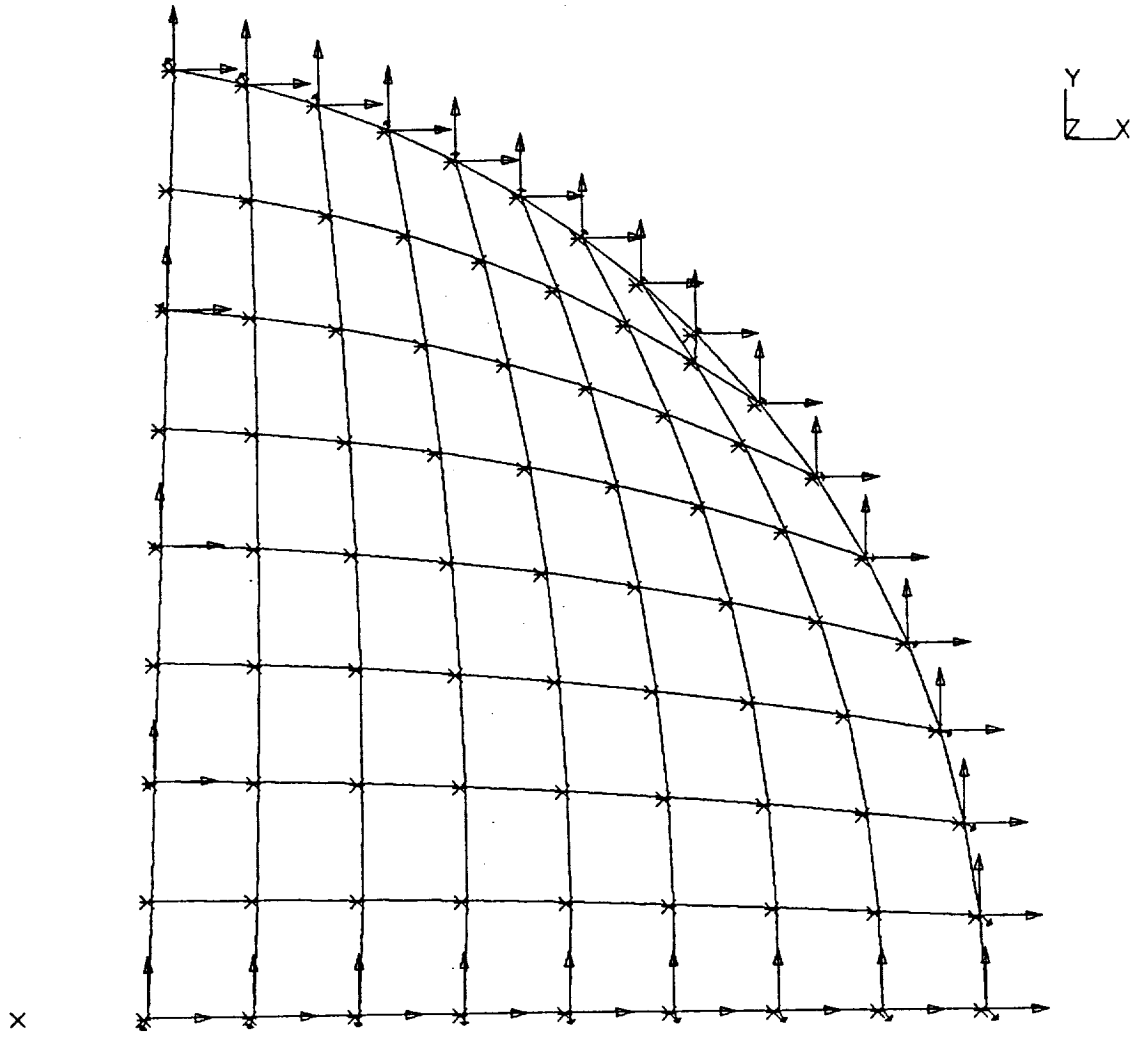

Figure 3.7-5. IRLE Top Plate NASTRAN Model

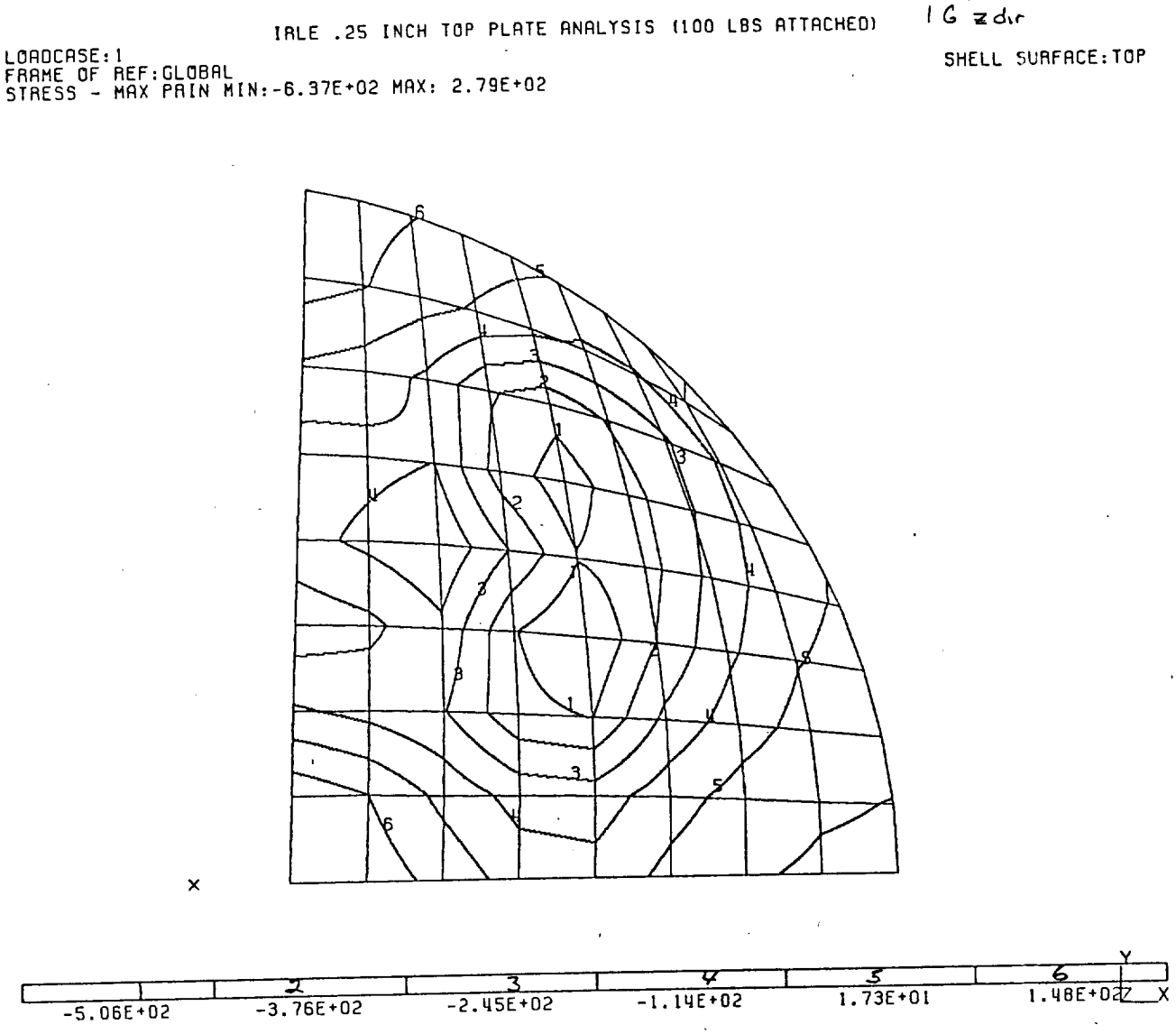

Figure 3.7-6. IRLE Top Plate Stress Analysis

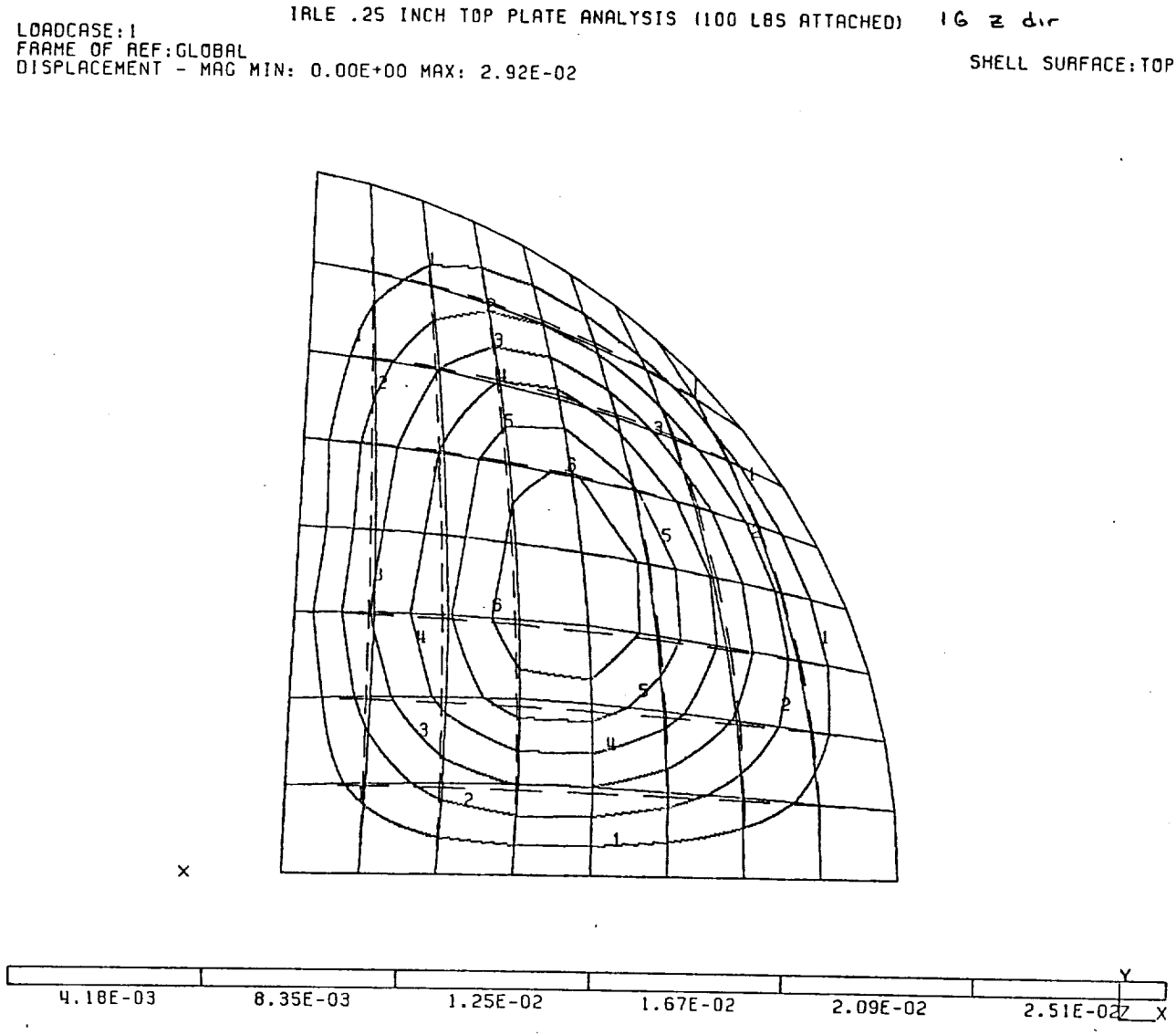

Figure 3.7-7. IRLE Top Plate Deflection Analysis

	Maximum Stresses:	Maximum Deflections:
1 g Z	-637 psi	2.92×10^{-2} in.

Stresses upon rocket lift-off, etc., do not approach yield strength of the material, therefore, no permanent deformations will occur.

3.7.5 Shroud/Top Plate Vibrations

The shroud is composed of a very thin skin, stiffened periodically by U-shaped internal stringers (see Figures 3.7-8 and 3.7-9). Analysis of the unstiffened skin showed that natural frequencies were well below 50 Hz with typical thin plate vibration modes dominating. By stiffening the skin (see Figure 3.7-10), the fundamental mode shape is now that of the entire shroud moving as an entity, thereby raising the fundamental frequency to 227 Hz. Thin plate vibration modes are now present only at higher frequencies of 721 and 1007 Hz (see Figures 3.7-11 and 3.7-12).

Natural Frequencies:
227 Hz
721 Hz
1007 Hz

Random vibration analysis should be completed in the future to provide force transmissibility information. Actual materials must be tested to obtain valid results from this analysis.

The aluminum top plate will be separated into two pieces. The larger piece, which was analyzed earlier, will carry most of the mass and will have the least amount of support. The smaller piece will have masses attached very near the supporting shroud walls. Since the plates are connected to the same shroud and are well supported along the boundary between them, contact between them due to vibration-induced deflections is not expected to occur. The methods of support seem quite adequate.

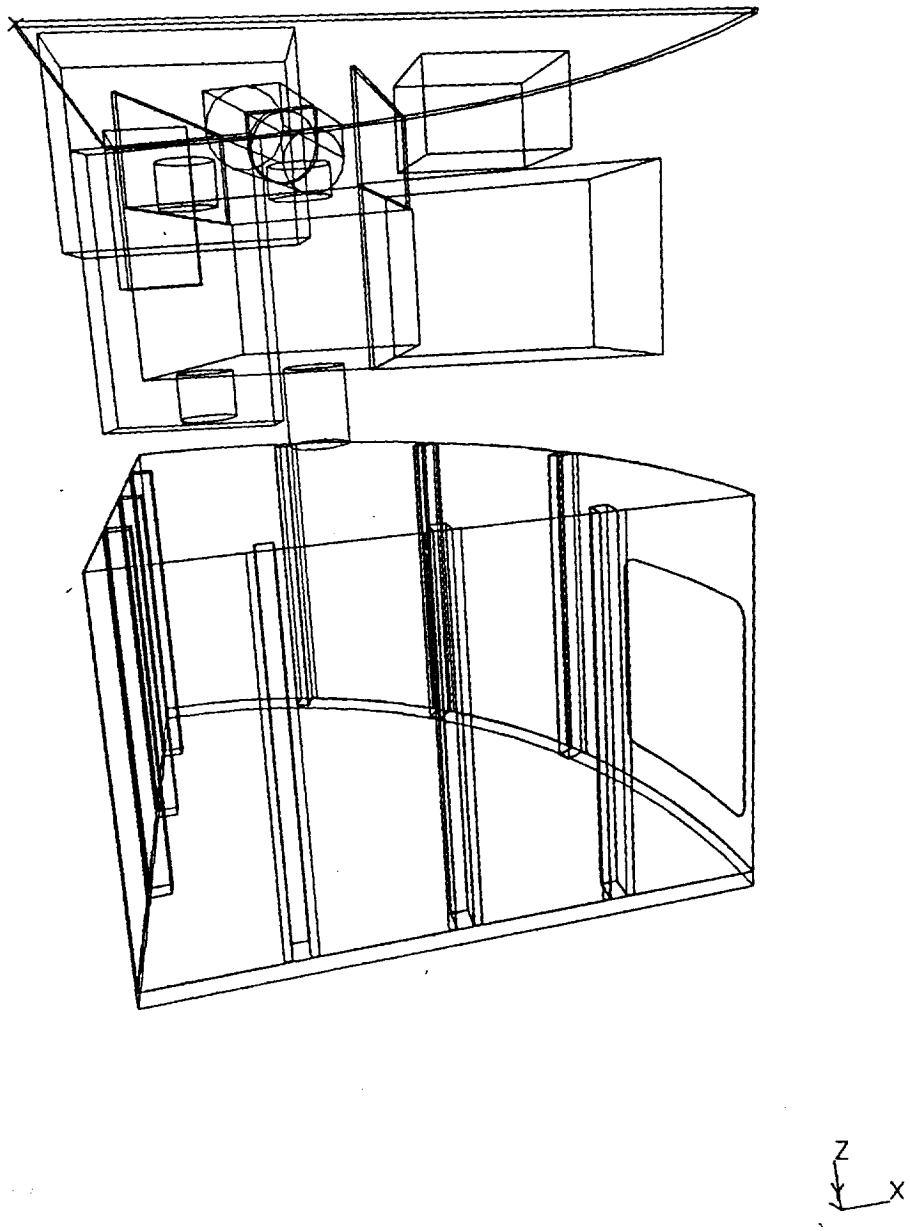

Figure 3.7-8. IRLE Three-Dimensional Conceptual Model

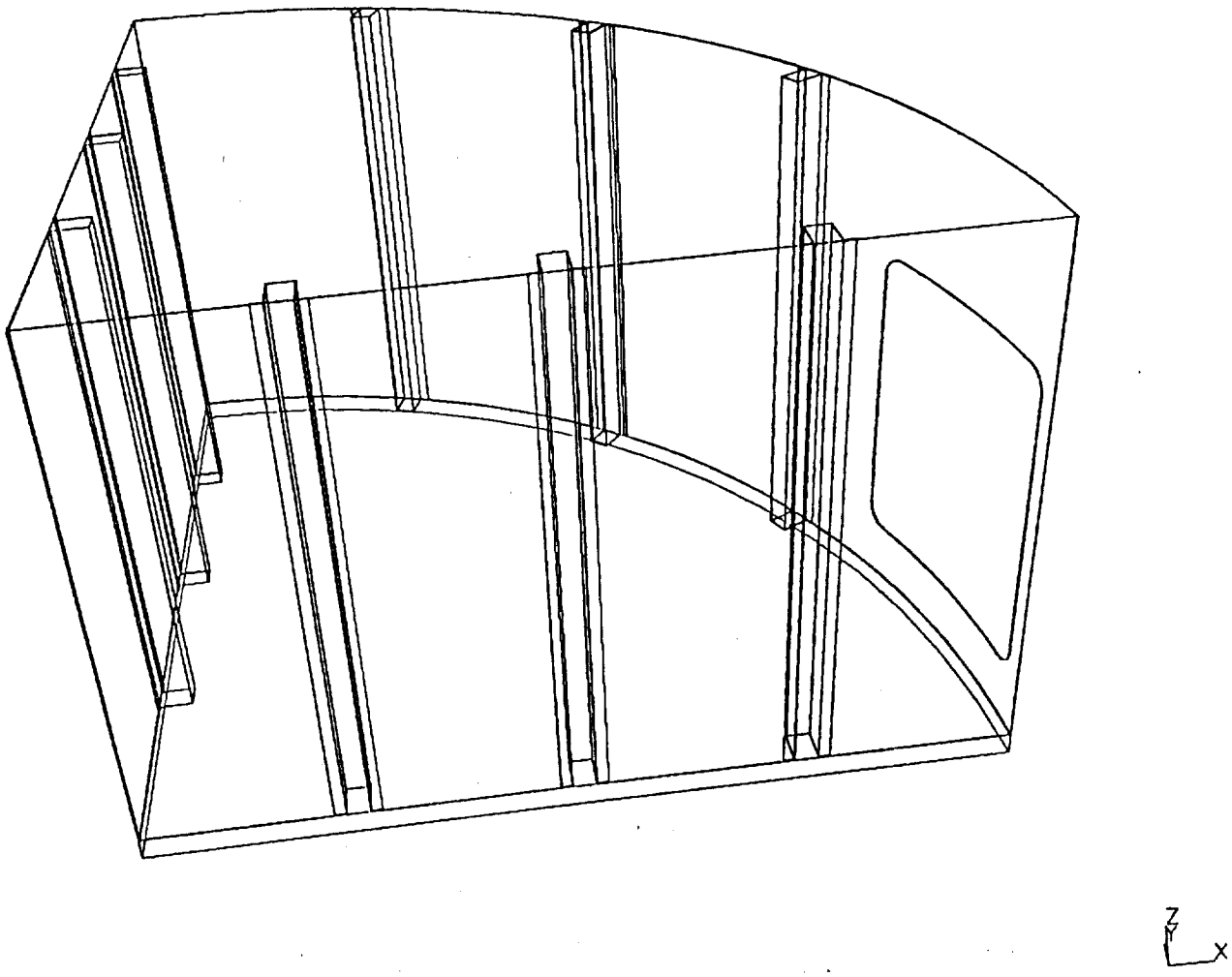

Figure 3.7-9. IRLE Three-Dimensional Shroud Model

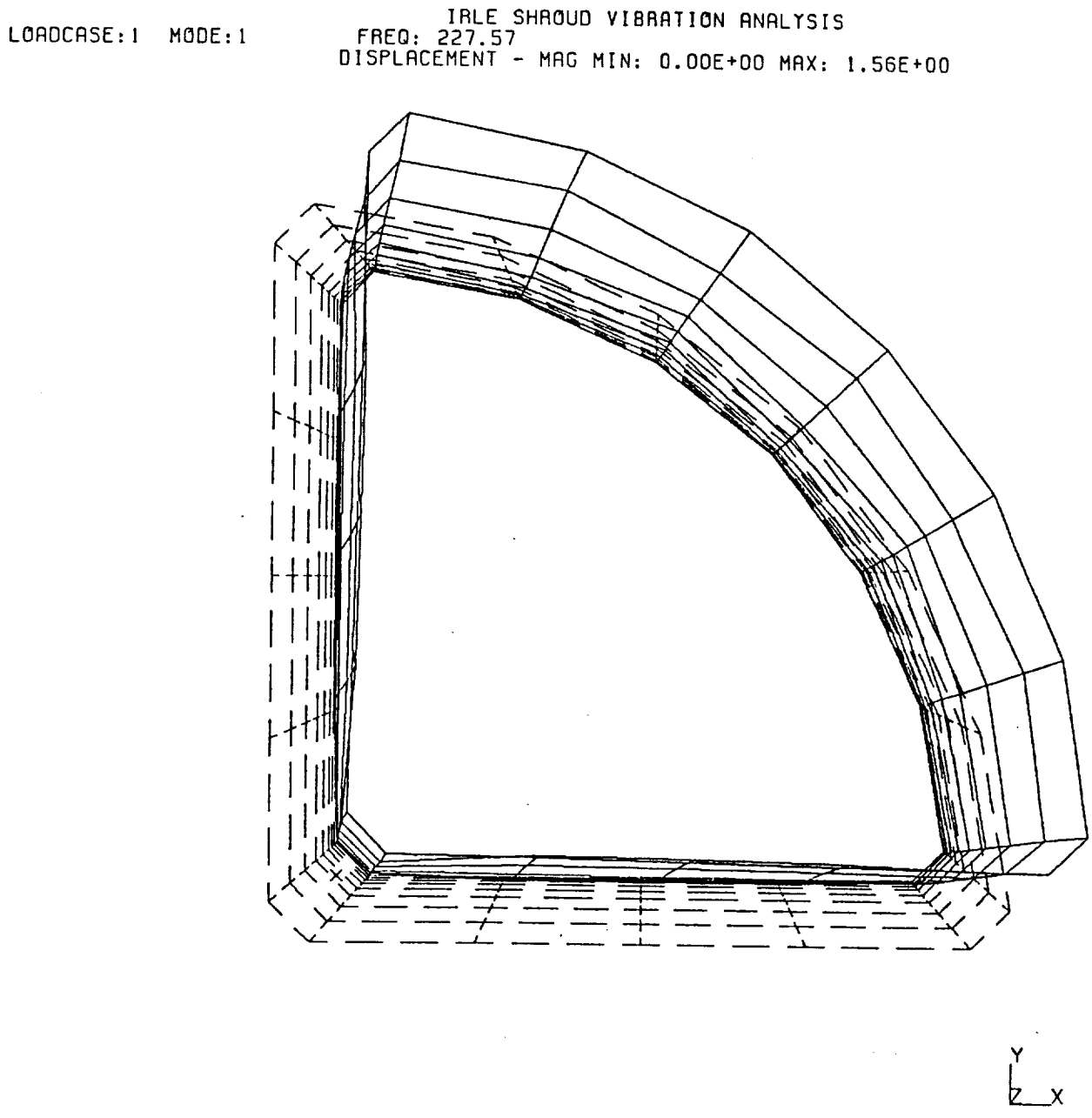

Figure 3.7-10. IRLE Shroud Vibration Analysis (Fundamental Mode)

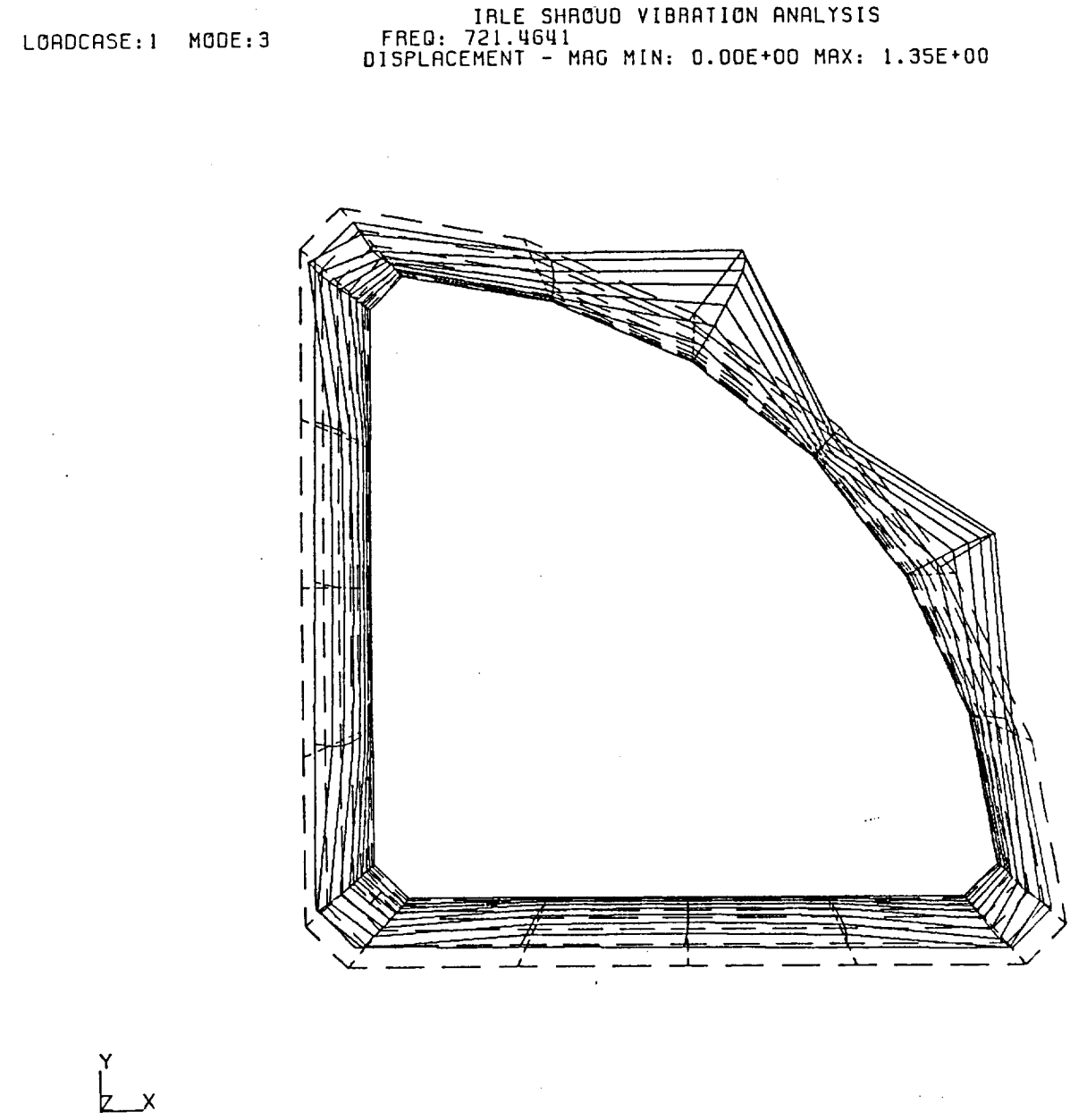

Figure 3.7-11. IRLE Shroud Vibration Analysis (Second Mode)

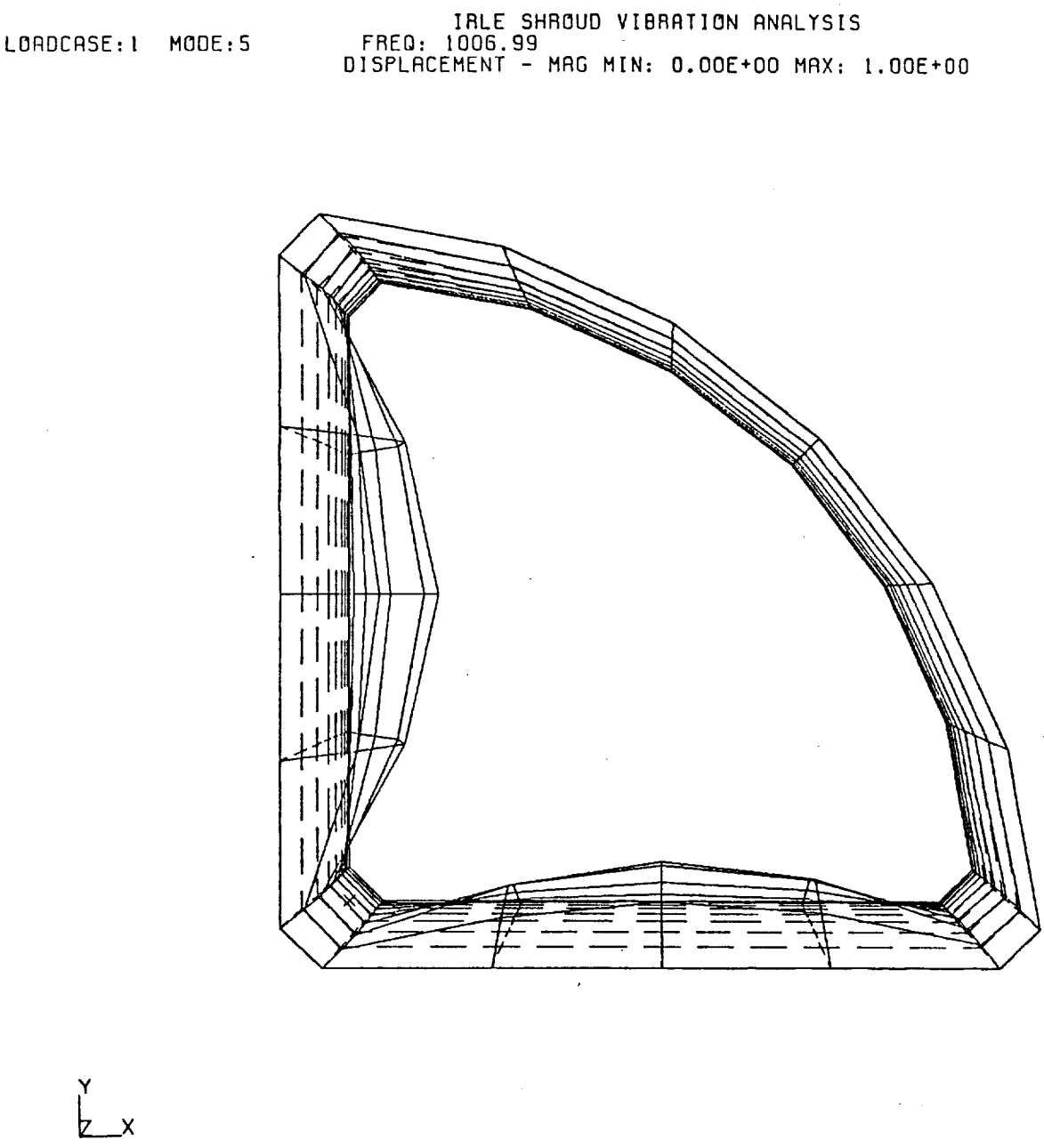

Figure 3.7-12. IRLE Shroud Vibration Analysis (Third Mode)

3.7.6 Structure Weight

The carbon/graphite shroud will be approximately .040 in. thick and supported by nine stringers or stiffeners. Masses of base connection flanges can only be estimated at this time. Density of the composite material is .06 lb/in^3.

Shroud:	3.45 kg
Stringers:	9 @ .13 kg = 1.17 kg
Base Connection Flanges:	1.04 kg
Total Support Structure Weight:	5.66 kg (excluding bolt weights)
Telescope/Dewar/Top Plate:	approximately 67.2 kg

4. GROUND SUPPORT EQUIPMENT

Ground operation and monitoring of IRLE by SDL/USU will be accomplished using the Instrument Test Operations Control Capability (I-TOCC) computer system that will be provided for each MELTER instrument by the Laboratory for Atmospheric and Space Physics (LASP) of the University of Colorado.

Costing and planning were performed assuming that three 386 PC computers, configured as shown in Figure 4-1, would be used for controlling and monitoring IRLE. The I-TOCC makes it possible to eliminate one of these 386 computers, because data capture and instrument control will be performed using the I-TOCC. An optical disk for data storage is still required. Two 386 computers will still be required for data analysis and development of flight software.

There is a data interface to the IRLE instrument through the spacecraft 1553 bus and also through a direct HPIB interface. The spacecraft 1553 bus allows the flight data to be obtained and recorded on an optical disk. The HPIB interface provides access to engineering data from the IRLE instrument that is not available through the 1553 bus. The HPIB board data lines and power connections are made through a ground test connector located on the IRLE instrument. The HPIB interface will not be used or powered during flight.

Ground control through the spacecraft 1553 bus and the HPIB interface allows both flight commands and engineering commands and data to be uploaded into the IRLE instrument. There is also a 1553 bus simulator to allow simulation of bus traffic during engineering checkout.

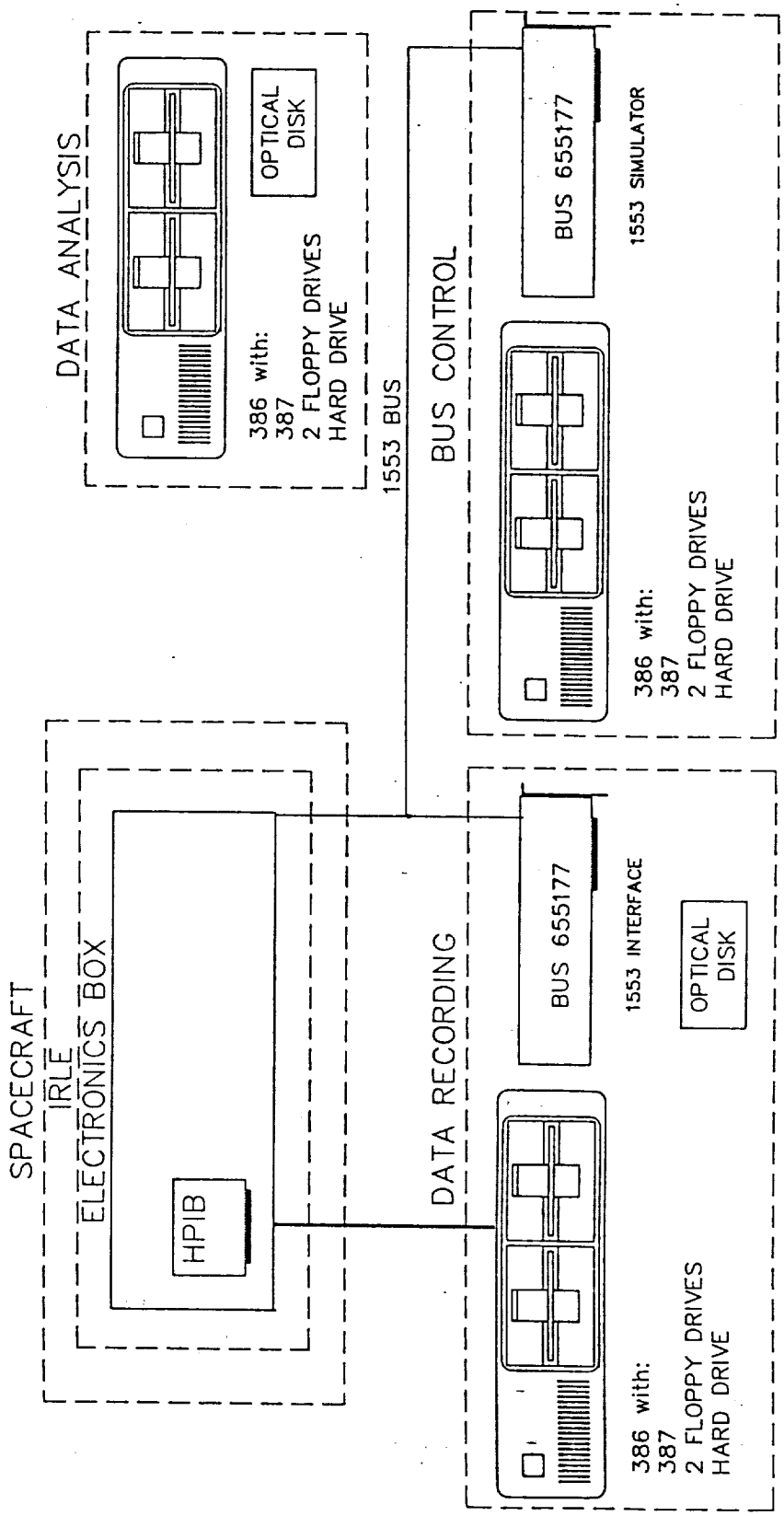

Figure 4-1. Ground Support Electrical Equipment

5. SENSOR CALIBRATION

5.1 CALIBRATION TEST CONFIGURATION

The calibration test configuration is shown schematically in Figure 5.1-1. The entire IRLE sensor will be installed in a test vacuum shell that is bolted to the SDL/USU calibrator. This test configuration allows the IRLE sensor to operate in the temperature range expected in orbit while viewing point sources, MTF reticles, Jones sources, and extended sources against a 10 Kelvin background.

The SDL/USU calibrator is an existing piece of equipment that was constructed for the SPIRIT II program. A brief description of this calibrator is given in paragraph 5.2. The cold entrance aperture of this calibrator is large enough, 11 by 22 in., to allow the IRLE to scan its full range (13 deg) against a 10 Kelvin background. The distance from the scan mirror to the entrance aperture of the calibrator is less than 31 in.

5.2 SDL/USU CALIBRATION FACILITY

The SDL/USU calibration facility consists of a calibrator, data capture equipment, and data analysis equipment. The SDL/USU calibrator, which was constructed to calibrate the SPIRIT II sensor, is a multi-function calibrator capable of functioning as a collimated source, a Jones source, an extended source, or a diffuse scatter source by changing its configuration as illustrated schematically in Figure 5.2-1. The calibrator can be changed from one configuration to another at cryogenic operating temperatures. The specifications of the calibrator in each of these four modes are provided in Table 5.2-1.

5.2.1 Collimator Mode

In the collimator mode, the SDL/USU calibrator is a folded, unobscured, off-axis, Gregorian telescope with a 200-in. focal length that provides distant small-area sources that fill the entire sensor entrance aperture. The collimated exit beam is directed by a single-axis, gimbal-mounted flat mirror over a range of 10 deg with a settability of 4.1 μrad and an accuracy of ±20.5 μrad.

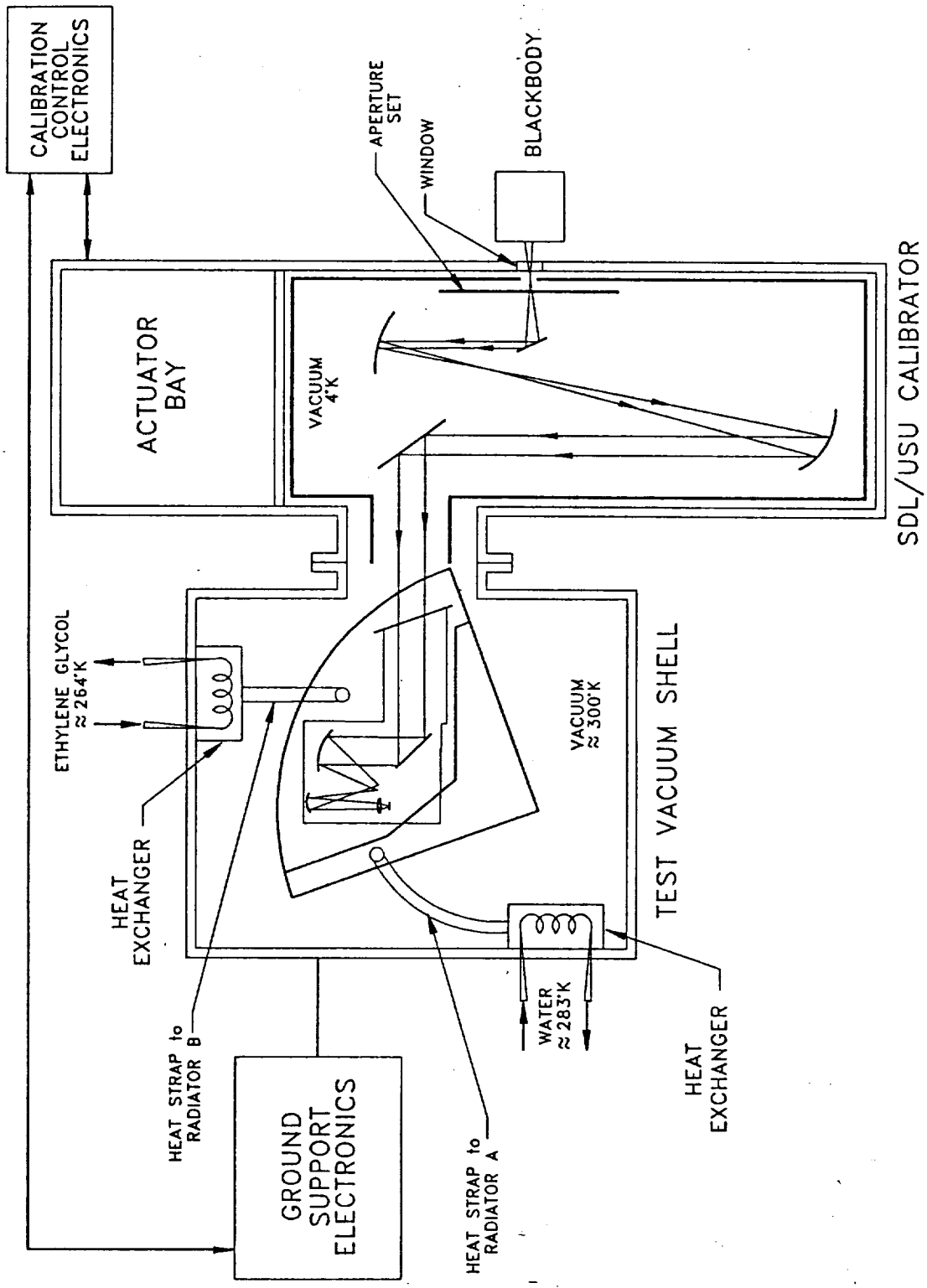

Figure 5.1-1. Calibration Test Configuration

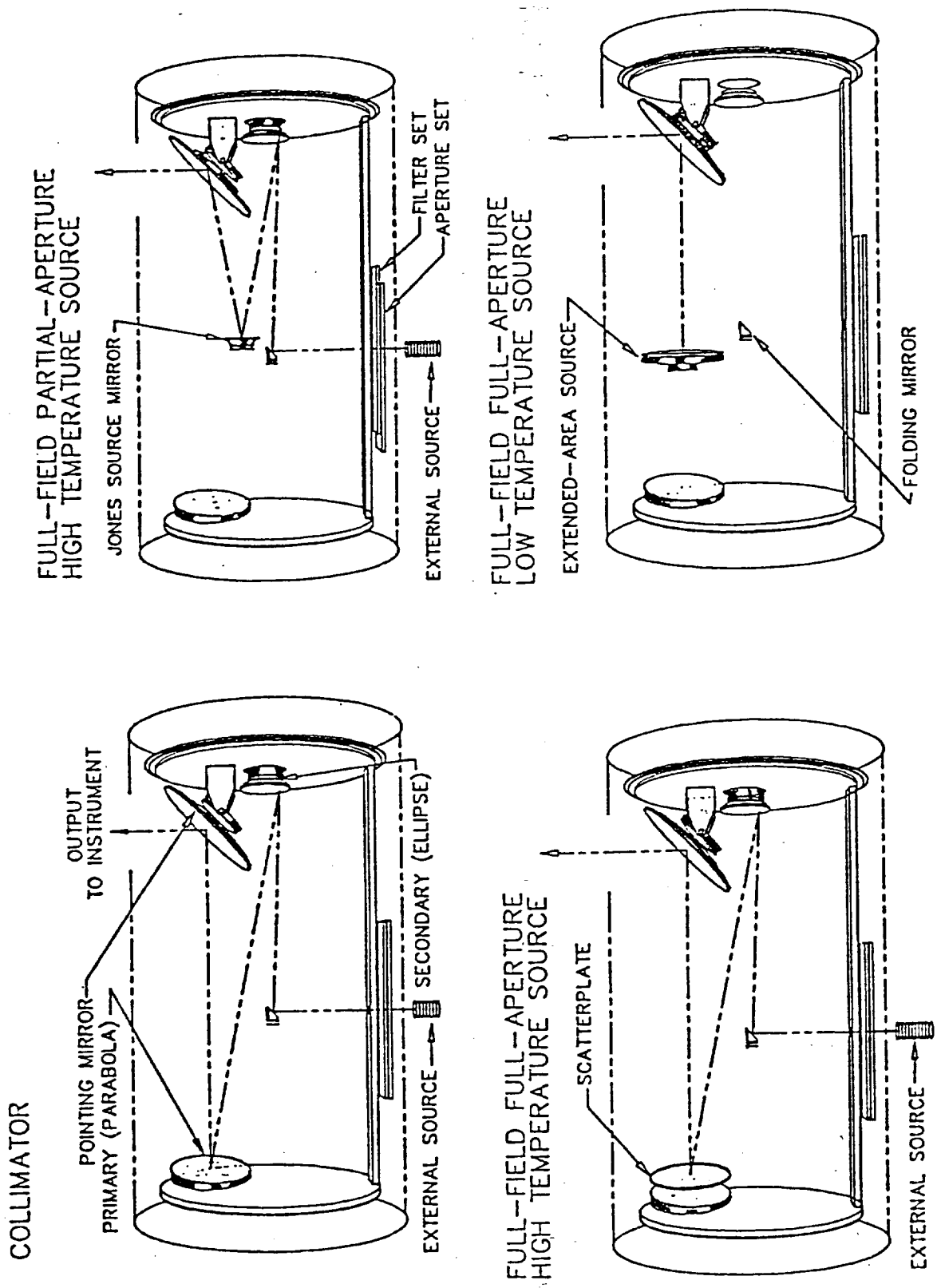

Figure 5.2-1. SDL/USU Calibration Source Configurations

Table 5.2-1. SDL/USU Calibrator Specification

COLLIMATOR	
Focal Length	200 in.
Beam Exit Geometry	21 x 11-in. elliptical
Apertures (11)	39.6 μrad - 1.266 mrad
Area Dynamic Range	1024:1
Area Resolution	2:1
Image Quality	70% of energy within 45x87 μrad at 10 μm
MTF Reticles (6)	0.38 c/mrad - 14.3 c/mrad
AC Scene Simulators (2)	
Filters (6)	
Source Positioning	
Full-Scale 2-D Travel	10 deg
Settability	4.1 μrad
Accuracy	±20.5 μrad
External Sources	
Blackbody Simulators	300 - 1200 K
Line Simulators	
Monochromator	3 - 25 μm
Absorption Cells	Water, Methane, Polystyrene, etc.
IR Laser	3 μm
Interferometer	Bomem
JONES SOURCE	
Apertures	See Collimator
Filters	See Collimator
External Sources	See Collimator
SCATTER SOURCE	
Apertures	See Collimator
Filters	See Collimator
External Sources	See Collimator
EXTENDED-AREA SOURCE	
Temperature Range	20 - 270 Kelvin
Temperature Uncertainty	±0.5 Kelvin

The collimator can provide test point sources of different sizes using a precision set of apertures in the focal plane. A MTF reticle can also be placed in the focal plane to measure the MTF of a sensor. The spectral output of the collimator can be controlled by either changing filters, located in the focal plane, or by changing the external source of radiation feeding the collimator. The radiation source can be either a blackbody, a monochromator, or an interferometer.

5.2.2 Jones Source Mode

In the Jones source mode, a flat pick-off mirror is inserted into the calibrator optical train directly after the elliptical secondary so that the image of the source is reimaged within the Jones cone of the sensor. When a point is imaged within the Jones cone, it completely floods the entire sensor focal plane. The Jones cone can be constructed, as illustrated in Figure 5.2-2, as follows.

1. Draw the chief ray, the ray through the center of the sensor entrance pupil to the edge of the field stop.

2. Draw a line parallel to the chief ray that passes through the edge of the sensor aperture stop, shown as the top dashed line in Figure 5.2-2.

If the sensor is symmetric about the optical axis, then the Jones cone is the right circular cone generated by rotating this dashed line about the optical axis. If the sensor is not symmetric about the optical axis, the procedure must be repeated at each azimuthal angle.

The Jones source completely floods the sensor focal plane, but it does not completely fill the sensor entrance aperture. The magnitude of the flux is controlled by changing the effective size of the source using a set of precision apertures.

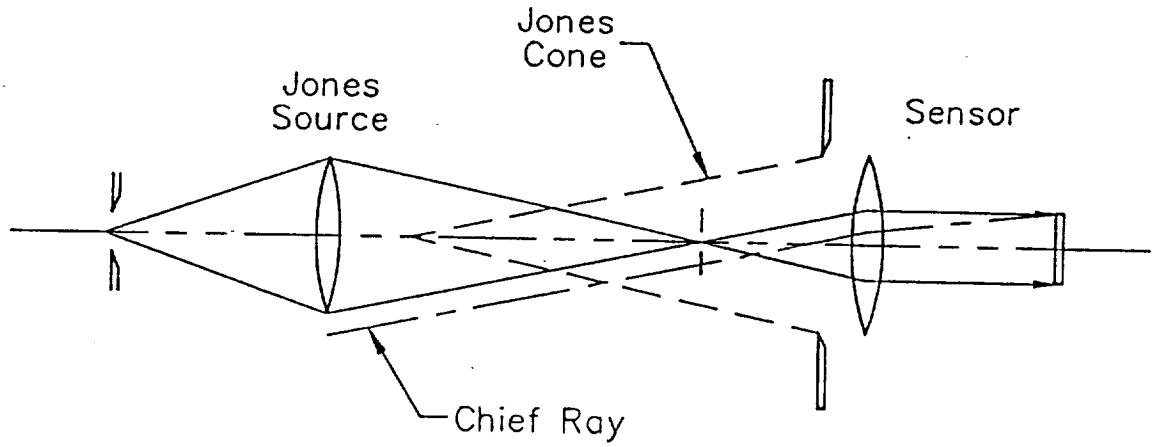

Figure 5.2-2. Jones Cone Definition

5.2.3 Extended-Area Source Mode

In the extended-area source mode a large, low-temperature source is inserted into the calibrator optical train so that it illuminates the flat, gimbal mirror and completely fills both the sensor entrance aperture and the sensor focal plane. The temperature of this extended source can be varied from 20 to 270 Kelvin with an uncertainty of ±0.5 Kelvin.

5.2.4 Scatter Source Mode

In the scatter plate mode, a rough plate is inserted directly in front of the calibrator primary mirror. This operation attenuates the radiation by a known ratio so that high temperature sources can be used without saturating the sensor. The calibrator completely fills both the sensor entrance aperture and the sensor focal plane. The magnitude of the flux can be varied by changing the effective size of the external source feeding the calibrator using a precision set of apertures.

5.3 CALIBRATION TESTS

Calibration tests are designed to calibrate individual sensor parameters independent of other parameters. These tests break down the function of a complex sensor into its fundamental parameters. The calibration tests measure the following parameters: noise response, temporal frequency response, linearity response, spatial response, relative spectral response, absolute response, and radiometric repeatability. In several cases, data from one experimental setup can be used to gather data on more than one sensor parameter by changing the way the data is analyzed.

5.3.1 Noise Response

5.3.1.1 Dark Signal. The purposes of this test are to measure the sensor noise with no signal present, to measure sensor offsets, to detect errors that look like signal, and to detect electrical crosstalk. This test will be conducted by operating the sensor while looking only at a 10 Kelvin scene.

5.3.1.2 Noise Over Dynamic Range. This test will measure the uncertainties of each detector throughout their dynamic range by using the data from the dc linearity test described in paragraph 5.3.3.1.

5.3.2 Temporal Frequency Response

The purpose of this test is to measure the temporal frequency response of the sensor. This test is accomplished by modulating the Jones source with an external chopper and measuring the power in the fundamental by Fourier analyzing the sensor output signal.

5.3.3 Linearity Response

5.3.3.1 DC Linearity. The purpose of this test is to determine the dc linearity of the sensor throughout the sensor dynamic range. This test is accomplished by measuring the sensor response to the Jones source as the input flux is varied by changing the precision apertures and the source temperature.

5.3.3.2 AC Linearity (Harmonic Distortion). The purpose of this test is to measure any harmonics produced by the sensor due to nonlinearities in its response. This test is accomplished by modulating the Jones source with an external interferometer and looking for response at harmonics of the modulation frequency.

5.3.4 Spatial Response

5.3.4.1 Field-of-View Maps. The purpose of this test is to map the responsivity versus field-of-view angle of all detectors. The collimator source is used to map the responsivity of each detector versus the angular position of the calibrator scan mirror.

5.3.4.2 Point-Source Modulation Transfer Function. The purpose of this test is to measure the MTF for each detector by Fourier transforming the point source response of each detector. The results are compared with the reticle MTF calibration. This test uses the calibrator in the collimator mode.

5.3.4.3 Reticle Modulation Transfer Function. The purpose of this test is to measure the MTF for each detector by measuring the modulation of bar-pattern scenes of various frequencies. This test is accomplished using the collimator and the calibrator scan mirror to scan the collimated bar patterns. A scan speed that results in detector output frequencies well below the sensor electrical bandwidth will be used.

5.3.4.4 Focal Plane Scatter. The purpose of this test is to measure the fraction of each detector's response due to sources outside its field of view. This test uses the collimator to map each detector response for regions both inside and outside its respective field stop.

5.3.4.5 Sensor Scan Mirror Pointing. The purpose of this test is to calibrate the angular position of the sensor scan mirror. The collimator will be used for this test.

5.3.5 Relative Spectral Response

The purpose of this test is to measure the relative spectral response of each detector. The external interferometer is used to modulate the Jones source. The output of the sensor will be Fourier transformed to give the relative spectral response versus wavelength. By using auxiliary filters, this technique has achieved out-of-band blocking transmission measurements down 5 or 6 orders of magnitude.

5.3.6 Absolute Response

5.3.6.1 Low-Temperature Extended-Area Measurements. The purpose of this test is to measure the absolute radiometric responsivity of channels 1 through 8 to an extended source. The low-temperature extended-area source is used for this test. This source provides inadequate flux to calibrate the short wavelength channel 9. Several different source temperatures will be used to evaluate spectral errors. The results of this test will be compared with the Jones source measurements. The extended source mode depends on only the radiance of the extended source and the reflectivity of the calibrator scan mirror, not on any geometric factors. For this reason, the extended source mode is more desirable for a radiance calibration than the Jones source calibration.

5.3.6.2 High-Temperature Jones-Source Measurements. The purpose of this test is to measure the absolute radiometric responsivity of each detector to a flood source. This test is used because the low-temperature extended source does not produce enough flux to calibrate the short wavelength channel 9. The Jones source test is not as desirable as the extended source test for absolute radiance calibrations because: (1) it requires knowledge of the area of the sensor entrance aperture and the area of the aperture in the focal plane of the calibrator, and (2) the response must be corrected for transmission losses in the calibrator entrance window and reflection losses at four calibrator mirror surfaces, and vignetting in the sensor will result in calibration errors.

5.3.7 Radiometric Repeatability

5.3.7.1 Internal Sources. The purpose of this test is to ascertain the repeatability of the internal sources and each detector. This test is accomplished by recording the response of each detector to the internal sources and to a cold scene during each day of the calibration period.

5.3.7.2 External Sources. The purpose of this test is to ascertain the long-term repeatability of the calibrator and each detector. This test is accomplished by recording the response of each detector to the Jones source during each day of the calibration period.

6. PROJECT PLAN

6.1 MILESTONE SCHEDULE

A milestone schedule is given in Figure 6.1-1. The schedule for each detailed task is included in the following Work Breakdown Structure (WBS) section. The schedule covers a period of 4-1/2 years, from 1 June 1990 to 14 December 1994. The schedule and the cost estimates continue to launch plus 30 days. The schedule is success oriented and includes no slack time. Long-lead parts, such as the telescope, cooler, detector array, and filters, must be ordered immediately following the preliminary design review (PDR). The chopper will also be ordered at PDR to allow maximum time for life tests.

6.2 WORK BREAKDOWN STRUCTURE

This section describes the WBS tasks and the schedule for each task.

6.2.1 Major Tasks and Schedules

The major tasks of the WBS and their schedules are:

WBS	Task Name	Start Date	End Date
00100	+ PROGRAM MANAGEMENT	1-Jun-90	15-Dec-94
00200	+ SYSTEM ENGINEERING	1-Jun-90	15-Dec-94
00300	+ FLIGHT HARDWARE	1-Jun-90	27-Jul-93
00400	+ GROUND EQUIPMENT	17-Sep-90	18-Jan-94
00500	+ FLIGHT & GROUND SOFTWARE	1-Jun-90	15-Jul-92
00600	+ PERFORMANCE ASSURANCE & SAFE	1-Jun-90	1-Jul-93
00700	+ INSTRU ASSEMBLY & VERFICATIO	18-May-92	4-Feb-93
00800	+ CALIBRATION	15-Jan-91	26-Jul-93
00900	+ INTEGRATION & TEST SUPPORT	2-Jan-92	15-Nov-94
01000	+ FLIGHT OPERATIONS SUPPORT	1-Feb-94	13-Dec-94

Schedule Name : IRLE9
Responsible : ROY ESPLIN
As-of Date : 13-Jun-89 Schedule File : D:\TL3\DATA\IRLE9

Select filter : MILESTONES

Task Name	Date
PROGRAM START	1-Jun-90
DELTA CoDR	17-Sep-90
PDR	15-Jan-91
FILTER AWARD	15-Jan-91
FPA AWARD	15-Jan-91
COOLER AWARD	15-Jan-91
THERMAL SWITCH AWARD	15-Jan-91
TELESCOPE AWARD	30-Jan-91
CHOPPER AWARD	15-Feb-91
CDR	16-Jul-91
CHOPPER DELIVERY	23-Aug-91
GSE EL HARDWARE COMPLET	27-Nov-91
THERMAL SWITCH DELIVERY	3-Feb-92
COOLER DELIVERY	3-Feb-92
FILTER DELIVERY	3-Feb-92
FPA DELIVERY	6-Apr-92
TELESCOPE DELIVERY	20-Apr-92
IRLE FAB COMPLETE	15-Jul-92
PERF TESTS COMPLETE	8-Oct-92
EMI TEST COMPLETE	23-Oct-92
VIBRATION TESTS COMPLET	16-Nov-92
THERMAL VAC TESTS COMPL	5-Feb-93
CALIBRATION COMPLETE	24-May-93
START OM INTEGRATION	16-Jul-93
START S/C INTEGRATION	18-Jan-94
START LANUNCH SUPPORT	15-Aug-94
LAUNCH	15-Nov-94
PROGRAM END	15-Dec-94

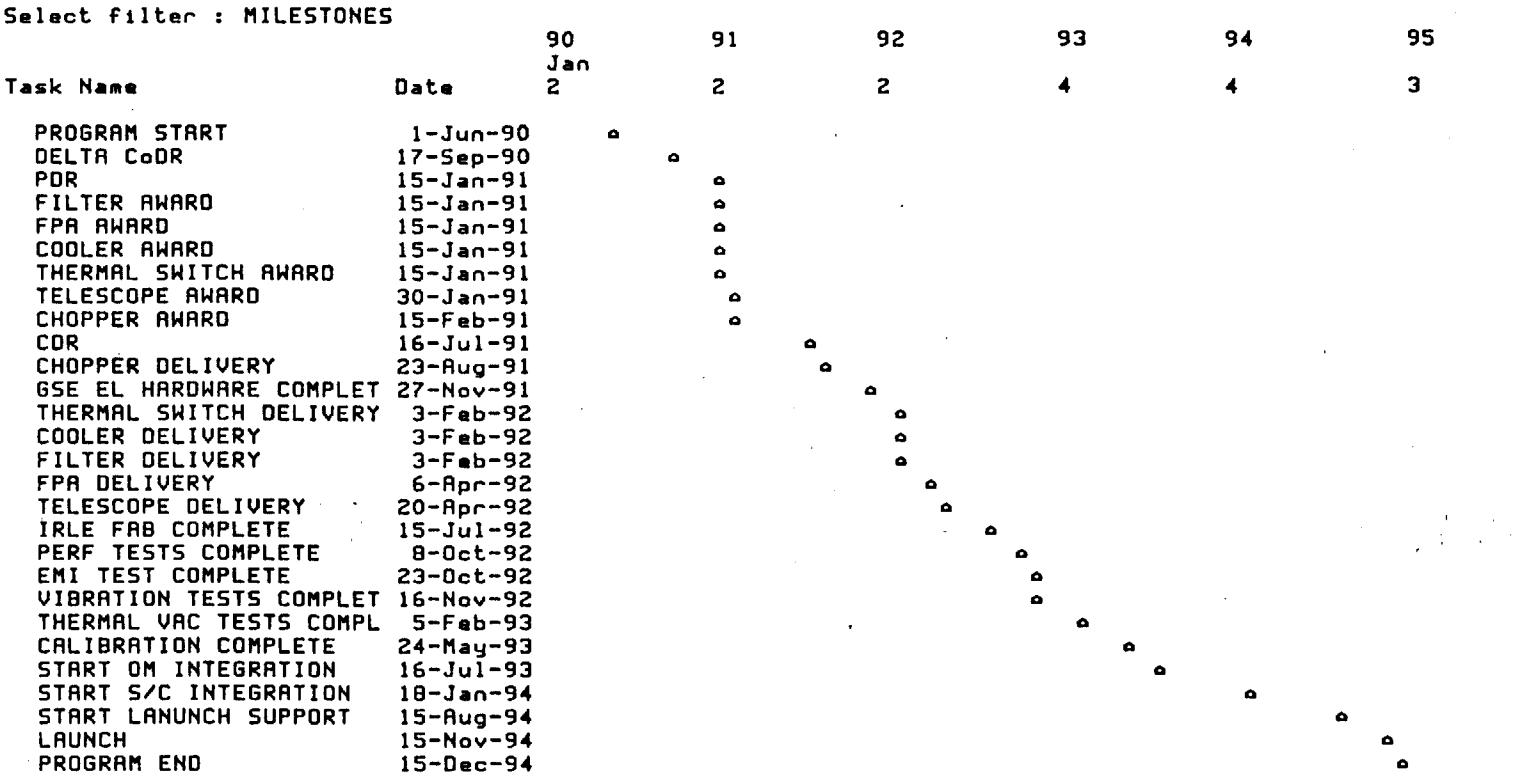

Detail Task (Started) (Slack)
Summary Task (Started) (Slack)
Milestone
Conflict
Resource delay
Scale: 1 month per character

Figure 6.1-1. IRLE Program Milestone Chart

6.2.2 Subtasks and Schedules

6.2.2.1 Program Management Tasks. The program management (WBS 00100) subtasks and their schedules are:

WBS	Task Name	Start Date	End Date
00100	PROGRAM MANAGEMENT	1-Jun-90	15-Dec-94
00110	PROGRAM MANAGEMENT	1-Jun-90	15-Dec-94
00111	TECH MANAGEMENT	1-Jun-90	15-Dec-94
00112	ADMINSTRATIVE MANAGEME	1-Jun-90	15-Dec-94
00113	MEETING TRAVEL	1-Jun-90	15-Dec-94
00113.1	DELTA CoDR	17-Sep-90	19-Sep-90
00113.2	PDR	15-Jan-91	17-Jan-91
00113.3	CDR	16-Jul-91	18-Jul-91
00113.4	TIM TRAVEL COSTS	1-Jun-90	15-Dec-94
00120	RESOURCE/SCEDULE CONTROL	1-Jun-90	15-Dec-94
00121	CSSR (COST REPORTING &	1-Jun-90	15-Dec-94
00130	DOCUMENTATION	1-Jun-90	15-Dec-94
00131	DELTA CoDR DOCUMENTS	31-Aug-90	14-Sep-90
00132	PDR DOCUMENTS	31-Dec-90	14-Jan-91
00133	CDR DOCUMENTS	1-Jul-91	15-Jul-91
00134	ICD & REPORTS	1-Jun-90	15-Dec-94
00140	SCIENCE MANAGEMENT	1-Jun-90	15-Dec-94
00150	SUBCONTRACT MANAGEMENT	15-Jan-91	5-Jun-92
00151	MANAGE COOLER SUB	15-Jan-91	5-May-92
00152	MANAGE FPA SUB	15-Jan-91	5-May-92
00152	MANAGE FILTER SUB	15-Jan-91	5-May-92
00153	MANAGE CHOPPER SUB	15-Feb-91	5-Jun-92
00154	MANAGE THERMAL SWITCH	15-Jan-91	5-May-92
00160	S/C/INSTRU INTEG CTRL	15-Jul-93	15-Aug-94

6.2.2.2 System Engineering. The system engineering (WBS 00200) subtasks and their schedules are:

WBS	Task Name	Start Date	End Date
00200	SYSTEM ENGINEERING	1-Jun-90	15-Dec-94
00210	DEVELOP SENSOR DESIGN REQ	1-Jun-90	1-Jul-91
00211	CONCEPTUAL DESIGN	1-Jun-90	4-Sep-90
00212	PRELI DESIGN	4-Sep-90	10-Jan-91
00213	FINAL DESIGN	11-Jan-91	1-Jul-91
00220	INSTRU INTEGR & TEST PLAN	13-May-94	15-Dec-94
00221	INTEG/TEST PLAN	13-May-94	15-Dec-94
00230	INST/S/C INTERF REQ	1-Jun-90	1-Jul-91
00231	CONCEPTUAL DESIGN	1-Jun-90	4-Sep-90
00232	PRELI DESIGN	4-Sep-90	2-Jan-91
00233	FINAL DESIGN	2-Jan-91	1-Jul-91
00240	INST MODELING & ANALYSIS	1-Jun-90	19-Jul-93
00241	PRELIM DESIGN	1-Jun-90	17-Dec-90
00241.1	RADIOMETRIC	15-Jun-90	17-Dec-90
00241.2	THERMAL	1-Jun-90	17-Dec-90
00241.3	STRUCTURAL	1-Jun-90	17-Dec-90
00242	FINAL DESIGN	1-Feb-91	3-Sep-91
00242.1	RADIOMETRIC MODEL	14-Feb-91	15-Aug-91
00242.2	THERMAL MODEL	1-Feb-91	15-Aug-91
00242.3	STRUCT MODEL	1-Feb-91	3-Sep-91
00243	VERIFY MODELS	16-Jul-92	19-Jul-93
00243.1	THERMAL	16-Jul-92	19-Jul-93
00243.2	STRUCTURE	16-Jul-92	16-Jul-93
00243.3	RADIOMETRIC	16-Jul-92	16-Jul-93
00250	CALIBRATION REQ/PLANNING	1-Jun-90	1-Jul-91
00251	PRELIMNARY DESIGN	1-Jun-90	2-Jan-91
00252	FINAL DESIGN	2-Jan-91	1-Jul-91
00260	GSE REQUIREMENTS/PLANNING	1-Jun-90	1-Jul-91
00261	PRELIMINARY DESIGN	1-Jun-90	2-Jan-91
00262	FINAL DESIGN	2-Jan-91	1-Jul-91
00270	COORD FLIGHT/GRND SOFTWAR	1-Jun-90	1-Jul-91
00271	PRELI DESIGN	1-Jun-90	2-Jan-91
00272	FINAL DESIGN	2-Jan-91	1-Jul-91

6.2.2.3 Flight Hardware. The flight hardware (WBS 00300) subtasks and their schedules are:

WBS Code	Task Name	Start Date	End Date
00300	FLIGHT HARDWARE	1-Jun-90	27-Jul-93
00310	OPTICS MODULE	1-Jun-90	27-Jul-93
00311	TELESCOPE & BAFFLE	1-Jun-90	22-Jul-92
00311.1	SELECT SUB	1-Jun-90	27-Jul-90
00311.2	PREL DESIGN SUBCONT	30-Jul-90	15-Jan-91
00311.3	MONITOR PREL DESIGN	30-Jul-90	15-Jan-91
00311.4	FOLLOW-ON SUBCONTRA	30-Jan-91	17-Apr-92
00311.5	MONITOR FOLLOW-ON S	30-Jan-91	22-Jul-92
00312	CHOPPER	17-Sep-90	27-Jul-93
00312.1	PREPARE RFQ	17-Sep-90	15-Oct-90
00312.2	SUBCONTRACT	15-Feb-91	22-Aug-91
00312.3	TEST BREADB CHOPPER	21-Jun-91	27-Jul-93
00313	ASSEM/WARM TEST MOD	20-Apr-92	15-May-92
00320	DETECTOR MODULE	1-Jun-90	29-Jun-92
00321	PRELI DESIGN DET MODUL	1-Jun-90	21-Nov-90
00321.1	FPA	1-Jun-90	2-Oct-90
00321.11	DEVELOP SPEC	1-Jun-90	27-Jul-90
00321.12	ISSUE RFQ	30-Jul-90	10-Aug-90
00321.13	TEST InGaAs DETE	1-Jun-90	2-Oct-90
00321.131	BUY SAMPLES	1-Jun-90	4-Sep-90
00321.132	TEST SAMPLES	5-Sep-90	2-Oct-90
00321.2	FILTERS	1-Jun-90	24-Aug-90
00321.21	DEVELOP SPEC	1-Jun-90	27-Jul-90
00321.22	ISSUE RFQ	13-Aug-90	24-Aug-90
00321.3	THERMAL SWITCHES	1-Jun-90	27-Jul-90
00321.31	DEVELOP SPEC	1-Jun-90	28-Jun-90
00321.32	ISSUE RFQ	29-Jun-90	27-Jul-90
00321.4	DEWAR	27-Aug-90	21-Nov-90
00321.41	THERMAL DESIGN	27-Aug-90	24-Sep-90
00321.42	MECHANICAL DESIG	11-Sep-90	21-Nov-90
00322	FINAL DESIGN	15-Jan-91	3-Apr-92
00322.1	FPA	15-Jan-91	3-Apr-92
00322.11	SUBCONTRACT	15-Jan-91	3-Apr-92
00322.12	MONITOR FPA SUBC	15-Jan-91	3-Apr-92
00322.2	FILTERS	15-Jan-91	31-Jan-92
00322.21	SUBCONTRACT	15-Jan-91	31-Jan-92
00322.22	MONITOR FILTER S	15-Jan-91	31-Jan-92

WBS Code	Task Name	Start Date	End Date
00322.3	THERMAL SWITCHES	15-Jan-91	31-Jan-92
00322.31	SUBCONTRACT	15-Jan-91	31-Jan-92
00322.32	MONITOR SUB	15-Jan-91	31-Jan-92
00322.4	DEWAR	22-Jan-91	29-May-91
00322.41	BREADBOARD LN TE	22-Jan-91	2-Apr-91
00322.411	DESIGN	22-Jan-91	19-Feb-91
00322.412	FAB	20-Feb-91	5-Mar-91
00322.413	TEST	6-Mar-91	2-Apr-91
00322.42	REDESIGN PF DEWA	3-Apr-91	29-May-91
00323	FAB & TEST PF MODULE	30-Sep-91	29-Jun-92
00323.1	PF DEWAR	30-Sep-91	24-Jan-92
00323.11	FAB	30-Sep-91	24-Dec-91
00323.12	TEST	26-Dec-91	24-Jan-92
00323.2	FAB HEAT SINKS	1-Nov-91	15-Nov-91
00323.3	SHIP FILTERS TO DET	3-Feb-92	4-Feb-92
00323.4	TEST THERM SWITCHES	3-Feb-92	2-Mar-92
00323.5	TEST COOLER	3-Feb-92	14-Feb-92
00323.6	TEST FPA IN LN DEWA	6-Apr-92	1-May-92
00323.7	INTEGRATE DET MOD	4-May-92	1-Jun-92
00323.8	TEST & CAL MODULE	2-Jun-92	29-Jun-92
00330	CRYOCOOLER	1-Jun-90	5-May-92
00331	DEVELOP SPEC	1-Jun-90	13-Jul-90
00332	ISSUE RFQ	16-Jul-90	10-Aug-90
00333	SUBCONTRACT	15-Jan-91	31-Jan-92
00334	MONITOR COOLER SUB	15-Jan-91	5-May-92

WBS Code	Task Name	Start Date	End Date
00340	ELECTRONICS	1-Jun-90	8-Jul-92
00341	PRELI DESIGN ELEC MODU	1-Jun-90	20-Nov-90
00341.1	PREAMPS	1-Jun-90	24-Aug-90
00341.2	POWER DISTRIBUTION	24-Aug-90	20-Nov-90
00341.3	DIG SIGNAL PROCESSO	1-Jun-90	28-Jun-90
00341.4	SCAN/FLIP CONTROL	29-Jun-90	27-Jul-90
00341.5	SYS CONTROL/HOUSEKE	1-Jun-90	10-Aug-90
00341.6	ELECTRONIC BOXES	1-Oct-90	22-Oct-90
00341.61	ELEC DESIGN	1-Oct-90	22-Oct-90
00341.62	MECH DESIGN	1-Oct-90	22-Oct-90
00342	FINAL DESIGN ELEC	22-Jan-91	28-Aug-91
00342.1	PREAMP	22-Jan-91	26-Aug-91
00342.11	BREADBOARD	22-Jan-91	3-Jun-91
00342.111	LAYOUT	22-Jan-91	11-Feb-91
00342.112	FAB	12-Feb-91	5-Mar-91
00342.113	TEST	6-May-91	3-Jun-91
00342.12	REDESIGN	16-Jul-91	26-Aug-91
00342.2	POWER DISTRIBUTION	22-Jan-91	15-Jul-91
00342.21	BREADBOARD	22-Jan-91	29-May-91
00342.211	LAYOUT	22-Jan-91	19-Mar-91
00342.212	FAB	20-Mar-91	30-Apr-91
00342.213	TEST	1-May-91	29-May-91
00342.22	REDESIGN	3-Jun-91	15-Jul-91
00342.3	DIGITAL SIGNAL PROC	22-Jan-91	12-Jun-91
00342.31	BREADBOARD	22-Jan-91	16-Apr-91
00342.311	LAYOUT	22-Jan-91	11-Feb-91
00342.312	FAB	12-Feb-91	5-Mar-91
00342.313	TEST/DEBUG	6-Mar-91	16-Apr-91
00342.32	REDESIGN	17-Apr-91	12-Jun-91
00342.4	SCAN/FLIP CONTROL	12-Feb-91	8-Aug-91
00342.41	BREADBOARD	12-Feb-91	29-May-91
00342.411	LAYOUT	12-Feb-91	5-Mar-91
00342.412	FAB	6-Mar-91	26-Mar-91
00342.413	TEST/DEBUG	17-Apr-91	29-May-91
00342.42	REDESIGN	13-Jun-91	8-Aug-91

WBS Code	Task Name	Start Date	End Date
00342.5	SYS CONTROL/HOUSEKE	6-Mar-91	25-Jul-91
00342.51	BREADBOARD	6-Mar-91	29-May-91
00342.511	LAYOUT	6-Mar-91	26-Mar-91
00342.512	FAB	27-Mar-91	16-Apr-91
00342.513	TEST/DEBUG	17-Apr-91	29-May-91
00342.52	REDESIGN	30-May-91	25-Jul-91
00342.6	ELEC BOX REDESIGN	1-Aug-91	28-Aug-91
00343	FAB & TEST PF MODULE	16-Sep-91	8-Jul-92
00343.1	PREAMP	16-Sep-91	16-Jan-92
00343.11	LAYOUT BOARD	16-Sep-91	4-Oct-91
00343.12	FAB	7-Oct-91	3-Dec-91
00343.13	TEST	4-Dec-91	16-Jan-92
00343.2	POWER DIST	7-Oct-91	16-Mar-92
00343.21	LAYOUT BOARD	7-Oct-91	25-Oct-91
00343.22	FAB	4-Dec-91	31-Jan-92
00343.23	TEST	3-Feb-92	16-Mar-92
00343.3	DIG SIG PROC	16-Sep-91	16-Jan-92
00343.31	LAYOUT BOARD	16-Sep-91	4-Oct-91
00343.32	FAB	7-Oct-91	3-Dec-91
00343.33	TEST/DEBUG	4-Dec-91	16-Jan-92
00343.4	SCAN/FLIP	7-Oct-91	16-Mar-92
00343.41	LAYOUT BOARD	7-Oct-91	25-Oct-91
00343.42	FAB	4-Dec-91	31-Jan-92
00343.43	TEST/DEBUG	3-Feb-92	16-Mar-92
00343.5	SYS/HOUSEKEEPING	16-Sep-91	27-Apr-92
00343.51	LAYOUT BOARD	16-Sep-91	4-Oct-91
00343.52	FAB	7-Oct-91	3-Dec-91
00343.53	TEST/DEBUG	17-Mar-92	27-Apr-92
00343.6	FAB ELEC BOXES	16-Sep-91	25-Oct-91

WBS Code	Task Name	Start Date	End Date
00343.7	INTEGRATE & TEST MO	28-Apr-92	8-Jul-92
00343.71	ASSEMBLY	28-Apr-92	11-May-92
00343.72	TROUBLESHOOT	12-May-92	9-Jun-92
00343.73	CHARACTERIZE	10-Jun-92	23-Jun-92
00343.74	ENVIRN TESTING	24-Jun-92	8-Jul-92
00350	SENSOR STRUCTURE	30-Jul-90	23-Jun-92
00351	PRELIMINARY DESIGN	30-Jul-90	14-Dec-90
00351.1	FRAME	30-Jul-90	24-Aug-90
00351.2	CONTAM COVER	31-Oct-90	29-Nov-90
00351.3	WIRING HARNESS	3-Dec-90	14-Dec-90
00352	FINAL DESIGN	4-Apr-91	13-Jun-91
00352.1	CONTAIM COVER REDES	4-Apr-91	30-May-91
00352.2	FRAME	31-May-91	13-Jun-91
00353	FAB & TEST PFM	1-Oct-91	23-Jun-92
00353.1	FAB FRAME	1-Oct-91	12-Nov-91
00353.2	FAB/TEST COVER	2-Jan-92	27-Mar-92
00353.3	FAB/TEST WIRE HARNE	31-Mar-92	11-May-92
00353.4	ASSEMBLE FRAME MODU	12-May-92	23-Jun-92
00360	THERMAL CONTROL	17-Sep-90	3-Apr-92
00361	PRELIMINARY DESIGN	17-Sep-90	20-Dec-90
00361.1	RADIATORS	25-Sep-90	30-Oct-90
00361.11	THERMAL DESIGN	25-Sep-90	30-Oct-90
00361.12	MECHANICAL DESIG	10-Oct-90	30-Oct-90
00361.2	HEAT SINKS	25-Sep-90	6-Dec-90
00361.21	OPTICS MODULE	16-Oct-90	20-Nov-90
00361.211	THERMAL DESIG	16-Oct-90	5-Nov-90
00361.212	MECH DESIGN	6-Nov-90	20-Nov-90
00361.22	COMPRESSOR H.S.	24-Oct-90	6-Dec-90
00361.221	THERM	24-Oct-90	21-Nov-90
00361.222	MECH	7-Nov-90	6-Dec-90
00361.23	DISPLACER H.S	25-Sep-90	30-Oct-90
00361.231	THERMAL	25-Sep-90	23-Oct-90
00361.232	MECH	2-Oct-90	30-Oct-90
00361.24	ELECTRONICS HEAT	23-Oct-90	6-Dec-90
00361.241	THERMAL DESIG	23-Nov-90	6-Dec-90
00361.242	MECHANICAL DE	23-Oct-90	5-Nov-90
00361.3	SURVIVAL HEATERS	17-Sep-90	28-Sep-90
00361.4	THERMAL BLANKET SPE	7-Dec-90	20-Dec-90

WBS Code	Task Name	Start Date	End Date
00362	FINAL DESIGN	25-Jan-91	19-Jun-91
00362.1	RADIATOR REDESIGN	25-Jan-91	19-Apr-91
00362.2	HEAT SINK REDESGN	30-May-91	19-Jun-91
00362.3	FINALIZE BLANKET SP	3-Jun-91	14-Jun-91
00363	FAB/ASSEM THERMAL CONT	28-Oct-91	3-Apr-92
00363.1	FAB RADIATORS	13-Nov-91	26-Dec-91
00363.2	FAB HEAT SINK	16-Mar-92	3-Apr-92
00363.3	BUY THERM BLANKETS	30-Mar-92	30-Mar-92
00363.4	FAB ELEC MODULE HEA	28-Oct-91	8-Nov-91

6.2.2.4 Ground Equipment. The ground equipment (WBS 00400) subtasks and their schedules are:

WBS Code	Task Name	Start Date	End Date
00400	GROUND EQUIPMENT	17-Sep-90	18-Jan-94
00410	ELECTRONIC GSE	23-Nov-90	26-Nov-91
00411	PRELIM DESIGN GSE	23-Nov-90	20-Dec-90
00411.1	SPEC COMP HARDWARE	23-Nov-90	20-Dec-90
00412	FINAL DESIGN	22-Jan-91	10-Apr-91
00412.1	ORDER COMP HARDWARE	22-Jan-91	22-Jan-91
00412.11	3-386 PC'S	22-Jan-91	22-Jan-91
00412.12	1-BUS65517 SIMUL	22-Jan-91	22-Jan-91
00412.13	1-BUS65515 INTER	22-Jan-91	22-Jan-91
00412.14	2-OPTITEK DRIVE	22-Jan-91	22-Jan-91
00412.15	2-HPIB INTERFACE	22-Jan-91	22-Jan-91
00412.2	ENG INTERFACE	22-Jan-91	10-Apr-91
00412.21	DESIGN BOARD	22-Jan-91	12-Feb-91
00412.22	FAB BREADBOARD	12-Feb-91	10-Apr-91
00413	FAB/ASSEM HARDWARE	1-Oct-91	26-Nov-91
00413.1	BUY GSE INSTRUMENTS	1-Oct-91	1-Oct-91
00413.11	INTERFACE ELECTR	1-Oct-91	1-Oct-91
00413.12	MISC. INSTRUMENT	1-Oct-91	1-Oct-91
00413.2	FAB RACKS	1-Oct-91	28-Oct-91
00413.3	FAB PF ENG INTERFAC	1-Oct-91	26-Nov-91
00420	GROUND HANDLING/SHIPPING	2-Jan-92	18-Jan-94
00421	DESIGN HANDLING EQUIPM	2-Jan-92	23-Jan-92
00422	FAB HANDLING EQUIPMENT	15-May-92	5-Jun-92
00423	PACK/SHIP THERMAL/VAC	16-Nov-92	7-Dec-92
00424	PACK/SHIP FROM THERM/V	5-Feb-93	26-Feb-93
00425	PACK/SHIP TO OM INTEGR	1-Jul-93	15-Jul-93
00426	PACK/SHIP TO S/C INTEG	4-Jan-94	18-Jan-94
00430	INTERFACE JIGS, ETC	17-Sep-90	27-Jan-92
00431	PREL DESIGN HEAT EXCHA	17-Sep-90	28-Sep-90
00432	DESIGN TEST HEAT EXCHA	2-May-91	30-May-91
00433	FAB HEAT EXCHANGER	27-Nov-91	27-Jan-92
00434	MISC	27-Nov-91	27-Jan-92

6.2.2.5 Flight and Ground Software. The flight and ground software (WBS 00500) subtasks and their schedules are:

WBS Code	Task Name	Start Date	End Date
00500	FLIGHT & GROUND SOFTWARE	1-Jun-90	15-Jul-92
00510	FLIGHT SOFTWARE	30-Jul-90	19-Mar-91
00511	PREL DESIGN	30-Jul-90	21-Nov-90
00511.1	DIG SIG PROC SOFTWA	30-Jul-90	24-Sep-90
00511.2	SCAN/FLIP SOFTWARE	25-Sep-90	21-Nov-90
00511.3	SYS CNTRL & HOUSEKE	13-Aug-90	6-Nov-90
00512	FINAL DESIGN	22-Jan-91	19-Mar-91
00512.1	DIG SIG PROC SOFTWA	22-Jan-91	19-Mar-91
00512.2	SCAN/FLIP SOFTWARE	22-Jan-91	19-Mar-91
00512.3	SYS CNTRL & HOUSEKE	22-Jan-91	19-Mar-91
00513	ADJUSTMENT	30-Jul-90	19-Mar-91
00520	GSE SOFTWARE	1-Jun-90	15-Jul-92
00521	PREL DESIGN	1-Jun-90	21-Nov-90
00521.1	ENG INTERFACE	1-Jun-90	13-Jul-90
00521.2	SPACE CRAFT SIMULAT	27-Aug-90	23-Oct-90
00521.3	DATA LOGGER	16-Jul-90	24-Aug-90
00521.4	OFFLINE DATA ANALYZ	24-Oct-90	21-Nov-90
00522	FINAL DESIGN	12-Feb-91	15-Jul-92
00522.1	ENG INTERFACE SOFTW	12-Feb-91	27-Mar-91
00522.2	SPACECRAFT SIMULATO	27-Mar-91	22-May-91
00522.3	DATA LOGGER	22-May-91	19-Jul-91
00522.4	THERMAL CONTROL SOF	31-May-91	12-Jul-91
00522.5	QUICKLOOK OFFLINE S	15-Jul-91	9-Sep-91
00522.6	COMPL ONLINE SOFTWA	16-Sep-91	9-Jan-92
00522.7	COMPL QUICKLOOK	10-Jan-92	23-Mar-92
00522.8	IN DEPTH OFFLINE SO	24-Mar-92	15-Jul-92
00523	ADJUSTMENT	1-Jun-90	15-Jul-92

6.2.2.6 Performance Assurance and Safety. The performance assurance and safety (WBS 00600) subtasks and their schedules are:

WBS Code	Task Name	Start Date	End Date
00600	PERFORMANCE ASSURANCE & SAFE	1-Jun-90	1-Jul-93
00610	RELIABILITY & QUALITY ASS	1-Jun-90	1-Jul-93
00620	PARTS, MATERIALS, & PROCE	1-Jun-90	1-Jul-92
00630	CONFIGURATION MANAGEMENT	1-Jun-90	1-Jul-92
00640	SYSTEMS SAFETY	1-Jun-90	1-Jul-93

6.2.2.7 Instrument Assembly and Verification. The instrument assembly and verification (WBS 00700) subtasks and their schedules are:

WBS Code	Task Name	Start Date	End Date
00700	INSTRU ASSEMBLY & VERFICATIO	18-May-92	4-Feb-93
00710	IRLE ASSEMBLY & INTEGRATI	18-May-92	15-Jun-92
00711	ASSEMBLY & INTEGRATION	18-May-92	15-Jun-92
00720	INSTRUMENT CHAR & PERF TE	16-Jun-92	7-Oct-92
00721	ENG CHECKOUT	16-Jun-92	7-Oct-92
00721.1	ADJUST/ALIGN IRLE	16-Jun-92	9-Sep-92
00721.2	ENG CAL/CHAR-PERFOR	10-Sep-92	7-Oct-92
00730	INSTRU ENVIR TEST	8-Oct-92	4-Feb-93
00731	EMI TESTING	8-Oct-92	22-Oct-92
00732	VIBRATION TESTING	23-Oct-92	13-Nov-92
00733	THERMAL VACCUM TESTING	8-Dec-92	4-Feb-93

6.2.2.8 Calibration. The calibration (WBS 00800) subtasks and their schedules are:

WBS Code	Task Name	Start Date	End Date
00800	CALIBRATION	15-Jan-91	26-Jul-93
00810	CALIBRATION PLAN	15-Jan-91	26-Jul-93
00811	CAL TEST PLAN	15-Jan-91	23-Jul-91
00812	CAL REPORT	24-May-93	26-Jul-93
00820	GROUND CAL EQUIPMENT	1-Feb-91	10-Mar-92
00821	SOFTWARE	1-Feb-91	10-Sep-91
00823	DESIGN HARDWARE	15-May-91	29-May-91
00824	FAB CAL EQUIPMENT	28-Jan-92	10-Mar-92
00830	GROUND CAL OPERATIONS	1-Mar-93	21-May-93

6.2.2.9 Integration and Test. The integration and test (WBS 00900) subtasks and their schedules are:

WBS Code	Task Name	Start Date	End Date
00900	INTEGRATION & TEST SUPPORT	2-Jan-92	15-Nov-94
00910	INTEGRATION PLAN	2-Jan-92	6-May-92
00920	IRLE/OM INTEGRATION & TES	1-Sep-93	1-Apr-94
00930	OM/S/C INTEGRATION & TEST	1-Apr-94	1-Jul-94
00940	PRE-LAUNCH SUPPORT	1-Jul-94	15-Nov-94

6.2.2.10 Flight Operations Support. The flight operations support (WBS 01000) subtasks and their schedules are:

WBS Code	Task Name	Start Date	End Date
01000	FLIGHT OPERATIONS SUPPORT	1-Feb-94	13-Dec-94
01010	PRE-LAUNCH PLANNING & SIM	1-Feb-94	19-Jul-94
01011	PLANNING	1-Feb-94	14-Feb-94
01012	SIMULATION EXERCISE	6-Jul-94	19-Jul-94
01020	POST-LAUNCH SUPPORT	15-Nov-94	29-Nov-94
01030	FLIGHT DATA VALIDATION SU	30-Nov-94	13-Dec-94

6.3 COST MODEL

All costs are given in terms of 1989 dollars. The total cost of the project is $10,699,765. Hourly labor rates are fully burdened. They include a 32 percent benefit rate and a 37 percent overhead rate. Hourly rates were computed using the following formula:

Hourly rate = 1.37(1.32 x pay rate).

6.3.1 Costs of Major Tasks

6.3.1.1 Total Costs. The total costs of each major task are:

PROGRAM MANAGEMENT	$1,169,310
SYSTEM ENGINEERING	$410,948
FLIGHT HARDWARE	$6,695,351
GROUND EQUIPMENT	$271,109
FLIGHT & GROUND SOFTWARE	$400,612
PERFORMANCE ASSURANCE & SAFETY	$345,743
INSTRU ASSEMBLY & VERFICATION	$466,489
CALIBRATION	$298,790
INTEGRATION & TEST SUPPORT	$528,540
FLIGHT OPERATIONS SUPPORT	$112,873
Total	$10,699,765

6.3.1.2 Costs by Fiscal Year. The fiscal year starts in October. The costs of the major tasks for fiscal years 1990 and 1991 are:

	FY-90	FY-91
PROGRAM MANAGEMENT	$88,090	$284,645
SYSTEM ENGINEERING	$117,936	$241,442
FLIGHT HARDWARE	$213,052	$3,771,476
GROUND EQUIPMENT	$3,747	$63,322
FLIGHT & GROUND SOFTWARE	$84,593	$224,917
PERFORMANCE ASSURANCE & SAFETY	$44,641	$133,390
INSTRU ASSEMBLY & VERFICATION		
CALIBRATION		$95,585
INTEGRATION & TEST SUPPORT		
FLIGHT OPERATIONS SUPPORT		
Total	$552,059	$4,814,777

The costs of the major tasks for fiscal years 1992 and 1993 are:

	FY-92	FY-93
PROGRAM MANAGEMENT	$246,762	$234,977
SYSTEM ENGINEERING	$6,187	$22,736
FLIGHT HARDWARE	$2,697,441	$13,381
GROUND EQUIPMENT	$187,991	$12,238
FLIGHT & GROUND SOFTWARE	$91,103	
PERFORMANCE ASSURANCE & SAFETY	$117,724	$49,988
INSTRU ASSEMBLY & VERFICATION	$264,256	$202,234
CALIBRATION	$90,162	$113,043
INTEGRATION & TEST SUPPORT	$23,479	$38,115
FLIGHT OPERATIONS SUPPORT		
Total	$3,725,106	$686,712

The costs of the major tasks for fiscal years 1994 and 1995 are:

	FY-94	FY-95
PROGRAM MANAGEMENT	$269,455	$45,381
SYSTEM ENGINEERING	$14,895	$7,752
FLIGHT HARDWARE		
GROUND EQUIPMENT	$3,810	
FLIGHT & GROUND SOFTWARE		
PERFORMANCE ASSURANCE & SAFETY		
INSTRU ASSEMBLY & VERFICATION		
CALIBRATION		
INTEGRATION & TEST SUPPORT	$425,066	$41,881
FLIGHT OPERATIONS SUPPORT	$29,119	$83,755
Total	$742,344	$178,768

6.3.2 Costs by Resource

Resource Cost Type	Full Name	Hourly Rate	Total
Resource	ACCOUNTANT	26.44	$181,008
Fixed	ADMINISTRATIVE MANAGEMENT		$200,000
Resource	CALIBRATION ENGINEER	33.42	$149,722
Resource	CIRCUIT BOARD DESIGNER	30.13	$48,449
Resource	MECHANICAL DESIGNER	30.13	$307,772
Resource	ELECTRICAL ENGINEER	33.42	$1,147,817
Resource	SENIOR ELECTRICAL ENG	46.77	$95,336
Fixed	EXPENDABLES		$6,000
Resource	GRAPHICS ARTIST	26.44	$139,709
Resource	MACHINIST	21.70	$127,040
Resource	MECHANICAL ENGINEER	33.42	$110,847
Fixed	PARTS AND MATERIALS		$426,950
Resource	QUALITY ASSURANCE &	26.44	$220,340
Resource	SENIOR SCIENTIST	62.03	$113,242
Fixed	SUBCONTRACTS		$5,355,745
Fixed	SUBCONTRACT MANAGEMENT		$46,250
Resource	SYSTEMS ENGINEER SR.	47.77	$558,118
Resource	THERMAL ENGINEER	33.42	$116,716
Resource	SENIOR THERMAL ENG	62.03	$212,639
Resource	TECHNICIANS	22.62	$537,596
Fixed	TRAVEL		$241,000
Resource	TECHWRITER	26.44	$357,469
	Total		$10,699,765

6.3.3 Costs of Subtasks

6.3.3.1 Program Management Subtasks. The costs of the program management subtasks (WBS 00100) are:

PROGRAM MANAGEMENT	$1,169,310
PROGRAM MANAGEMENT	$384,011
TECH MANAGEMENT	$109,011
ADMINSTRATIVE MANAGEMENT	$200,000
MEETING TRAVEL	$75,000
DELTA CoDR	$5,000
PDR	$10,000
CDR	$10,000
TIM TRAVEL COSTS	$50,000
RESOURCE/SCEDULE CONTROL	$181,008
CSSR (COST REPORTING & TRA	$181,008
DOCUMENTATION	$387,053
DELTA CoDR DOCUMENTS	$8,346
PDR DOCUMENTS	$8,346
CDR DOCUMENTS	$8,346
ICD & REPORTS	$362,016
SCIENCE MANAGEMENT	$113,242
SUBCONTRACT MANAGEMENT	$46,250
MANAGE COOLER SUB	$9,250
MANAGE FPA SUB	$9,250
MANAGE FILTER SUB	$9,250
MANAGE CHOPPER SUB	$9,250
MANAGE THERMAL SWITCH SUB	$9,250
S/C/INSTRU INTEG CTRL	$57,745
Total	$1,169,310

6.3.3.2 System Engineering Subtasks. The costs of the system engineering subtasks (WBS 00200) are:

SYSTEM ENGINEERING	$410,948
DEVELOP SENSOR DESIGN REQUIR	$108,377
CONCEPTUAL DESIGN	$50,157
PRELI DESIGN	$22,045
FINAL DESIGN	$36,174
INSTRU INTEGR & TEST PLAN	$22,647
INTEG/TEST PLAN	$22,647
INST/S/C INTERF REQ	$102,080
CONCEPTUAL DESIGN	$25,079
PRELI DESIGN	$29,124
FINAL DESIGN	$47,877
INST MODELING & ANALYSIS	$144,138
PRELIM DESIGN	$35,528
RADIOMETRIC	$7,280
THERMAL	$19,091
STRUCTURAL	$9,157
FINAL DESIGN	$79,687
RADIOMETRIC MODEL	$24,458
THERMAL MODEL	$35,310
STRUCT MODEL	$19,918
VERIFY MODELS	$28,923
THERMAL	$12,555
STRUCTURE	$6,737
RADIOMETRIC	$9,630
CALIBRATION REQ/PLANNING	$10,433
PRELIMNARY DESIGN	$5,618
FINAL DESIGN	$4,815
GSE REQUIREMENTS/PLANNING	$10,433
PRELIMINARY DESIGN	$5,618
FINAL DESIGN	$4,815
COORD FLIGHT/GRND SOFTWARE	$12,841
PRELI DESIGN	$5,618
FINAL DESIGN	$7,223
Total	$410,948

6.3.3.3 Flight Hardware. The costs of the flight hardware subtasks (WBS 00300) are:

FLIGHT HARDWARE	$6,695,351
OPTICS MODULE	$2,633,046
TELESCOPE & BAFFLE	$2,512,173
SELECT SUB	$5,822
PREL DESIGN SUBCONTRACT	$100,000
MONITOR PREL DESIGN SUB	$30,685
FOLLOW-ON SUBCONTRACT	$2,300,000
MONITOR FOLLOW-ON SUBCON	$75,667
CHOPPER	$107,537
PREPARE RFQ	$3,822
SUBCONTRACT	$69,250
TEST BREADB CHOPPER	$34,465
ASSEM/WARM TEST MOD	$13,336
DETECTOR MODULE	$1,594,548
PRELI DESIGN DET MODULE	$79,483
FPA	$21,390
DEVELOP SPEC	$7,822
ISSUE RFQ	$2,866
TEST InGaAs DETECTORS	$10,702
BUY SAMPLES	$3,261
TEST SAMPLES	$7,441
FILTERS	$12,509
DEVELOP SPEC	$9,643
ISSUE RFQ	$2,866
THERMAL SWITCHES	$10,310
DEVELOP SPEC	$5,155
ISSUE RFQ	$5,155
DEWAR	$35,274
THERMAL DESIGN	$7,828
MECHANICAL DESIGN	$27,446
FINAL DESIGN	$1,417,471
FPA	$1,015,771
SUBCONTRACT	$1,000,000
MONITOR FPA SUBCONTRAC	$15,771
FILTERS	$260,884
SUBCONTRACT	$248,795
MONITOR FILTER SUBCONT	$12,089
THERMAL SWITCHES	$81,550
SUBCONTRACT	$75,000

MONITOR SUB	$6,550
DEWAR	$59,266
BREADBOARD LN TEST DEW	$29,673
DESIGN	$13,308
FAB	$4,472
TEST	$11,893
REDESIGN PF DEWAR	$29,593
FAB & TEST PF MODULE	$97,595
PF DEWAR	$37,406
FAB	$27,448
TEST	$9,959
FAB HEAT SINKS	$4,472
SHIP FILTERS TO DET SUB	$864
TEST THERM SWITCHES	$13,559
TEST COOLER	$6,681
TEST FPA IN LN DEWAR	$13,673
INTEGRATE DET MOD	$9,676
TEST & CAL MODULE	$11,262
CRYOCOOLER	$1,516,775
DEVELOP SPEC	$7,732
ISSUE RFQ	$5,155
SUBCONTRACT	$1,487,700
MONITOR COOLER SUB	$16,188
ELECTRONICS	$685,664
PRELI DESIGN ELEC MODULE	$75,805
PREAMPS	$20,532
POWER DISTRIBUTION SYS	$16,042
DIG SIGNAL PROCESSOR	$6,844
SCAN/FLIP CONTROL	$6,844
SYS CONTROL/HOUSEKEEPING	$17,110
ELECTRONIC BOXES	$8,434
ELEC DESIGN	$1,203
MECH DESIGN	$7,231
FINAL DESIGN ELEC	$197,230
PREAMP	$30,282
BREADBOARD	$21,139
LAYOUT	$3,616
FAB	$8,557
TEST	$8,966
REDESIGN	$9,143
POWER DISTRIBUTION SYSTE	$35,466
BREADBOARD	$26,322

LAYOUT	$9,642
FAB	$7,714
TEST	$8,966
REDESIGN	$9,143
DIGITAL SIGNAL PROCESSOR	$40,613
BREADBOARD	$28,422
LAYOUT	$3,616
FAB	$11,357
TEST/DEBUG	$13,450
REDESIGN	$12,191
SCAN/FLIP CONTROL	$35,613
BREADBOARD	$23,422
LAYOUT	$3,616
FAB	$6,357
TEST/DEBUG	$13,450
REDESIGN	$12,191
SYS CONTROL/HOUSEKEEPING	$45,613
BREADBOARD	$33,422
LAYOUT	$3,616
FAB	$16,357
TEST/DEBUG	$13,450
REDESIGN	$12,191
ELEC BOX REDESIGN	$9,642
FAB & TEST PF MODULE	$412,629
PREAMP	$29,884
LAYOUT BOARD	$3,616
FAB	$12,819
TEST	$13,450
POWER DIST	$104,800
LAYOUT BOARD	$3,616
FAB	$10,619
TEST	$13,450
DIG SIG PROC	$86,250
LAYOUT BOARD	$3,616
FAB	$10,619
TEST/DEBUG	$13,450
SCAN/FLIP	$25,684
LAYOUT BOARD	$3,616
FAB	$8,619
TEST/DEBUG	$13,450
SYS/HOUSEKEEPING	$25,684
LAYOUT BOARD	$3,616

FAB	$8,619
TEST/DEBUG	$13,450
FAB ELEC BOXES	$12,646
INTEGRATE & TEST MODULE	$127,680
ASSEMBLY	$6,634
TROUBLESHOOT	$26,899
CHARACTERIZE	$13,450
ENVIRN TESTING	$13,450
SENSOR STRUCTURE	$134,878
PRELIMINARY DESIGN	$38,644
FRAME	$18,655
CONTAM COVER	$12,315
WIRING HARNESS	$7,674
FINAL DESIGN	$29,714
CONTAIM COVER REDESIGN	$24,630
FRAME	$5,084
FAB & TEST PFM	$66,520
FAB FRAME	$17,247
FAB/TEST COVER	$31,400
FAB/TEST WIRE HARNESS	$5,429
ASSEMBLE FRAME MODULE	$12,445
THERMAL CONTROL	$130,439
PRELIMINARY DESIGN	$64,824
RADIATORS	$14,677
THERMAL DESIGN	$6,443
MECHANICAL DESIGN	$8,234
HEAT SINKS	$41,822
OPTICS MODULE	$8,315
THERMAL DESIGN	$3,494
MECH DESIGN	$4,821
COMPRESSOR H.S.	$9,976
THERM	$5,155
MECH	$4,821
DISPLACER H.S	$14,796
THERMAL	$5,155
MECH	$9,642
ELECTRONICS HEAT SINK	$8,735
THERMAL DESIGN	$3,914
MECHANICAL DESIGN	$4,821
SURVIVAL HEATERS	$5,155
THERMAL BLANKET SPECS	$3,170
FINAL DESIGN	$37,745

RADIATOR REDESIGN	$25,461
HEAT SINK REDESGN	$8,370
FINALIZE BLANKET SPEC	$3,914
FAB/ASSEM THERMAL CONTROL	$27,870
FAB RADIATORS	$12,724
FAB HEAT SINK	$7,016
BUY THERM BLANKETS	$1,248
FAB ELEC MODULE HEAT SIN	$6,882
Total	$6,695,351

6.3.3.4 Ground Equipment. The costs of the ground equipment subtasks (WBS 00400) are:

GROUND EQUIPMENT	$271,109
ELECTRONIC GSE	$198,306
PRELIM DESIGN GSE	$5,347
SPEC COMP HARDWARE	$5,347
FINAL DESIGN	$50,480
ORDER COMP HARDWARE	$41,250
3-386 PC'S	$2,500
1-BUS65517 SIMULATOR	$12,500
1-BUS65515 INTERFACE	$7,000
2-OPTITEK DRIVE	$16,500
2-HPIB INTERFACES	$2,750
ENG INTERFACE	$9,230
DESIGN BOARD	$4,010
FAB BREADBOARD	$5,220
FAB/ASSEM HARDWARE	$142,478
BUY GSE INSTRUMENTS	$113,700
INTERFACE ELECTRONICS	$13,700
MISC. INSTRUMENTS	$100,000
FAB RACKS	$17,233
FAB PF ENG INTERFACE	$11,545
GROUND HANDLING/SHIPPING EQU	$35,913
DESIGN HANDLING EQUIPMENT	$7,231
FAB HANDLING EQUIPMENT	$12,634
PACK/SHIP THERMAL/VAC TEST	$4,714
PACK/SHIP FROM THERM/V TO	$3,714
PACK/SHIP TO OM INTEGRATON	$3,810
PACK/SHIP TO S/C INTEGRATI	$3,810
INTERFACE JIGS, ETC	$36,890
PREL DESIGN HEAT EXCHANGER	$3,747
DESIGN TEST HEAT EXCHANGER	$7,494
FAB HEAT EXCHANGER	$15,648
MISC	$10,000
Total	$271,109

6.3.3.5 Flight and Ground Software. The costs of the flight and ground software subtasks are:

FLIGHT & GROUND SOFTWARE	$400,612
FLIGHT SOFTWARE	$137,530
PREL DESIGN	$37,430
DIG SIG PROC SOFTWARE	$10,694
SCAN/FLIP SOFTWARE	$10,694
SYS CNTRL & HOUSEKEEP SO	$16,042
FINAL DESIGN	$32,083
DIG SIG PROC SOFTWARE	$10,694
SCAN/FLIP SOFTWARE	$10,694
SYS CNTRL & HOUSEKEEP SO	$10,694
ADJUSTMENT	$68,016
GSE SOFTWARE	$263,082
PREL DESIGN	$32,083
ENG INTERFACE	$8,021
SPACE CRAFT SIMULATOR	$10,694
DATA LOGGER	$8,021
OFFLINE DATA ANALYZER	$5,347
FINAL DESIGN	$88,229
ENG INTERFACE SOFTWARE	$8,021
SPACECRAFT SIMULATOR	$10,694
DATA LOGGER	$10,694
THERMAL CONTROL SOFTWARE	$8,021
QUICKLOOK OFFLINE SOFTWA	$10,694
COMPL ONLINE SOFTWARE	$16,042
COMPL QUICKLOOK	$13,368
IN DEPTH OFFLINE SOFTWAR	$10,694
ADJUSTMENT	$142,770
Total	$400,612

6.3.3.6 Performance Assurance and Safety. The costs of the performance assurance and safety subtasks (WBS 00600) are:

PERFORMANCE ASSURANCE & SAFETY	$345,743
RELIABILITY & QUALITY ASSURA	$143,852
PARTS, MATERIALS, & PROCESSE	$102,762
CONFIGURATION MANAGEMENT	$36,646
SYSTEMS SAFETY	$62,484
Total	$345,743

6.3.3.7 Instrument Assembly and Verification. The costs of the instrument assembly and verification subtasks (WBS 00700) are:

INSTRU ASSEMBLY & VERFICATION	$466,489
IRLE ASSEMBLY & INTEGRATION	$87,354
ASSEMBLY & INTEGRATION	$87,354
INSTRUMENT CHAR & PERF TEST	$186,900
ENG CHECKOUT	$186,900
ADJUST/ALIGN IRLE	$146,908
ENG CAL/CHAR-PERFORMANCE	$39,992
INSTRU ENVIR TEST	$192,236
EMI TESTING	$55,546
VIBRATION TESTING	$35,188
THERMAL VACCUM TESTING	$101,502
Total	$466,489

6.3.3.8 Calibration. The costs of the calibration subtasks (WBS 00800) are:

CALIBRATION	$298,790
CALIBRATION PLAN	$41,657
CAL TEST PLAN	$8,823
CAL REPORT	$32,835
GROUND CAL EQUIPMENT	$176,925
SOFTWARE	$82,347
DESIGN HARDWARE	$4,416
FAB CAL EQUIPMENT	$90,162
GROUND CAL OPERATIONS	$80,208
Total	$298,790

6.3.3.9 Integration and Test Support. The costs of the integration and test support subtasks (WBS 00900) are:

INTEGRATION & TEST SUPPORT	$528,540
INTEGRATION PLAN	$23,479
IRLE/OM INTEGRATION & TEST	$263,174
OM/S/C INTEGRATION & TEST	$110,661
PRE-LAUNCH SUPPORT	$131,226
Total	$528,540

6.3.3.10 Flight Operations Support. The costs of the flight operations subtasks (WBS 01000) are:

FLIGHT OPERATIONS SUPPORT	$112,873
PRE-LAUNCH PLANNING & SIMULA	$29,119
PLANNING	$6,331
SIMULATION EXERCISE	$22,788
POST-LAUNCH SUPPORT	$45,282
FLIGHT DATA VALIDATION SUPPO	$38,473
Total	$112,873